Tampereen yliopisto

Niko Mäkipää

SURFACE CHARACTERIZATION OF GROUND SURFACES: EFFECTS OF GRINDING

Materials Science and Environmental Engineering unit
Master's Thesis
October 2019

ABSTRACT

Mäkipää, Niko: Surface characterization of ground surfaces: effects of grinding
Master's Thesis
Tampere University
Degree Programme in Materials Science and Engineering
October 2019

Thesis was focused on to the effects of grinding and the surface characterization of the ground surfaces. Main focus was in Barkhausen noise (BN) and its use in surface characterization measurements done to the assigned sample batches. Grinding wheel types used in grinding were Aluminium oxide (Al_2O_3) and cubic boron nitrade (CBN), CBN was further divided to B126 and B181 wheels based on the grit size. Purpose of the thesis was to examine how well and reliably can BN be used as the detection method for grinding process, indicating for example grinding burns. In addition, the goal was to find out the differences between the grinding wheels through theory and measurements to finalize an opinion which of the wheels suits the grinding operation of the component better. The suitability was based on the residual stresses that rise inevitability during grinding. The objective of the thesis was to contribute information and help industrial quality control to move from destructive and time consuming testing methods to non-destructive testing (NDT) methods.

The grinding samples were all same size and produced from 20MnCrS5 steel. Samples were carburized case hardened with oil quenching before grinding. The laboratory testing started with the use of NDT methods, once the sample batches arrived to university after grinding processes. Before starting with X-ray diffraction based residual stress measurements, visual inspection indicated the grinding direction in the CBN ground samples. Based on earlier measurements during this project and information found in theory, residual stress deviation depends on the direction of the grinding. By measuring the residual stresses, direction of the grinding was solved based on the values acquired. After this, the surface measurements were started by using BN. Barkhausen experiments included using two different sensors (S6287 and S4740) and two different kind of softwares to collect the measured data (MicroScan and PCCaseDepth) The results of BN measurements were compared to X-ray diffraction results and closer to the end with the destructive results. These results were involved as supportive measurements to see the realisticity of the BN results and to give values to see correlation with the BN values.

Final clarity of the results was ensured with destructive testing (residual stress depth profile, hardness measurements and micostructural observation). This was done to verify that the BN results were realistic. For an original, non-ground sample residual stress depth profile was done. Normally ground and intentionally made grinding burn samples were prepared for the optical microscopy and hardness measurements. Based on these values gathered on the measurements and comparing them to theory, the reliability of the BN measurements was determined to be quite good, offering realistic and theory supported results with good correlation to the most values related to the study.

Due to the fact that selected grinding parameters didn't use the full potential of the grinding wheels, the results resembled quite a lot each other between normally ground batches. Leading up to the conclusion that the selection of the grinding wheel should more likely be based on for example either volume of the component batch or required surface roughness. Differences were detected in the intentionally caused grinding burn samples. In the Al_2O_3 wheel ground samples temper burn was detected, while in the CBN B126 grinding burn results turn out to be questionable because the whole case depth was ground off. This effort wasn't wasted, since this result showed that the severity of the grinding burn can't be judged just by the visual burn on the surface.

At the beginning it was informed that the user of grinding wheel CBN B181 noticed issues when grinding with wheel. Results gathered with grinding wheel CBN B181 showed anomalies in only a few measurements that all can be explained with normal deviation. Based on the results it is hard to define, did the issues noticed with the wheel have influence to the results.

Keywords: Barkhausen noise, case depth, residual stress measurements, grinding

TIIVISTELMÄ

Mäkipää, Niko: Hiotun pinnan karakterisointi – hionnan vaikutusten määrittely
Diplomityö
Tampereen yliopisto
Materiaalitekniikan DI-tutkinto-ohjelma
Lokakuu 2019

Työssä perehdytään hionnan vaikutuksiin ja hiotun pinnan karakterisointiin. Työn pääpaino on ainetta rikkomattoman koetustavan, Barkhausen kohinan (BN), avulla suoritettavissa mittauksissa. Mittauksilla karakterisoidaan eri hiontalaikoilla hiottuja näytteiden pintakerroksia. Työssä käytössä olevat hiontalaikat ovat alumiinioksidipohjainen hintalaikka (Al_2O_3) ja kuutiollinen boorinitridi-hiontalaikka (CBN), joista CBN on jaoteltu vielä hiontalaikan abrasiivisten kiteiden koon mukaan B126 ja B181 hiontalaikkoihin. Työssä selvitetään kuinka hyvin ja luotettavasti Barkhausen kohinan avulla voidaan määrittää hionnan vaikutuksia, esimerkiksi mahdollisia hiontapalamisia. Tämän lisäksi selvitellään hiontalaikkojen eroja teorian ja mittausten avulla sekä kehitetään ratkaisu, kumpi hiontalaikoista soveltuisi paremmin osaksi työssä tutkittavien kappaleiden valmistusprosessia. Valmistuksen soveltuvuus perustuu jäännösjännityksiin, joita hionnassa väistämättä syntyy. Tutkimuksen päämäärä on edesauttaa teollisuuden laaduntarkastuksen siirtymistä ainetta rikkovista ja aikaa vievistä mittauksista nopeampaan, ainetta rikkomattoman laaduntarkastuksen suuntaan.

Hiontanäytteet olivat samankokoisia ja valmistettu 20MnCrS5 teräksestä. Hiiletyskarkaisu suoritettiin näytteille ennen hiontojen suorittamista. Laboratoriotestit aloitettiin ainetta rikkomattomilla mittauksilla, kun kaikki näytesarjat oli saatu hiottua ja toimitettua yliopistolle. Ennen röntgendifraktioon perustuvan jäännösjännitysmittauksen aloitusta, visuaalisella tarkastuksella näytteiden pinnat tarkastettiin hiontavirheiden varalta. Perustuen projektin aiemmin hiottujen kappaleiden ja teorian osoittamiin arvoihin jäännösjännitysten jakautumisesta eri suuntiin, näytteiden hionnan suunta pääteltiin jäännösjännitysten arvoista. Tämän jälkeen suoritettiin pinnan mittaukset Barkhausenin kohinan avulla. Barkhausenin mittaukset sisälsivät mittauksia hyödyntäen kahta erilaista sensoria (S6387 ja S4740) ja kahta eri datan keräämistarkoitukseen käytettävää ohjelmaa (MicroScan ja PCCaseDepth). BN mittaustuloksia vertailtiin röntgendifraktioon perustuvan jäännösjännitysmittauksen avulla mitattuihin tuloksiin sekä lopuksi ainetta rikkoviin mittaustuloksiin. Nämä toimivat tukena tulosten luotettavuudelle ja antoivat vertailukohtia siihen, miten BN mittaustulokset korreloivat toisten arvojen kanssa.

Tulosten tarkastelu suoritettiin lopuksi ainetta rikkovilla tutkimusmenetelmillä (jäännösjännitys-syvyysprofiili, kovuusmittaukset, optinen mikrorakenteen havainnointi). Näin varmistettiin Barkhausenin kohinan avulla mitattujen tulosten paikkansapitävyys. Alkuperäiselle hiomattomalle näytteelle suoritettiin jäännösjännitys-syvyysprofilointi, hiotut ja tahallisesti aiheutetut hiontapalamisnäytteet leikattiin ja valmisteltiin optista mikroskopiaa ja kovuusmittauksia varten. Saatujen tulosten ja teoriaan vertailun perusteella voidaan Barkhausenin kohinan todeta antaneen suhteellisen hyviä, realistisia ja teorian tukemia tuloksia sekä korreloivan hyvin useiden muiden työssä tutkittujen arvojen kanssa.

Koska työhön valitut hiontaparametrit eivät täysin hyödyntäneet hiontalaikkojen potentiaalia, tulokset muistuttivat paljon toisiaan normaalihionnassa, johtaen hiontalaikan valinnan perustumaan esimerkiksi hiontaerän kokoon ja tarvittavaan pinnanlaatuun. Eroja kuitenkin syntyi, kun näytteisiin tuotettiin tahallisesti hiontapalamista. Al_2O_3 laikalla hiotuissa näytteissä ilmeni pintapäästymistä. CBN B126 laikan tulokset jäivät kyseenalaisiksi, koska koko karkaisukerros oli hiottu pois. Tämä kuitenkin antoi tiedon, että pinnalle muodustuneen hiontapalamisen vakavuutta ei pystytä tulkitsemaan pelkästään tutkimalla pinnan ulkonäköä visuaalisella tarkastuksella.

Työn alkupuolella CBN B181 laikalla hionnan suorittanut ilmoitti, että joitain ongelmia oli havaittavissa hionnan suorituksen aikana. Hiontalaikalla saaduissa tuloksissa poikkeamia aiheutui vain muutamassa mittauksessa ja nekin ovat selitettävissä normaalina poikkeamana. Tulosten perusteella on siis hankalaa todeta, oliko havaituilla ongelmilla vaikutusta tuloksiin.

Avainsanat: Barkhausen kohina, case depth, jäännösjännitysmittaukset, hionta

PREFACE

The research and experimental work for this thesis was carried out in the Materials Science and Environmental Engineering unit, Tampere University, during year 2019. This thesis was done as a part of an Academy of Finland funded project “FUNBARK” in collaboration with Newcastle University Design unit and industrial companies. This work made use of Tampere Microscopy Center facilities at Tampere University.

From the bottom of my heart I want to thank Professor Minnamari Vippola and D.Sc. Suvi Santa-aho for all the guidance and support they have given to me during this process. I’m grateful of all the help and guidance I received from the staff and colleagues in the Department of Materials Science. Special thanks to Leevi Kurki, who helped me with the measurements and sample preparation and D.Sc. Aki Sorsa, for helping with the calculations. Also thanks to Cristopher Aylott for the fast replies to questions regarding grinding parameters and conditions.

As my final sincere thanks, I want to thank my parents for all the support and advices they have given to me.

Tampere 7.10.2019

Niko Mäkipää

TABLE OF CONTENTS

1. INTRODUCTION 1
2. THEORETICAL BACKGROUND 4
2.1 Carburizing 4
2.2 Case depth 8
2.3 Grinding 9
2.3.1 Variables in grinding 11
2.3.2 CBN grinding wheel 12
2.3.3 Al_2O_3 grinding wheel 14
2.3.4 Comparison of CBN and Al_2O_3 grinding wheels 14
2.4 Grinding induced surface layer transformations 15
2.4.1 Residual stress 15
2.4.2 Grinding burn 20
2.5 Inspection methods for grinding burn detection 23
2.5.1 Nital etching 24
2.5.2 Acoustic emission 25
2.5.3 XRD for residual stress measurements 25
2.5.4 Eddy current 26
2.5.5 Metallography 26
2.6 Recent studies with the common inspection methods 27
2.6.1 Nital etching study 27
2.6.2 XRD study 28
3. BARKHAUSEN NOISE 30
3.1 Grinding wheel characteristics and their influence on Barkhausen noise 34
3.1.1 Grinding parameters affecting to the BN results 35
3.1.2 Wheel characteristics 38
3.1.3 Recent studies of Barkhausen noise as a tool in the quality control/inspection process 40
4. ISSUES AFFECTING TO THE GRINDING OUTCOME AND TO THE SURFACE CHARACTERISTICS 44
5. EXPERIMENTAL: MATERIALS AND METHODS 46
5.1 Samples 46
5.1.1 Samples ground with Al_2O_3 wheel 49
5.1.2 Samples ground with CBN wheels 50
5.2 Preparation of the samples and equipment used in the measurements 51
5.2.1 X-ray diffraction measurements 51
5.2.2 Barkhausen noise measurements 53
5.2.3 Case depth studies with PCCaseDepth 57
5.2.4 Surface roughness studies 58
5.2.5 Residual stress depth profile 60
5.2.6 Microstructural observation 61
5.2.7 Hardness measurements 63

6. RESULTS AND DISCUSSION 65
6.1 Overall results 65
6.1.1 Residual stress results 65
6.1.2 Barkhausen noise results 72
6.1.3 Surface roughness results 78
6.1.4 PCCaseDepth results 80
6.1.5 Destructive testing results 81
6.1.6 Results from intentional caused grinding burn samples 93
6.2 Conclusions drawn from the measurement results and comparison to literature 103
7. ANALYZING SOURCES OF ERRORS 107
8. DISCUSSION OF BN ACCURACY 110
9. FUTURE OF GRINDING BURN DETECTION 112
9.1 Grinding temperature modeling 112
10. FINAL CONCLUSIONS 114
REFERENCES 116

ABBREVIATIONS AND NOTATION

AE	Acoustic emission
AL_2O_3	Aluminium oxide
BCC	Body-centered cubic
BN	Barkhausen noise
BNA	Barkhausen noise analysis
CBN	Cubic boron nitride
CHD	Case hardening depth measurement
Corundum	Natural aluminium oxide
ECT	Eddy current testing
FFT	Fast Fourier transform
HAZ	Heat-affected zone
HL	Hardness limit
HRC	Rockwell C hardness
HV	Vickers hardness
LST	Laser surface treatment
MBE	Magnetic Barkhausen emission
MBN	Magnetic Barkhausen noise
MQC	Metallurgical quality control
MQL	Minimum quantity lubrication
NDT	Non-destructive testing
RMS	Root-mean-square of Barkhausen noise voltage signal
UTM	Untempered martensite
WL	White layer
XRD	X-ray diffraction
-Ve rake	Negative angle velocity
+Ve rake	Positive angle velocity
a_p	Grinding depth
q_{ch}	Heat flux entering to the chip, W/mm^2
q_f	Heat flux entering in to the coolant, W/mm^2
q_s	Heat flux entering to the grinding wheel, W/mm^2
q_w	The heat flux entering to the workpiece, W/mm^2
R_a	Surface roughness
R_q	RMS roughness
R_t	Maximum peak to valley height of roughness profile
R_z	Mean peak to valley height of roughness profile
S_a	Average height of the area
v_s	Wheel speed
v_w	Workpiece speed
$\sigma_{comp,max}$	Maximum compressive residual stresses
σ_s	Surface residual stresses
σ_{xx}	Compressive stress distribution to grinding direction
σ_{yy}	Compressive stress distribution to perpendicular direction

1. INTRODUCTION

This thesis was done as a part of an Academy of Finland funded project called FUNBARK. The project was started in order to further study the Barkhausen noise (BN) as a non-destructive testing (NDT) method for industry to use as an inspection and quality control method for manufactured components. The focus point of this thesis was in grinding related components. Grinding is one of the last procedures in finalizing the component surface after heat-treatments to establish required roughness and tolerances. For example, the grinding always results as residual stresses and by measuring these stresses it is possible to determine grinding burns. Grinding burn is in worst case detrimental to component and at minimum reduces the service life of the component. Since the project involved around BN, it was the focal point of this thesis. Other methods will also be introduced to offer more comprehensive understanding of utilizing NDT methods. [9, 10, 30]

One part of the thesis was characterization of the ground surfaces and the effects of grinding procedure. The main focus of the project was in one NDT method, Barkhausen noise, and experimental studies using BN measurements to characterize the ground surfaces. The goal of this thesis was to find answers to questions related to grinding wheel differences (which of the used ones was the most suitable), grinding burn detection by using BN and reliability of Barkhausen noise as a detecting method for grinding burns.

The thesis starts with a theoretical section to showcase and introduce the topic giving it a backbone where to rely on. In the theoretical part carburizing, grinding and variables related to grinding are reviewed with a showcasing of the grinding wheels and comparison of wheel properties. In carburizing chapter, the heat-treatments for manufacturing the components are explained, followed by retained austenite and decarburizing, offering perception of the possible material state after heat-treatment process or processes.

In this thesis two different types of grinding wheels were used to ground the samples; Aluminium oxide (Al_2O_3) and cubic boron nitride (CBN). Two CBN wheels were used, B126 and B181, having different grain sizes. B126 had smaller abrasive grains than B181. Different wheels were included to the thesis in order to do a comparison with the results and see the differences and similarities shared by these grinding wheels. Eventually answering to the question: “Which one is better or more suitable wheel for grinding these specific samples studied in the thesis?”. Also residual stresses and defining of them was included to the theoretical part. After this one type of thermal damage, grinding

burn, was explained with the reasons why it happens and how it is inspected in industry. This includes couple of actual recently made studies to further inform how different inspection methods are actually used in quality control.

Then moving to the main topic, BN, introducing the theory and parameters that effect to the BN values. Basically going through what causes the BN and why it can be used as a quality control and inspection method. Starting with the domain wall motion and pinning sites during applied magnetic field continuing with the explanation of the hysteresis curve. Explaining the magnetization of the ferromagnetic material and irreversible discontinuous jumps that are observed as Barkhausen noise. Followed by introduction of recent studies that included BN as a quality control and inspection method. Finally ending the theory section with case depth determination with BN theory and showcasing of parameters influencing to the grinding outcome and surface characteristics. [28, 34, 39]

After theoretical part of the thesis, both the studied sample sets and the grinding wheels were introduced with the specifications. Ferromagnetic 20MnCrS5 was the material from what every sample regardless of batch was manufactured. In total 35 components were used during the measurements. These were divided into three batches of nine samples and layer ground off varied from 0.1-0.7, 0.9 and 1.1 mm with each wheel. One sample was left non-ground to do residual stress depth profile and three to do hardness depth profile. The five left over samples were ground to intentionally cause grinding burn (three ground with Al_2O_3 and two with CBN). This was followed by the detailed introduction of the research methods used to measure the samples. The research methods included X-ray diffraction (XRD), BN, hardness measurements, microstructural observations with microscope and surface roughness studies.

In the results part of the thesis, all of the measurement results were gathered together, interpreted and explained by reflecting results to theory and earlier studies. In addition, comparison between the sample batches was done in order to be able to evaluate the suitability of the grinding wheels head to head. BN was found to correlate well with most of the measurements, indicating case depth of carburized samples and relation of the severity of the grinding burns in N samples (samples ground with Al_2O_3 until intentionally caused grinding burns).

Finally, conclusions were made about the wheels, deviation of the results and parameters that would have helped to achieve better results. Conclusions were reflected to theory and earlier studies related to topic. Based on the collected data, similar results were measured from each wheel meaning that the decision of the wheel might be better to be based on other variables. For example, either to the tolerances for surface roughness or

the cost of the wheel based on the volume of the components needed to be ground. This was followed by discussion of the accuracy of the BN. Considering how well BN correlated with the other measurement results and the other measurements also backed up the BN results clearly indicating method to be reliable. Thus, other methods were needed in some cases to help seeing the changes in microstructure (hardness measurements).

Before final conclusions concerning the thesis, eyesight will be turned into the future with a possible future method of grinding burn inspection. The method introduced was grinding temperature modelling. The method sums up the variables that are related to grinding and gives prediction of maximum grinding temperature based on the parameters related to grinding. [52]

Ending the thesis with final conclusions about the measurements, results and discussion what could have been done differently in order to get more clear results. Temperature measurement during grinding and varying the grinding parameters were the most influencial issues that would have offered more information related to results, more likely offering desicive answer to the selection of the wheel. During this thesis, varying of the parameters was not possible, opening the possibility for further studies on the matter.

2. THEORETICAL BACKGROUND

In this chapter, carburizing, the one heat treatment for the case hardened material is discussed. This is followed by theory behind retained austenite and case depth measurement. Next grinding has been broken into topics of variables, grinding wheels and induced surface layer transformations, including residual stresses and grinding burn. Finally ending the chapter with introduction of the common inspection methods for detecting grinding induced damage. Two of the methods are also presented in a form of a study that has been recently made in order to get an idea of the other methods before introducing Barkhausen noise.

2.1 Carburizing

Carburizing is a heat treatment process affecting to the material properties. With carburizing, the material properties can be enhanced to endure wear in use and that way have a longer life cycle. Carburized case hardened material is diffused with carbon to get surface layers with high carbon content. [1]

Carburizing is one of the most used thermomechanical diffusion processes in industry. Carburizing is mainly used for low-carbon and low-alloy steels to create wear resistant and hard layer on the surface. Carburizing is done in high temperatures meaning that while cooling austenite transformation follows. [2] Generally the temperatures are somewhere between 850 ºC and 980 ºC. When going above the 980 ºC the carburizing time could be reduced significantly, although this requires high temperature grain coarsening resistant steels and furnaces that are designed properly to match the requirements. [3]

The benefit that carburizing offers is the compressive residual stress for parts that are highly stressed in use. Having case microstructure with high strength and hard case and core interacting together, it will enhance the properties of the material. This creates compressive stress to the case, and better surface properties with a high wear resistance. Typically carburizing process is done in two steps. In the first step carbon potential is near carbon's solubility to austenite at 1.0-1.2 wt.% and then carbon potential value is lowered to a level where it maintains surface carbon between 0.6 and 0.9 wt.%. The latter process is dependent on alloy content and temperature. In the second step excess carbon diffuses deeper. This is also known as diffuse carburizing. When the required case depth has been reached, material is quenched and tempered. With quenching

though, low-carbon core and high martensitic case are achieved. Pearlite is not tolerated, but depending on the application, small amounts of bainite are acceptable. [2]

Additional carbon content in steel after 0,65 wt.% improves hardenability but doesn't effect on the hardness. Performance characteristics like wear, sliding and rolling contact fatigue of the microstructural properties can be enhanced due to higher carbon content. If the carbon content ends up too high, there is possibility for retained austenite and harmful carbide formation affecting to the performance of the material. Due to carbides, brittle martensite may appear in the material. [3] Two methods in the quenching are used to harden the component. First one is direct quenching and the second one is reaustenising and then quenching. The more highly alloyed the steel is, the more reheating treatments are required. Reheating is used for carburized steel unless it is known to resist excessive grain growth. Controversy can be seen when asked about reheating: "Is the reheating actually necessary or would it be more beneficial to directly quench the material?". One benefit from reheating treatment is that the amount of retained austenite is reduced in reheated microstructure. However, there are controversial opinions about the effect that retained austenite has on the performance, only certainty is that it is not always catastrophic. One challenge of reheating is the chance for greater distortion. During quenching high stresses are developed, so tempering is considered most of the times as a necessary procedure after case hardening. Conditions for tempering (temperature and time) are depended on residual stress, hardness, toughness, strength and retained austenite. Typical example hardness values for case hardened, carburized and tempered steels are 57-62 Rockwell C hardness (HRC) (case) and 25-42 (core). [2]

Macherauch and Vöhringer have stated [2] that "hardening residual stress state" is the result of austenized steel parts rapidly quenched to room temperature. This state can't be illustrated with thermal and transformation stress superpositions. They stated that during quenching, volume increase happens together with martensitic local transformation shifting of the existing stresses to more negative magnitudes. Meaning that transformation occuring in tensile regions reduces the stresses while transformations on compressive regions enhances the stresses. During cooling, core and surface shrinking stresses change their signs. This means that the relative position (both in the core and surface) of the initiation time of transformation is important for the hardening residual stresses remain after cooling. [2]

Figure 1. presents a typical diagram of residual stress profile for carburized and hardened steels [2]. From the Figure 1. it can be seen that when the distance from the surface increases the carbon content and the amount of retained austenite decreases. In the last

diagram as the distance increases, the compressive residual stress decreases and eventually the stress becomes tensile. That happens by the ending of the carburized layer since the material is softer under the case depth of carburized sample. The ratio of the core and case thickness affects to the compressive residual stress magnitude on the surface. Case thickness is the distance from the surface to the point where the hardness of 550 Vickers hardness (HV) is located. High compressive residual stress on the surface is achieved when the thickness of the core is greater than the case. Core tensile residual stress is high and surface compressive residual stress is low when it's the opposite way. Using this as a reference and calculating the effect of retained austenite, residual stress level increases when case hardening depth increases. [2]

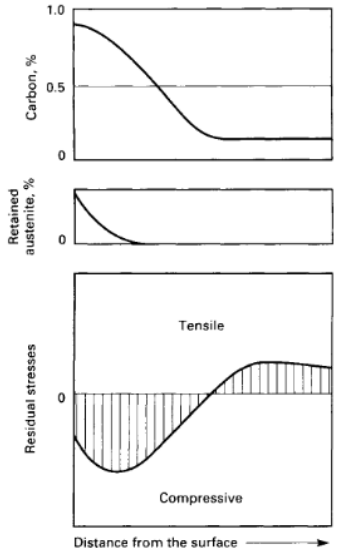

Figure 1. *Typical residual profile for carburized and hardened steels. Showcasing carbon and retained austenite content followed by residual stress as a function of depth. [2]*

Better consistence can be achieved for deformation of carburized samples if the carbon potential is controlled carefully and more accurately. Concerning heat treatment, the distortion, is most likely generated in quenching. Intensity of the cooling process has an increasing effect on the distortion. The distortion increases also when uneven hardening happens with the occurrence of soft spots. In steel transformation during heat treating, the present microstructures control the properties like hardness, strength and toughness. The process starts with heating the steel to the austenitizing temperature and then, to avoid pearlite, cooling the component rapidly to maximize martensite formation. With this process, the as-quenched hardness is formed for the steel component. For the quenched-hardenable steels most common transformation products that can be formed are: ferrite, martensite, pearlite, bainite and cementite. Proportions and formation for

each microstructure phase is dependent on alloy's elemental composition and cooling history (including time and temperature). [2]

The surface conditions effects in quench cooling process are important since the conditions can vary. The variations can be for example due to surface roughness, contamination, oxidation or coatings. Surface texture and roughness, while these affect to cooling characteristics of quenching, also affect to the stress and distortion values. Surface roughness can increasingly affect to the tendency of the quench cracking if roughness is higher than 1 µm. Odds of quench cracking occurance are increased if the texture (lapping) of the surface and the roughness stays similar. This means higher occurrence of quench cracks compared to grinding. [2] Usually tempering is carried out after carburizing. Tempering can't change the inner stress induced plastic distortion. The main decider for distortion is the quenching process in the quench-temper process. Tempering process involves heating in this case hardened steel under the eutectoid temperature to increase the toughness and reduce the hardness. Tempering is considered as a four stage process. These stages include the following actions. Martensite structure is tempered and retained austenite is transformed to martensite. The martensites decomposition products are tempered above 480 ºC and decomposing the retained austenite to martensite is done. [2]

Decarburization

Decarburization is a carbon removal process for steels. It is a serious problem for steel components, lowering the wear resistance and allowing the fatique failures to occur easier [4]. Process itself is done similar fashion than carburizing. Before decarburizing it is essential to identify the amount of excess carbon in order to control the process so that no excess decarburization occur. In order to guarantee fixed removal of carbon the gas furnace is used with oxidizing atmosphere above 900 ºC. Mostly unwanted since the removal of the carbon content from the steel surface makes the surface softer and ductile which rarely is wanted. This can be used when the carbon content in the surface has exceeded the wanted amount and is needed to lower back to the desired level. Decarburization can be caused for example by other heat treatments and poorly controlled carburizing process. High carbon skin can be caused by using carburized salt bath instead of neutral. Also high carbon gaseous atmosphere can cause this in furnaces (gas or electric). The process is unusual and requires capable team and equipment. [5]

Retained austenite

When the rapid cooling from the austenitizing temperature quenching is occurring, some of the austenite doesn't transform to martensite and this non-transforming austenite is called retained austenite. This is due to the unfinished martensite transformation when the structural transformation of the austenite to martensite is prevented by small volumes of the stress field of the nearby martensite needles. [6] The retained austenite can be considered as a possible surface layer which is consequence of carburizing process and affects to the surface layer properties by lowering its hardness. When the carburizing takes more time and is therefore elongated due to the need of deeper case depth, high surface carbon content is produced by the carbon potential. This possibly results as an excessive amount of retained austenite. [3]

2.2 Case depth

Case hardening is thermal treatment that produces wear resistant and hard layer while leaving the core ductile and soft. Process controlling of case hardening is critical in order to produce components performing in the intended use with correct case depths. Measuring the depth can be used as determination method for the performance of the material to see if the manufactured component performs as designed. Case depth can be divided to total and effective case depth. [7] Case depth is measured using standardized case hardening depth (CHD) [57] measurement procedure, in this thesis HV1 (Vickers hardness 1) testing method was used [8].

Total case depth

Total case depth is the distance of the carbon diffused from the surface towards the center of the sample. The distance can be seen with microscope from the perpendicular cut of the surface. The case starts from the surface and ends at the point where the core material and outer case layers can't be visually separated. Measuring of total case depth is specified mainly on parts with a requirement of thinner case. Measuring is done visually from the cross section (sample is cut from the surface to perpendicular direction) using etchant to create contrast. From the contrast case and core can be differentiated. [7] In this work the total case depth is observed from the hardness depth profiles from the point where the hardness value hardly changes anymore. This is visualized in Figure 2.

Effective case depth

Effective case depth is specified distance from the surface until the standard mentioned hardness level is crossed. In this case for carburized samples 550 HV is used according to standard ISO 18203:2016 [57] (to calculate the case hardening depth). This is meant to measure the depth of the effective case depth, since defining it is required in critical usage conditions. The effective case depth measurement is done by using microhardness testing methods, meaning creation of dents to the cross section to the standard specified hardness. When the hardness level has been reached, the distance (effective case depth), is measured. [7] This is visualized in Figure 2.

Since the HV1 was the used testing method, 550 HV is the hardness limit (HL) that is used as the effective case depth for the carburized sample material used in the experiments.

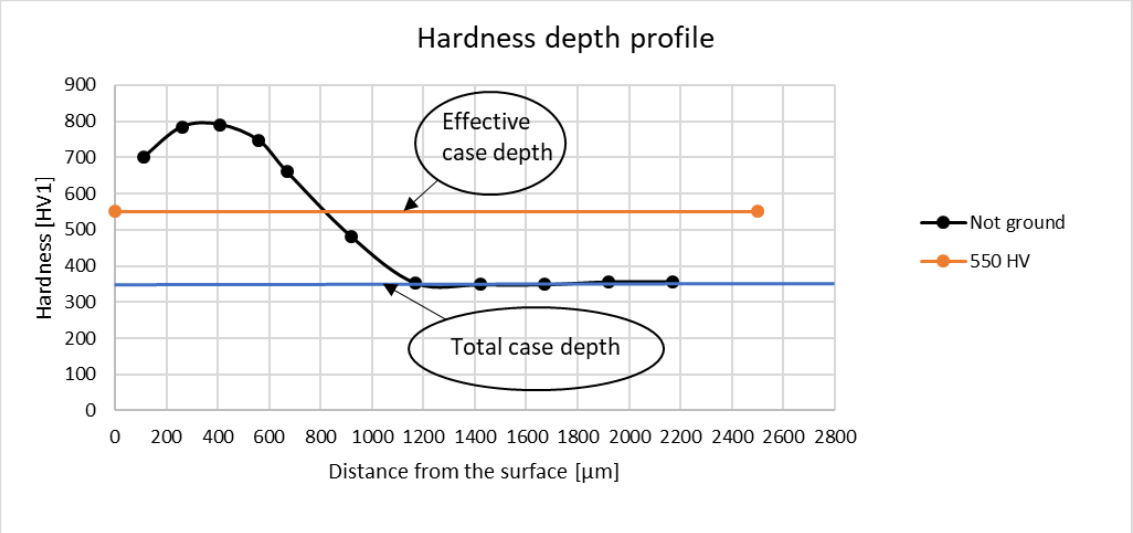

Figure 2. *The total and effective case depth demonstrated.*

2.3 Grinding

Case hardening is done to provide the component with a hard surface and tough core which is quite commonly required in critical component production [6]. Grinding can be considered as the final step of the manufacturing process where the dimensional tolerances and surface finish are determined [9]. When grinding has been performed well, compressive stress state is achieved with better surface integrity and surface tolerances. Thus, enhancing the properties of the component to be suited for the task required to perform through its lifecycle. [6, 10]

Grinding can also be considered as a machining method that forms chips. Temperature increase and plastic deformation are the results of the cutting energy. Three factors can be isolated as the possible cause of residual stress generation in the ground surface: plastic deformation, temperature increase and rapid heating and cooling cycle. The total sum of the residual stresses is balance between these three factors. [2]

Grinding can induce either compressive or tensile residual stress to the sample in grinding. Depending on multiple factors the stress type and value can be calculated. In grinding, the main problems are generated through high temperatures that occur in workpiece and grinding wheel contact [11]. The contact of the grinding wheel and the workpiece is presented in the Figure 3. [12]

Figure 3. presents the transfer paths that the heat generated in the contact zone mainly transmits. The heat flux entering to the workpiece is marked as q_w, heat flux entering to the chip as q_{ch}, heat flux entering to the grinding wheel as q_s and heat flux entering to the coolant as q_f. Total heat flux can be calculated when all of these values are added together. The unit for heat flux is W/mm^2. The wheel speed is marked as v_s and workpiece speed is v_w. [12] Wheel speed is the speed of the grinding wheel, also known and referred later on as grinding speed [13] and cutting speed [14]. Workpiece speed is the speed that ground component moves, also known and referred as table speed and work speed [15]. Work speed is also known as feed rate while infeed can be considered as depth of cut [14].

During grinding residual stresses develop to the ground sample surface layer [10]. Due to the increase of specific energy and too high increase in grinding zone temperature thermal damage can occur. Due to this compressive residual stresses in the surface may transform to tensile residual stresses and a change of the surface hardness due to microstructure changes may occur. In order to monitor produced components efficiently (at the rate of production) in case of a thermal damage, non-destructive testing methods are used to detect thermal damage during production. [9]

There are great variety of grinding wheel materials and parameters related to grinding. The parameters may influence in different ways for the formation of thermal damages. The following chapters immerse to this topic through the samples provided for this thesis.

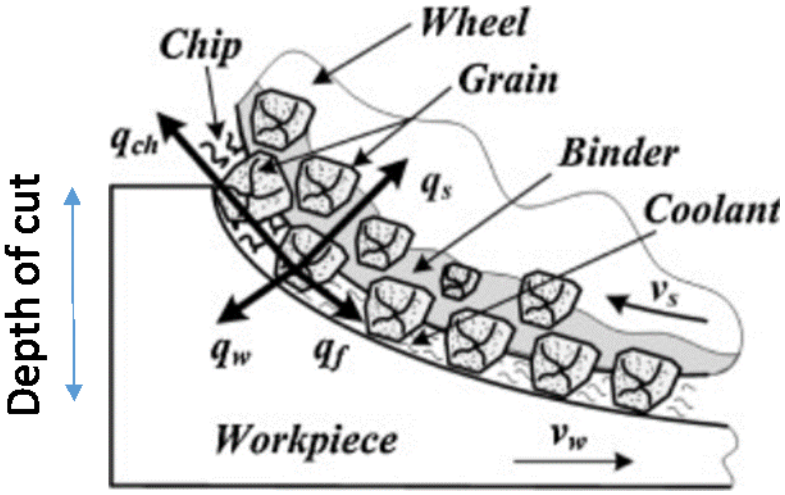

Figure 3. *Grinding wheel – workpiece contact during grinding. [12]*

2.3.1 Variables in grinding

There are different kinds of grinding wheels to choose from and grinding wheels can simply be divided into superabrasives and conventional abrasives. These are divided into different categories based on the hardness that is usually referred as Knoop hardness (kg/cm^3). In the Table 1. the Knoop hardness values are introduced for the grinding wheels that are used for the sample batches in the thesis. Superabrasive cubic boron nitride (CBN) and conventional abrasive aluminium oxide (Al_2O_3) are two the selected wheel types that will be used in this thesis and discussed. There are still few different abrasives that can be included between these two categories, as sintered ceramic abrasives and sintered aluminum oxide abrasives. [16]

Table 1. *Knoop hardness values for the grinding wheels used. [16]*

Knoop hardness	**Kg/cm^3**
CBN	4500
Al_2O_3	1370-2260

Hardness is the most important attribute of the abrasives and the classification to these different categories is done based on that parameter. Friability is another quality that determines in which kind of situations the abrasive is best to be used. Friability means the grains tendency to fracture under pressure. The higher the friability the better it suits to be used for low grinding forces. [16] Friability is usually higher in harder abrasives meaning that harder abrasives are suitable for precision-grinding and larger, tougher

abrasives suit better for heavy-duty grinding [17]. Due to the fact that fracture produces new, sharp edges it can be seen as an advantage as it maintains sharpness of the wheel. Important qualities for abrasive grains are wear resistance and grinding temperatures. Purity of the abrasive has significant effect on its conductivity. Wear resistance of the abrasive depends from hardness of the abrasive at high contact pressure, affecting parameters like hardness and chemical composition of the work material. The chemical composition of the ground material determines the abrasive based on the suitability for the chemical composition. [16]

2.3.2 CBN grinding wheel

CBN is commonly used superabrasive, the hardest after diamond. CBN has low wear rate and it can hold close size tolerances for the parts produced. It is thermally stable up to 1500 ºC. CBN's wear rate increases if water-based fluids are used. [16] CBN wheels are industrially considered attractive and longer term options for grinding due to low cost/ground workpiece, reduced thermal damage, high reliability and productivity. The sample finish is also great and machining induced compressive residual stresses are increased. CBN reaches its end of life when grits wear to pretermined level. [18] It is stated that thermal damage is less likely to happen with CBN than with aluminium oxide wheel and produced residual stresses are compressive. This means that with CBN, temperatures at the surface should stay lower. Due to high thermal conductivity more of the grinding heat transports to the grains instead of the sample. CBN has roughly 35x better thermal conductivity than aluminium oxide. Additional factor also could be the grinding fluid that is used. Most of the CBN wheels that are used are vitrified and electroplated CBN wheels. In vitrified CBN, cooling with the fluid in the grinding zone is provided due to the structural porosity. [19]

Thermal conductivity is the reason why, for example, CBN has low energy partition. Thermal conductivity guides the evolved grinding heat to grains instead of to the workpiece. It can be said that the higher thermal conductivity will provide enhanced heat removal during grinding as a sort of cooling fluid due to the enhanced heat removal. [19] CBN is brittle material but the six cleavage planes in the structure gives better breakdown control to CBN grains. Due to it's characteristics CBN is less tough than diamond and has lower hardness as well. These properties open the possibility for CBN being suitable to be dressed with diamond rotary tools. CBN grinding wheels can be further divided into vitrified and electroplated wheels. [14, 20]

Vitrified wheels

Vitrified bonds are assembled from set of glasses. These glasses are formed from clays, low-melting point mineral siliceous clay and chemical siliceous clay with pre-ground glass that oxide content has pre-determined. This mix is then placed in high temperature to go through vitrification heat process in order to merge the constituents together. [21] Vitrified bonds are unaffected by temperatures (heat, cold) and are made in wider range of hardness compared to other bonds. Vitrified bonds can also withstand acids, oils and water. Bonding adapts to all kind of grinding with the exception of the situations where the wheel is too thin, preventing the wheel to endure the side pressures. The porous structure combined with strength enables the grinding wheel to shine in operations demanding high stock removal. High elasticity modulus means that vitrified wheels are suitable for precision grinding as well. Due to the level of porosity, it is possible to tailor the bond structure in order to regularise continuous and self-sharpening grinding. [20, 22]

Mechanical strength compared to conventional grinding wheels with same grain size is higher for vitrified bonded abrasives due to lower wear rate and importance of not breaking grains away off the bond. [23]

Electroplated wheels

Electroplated wheel production starts with the precion work of producing wheel blank with surface hardening treatment. Then the grit material is applied using nickel electroplating methods to attach the grit material to unmasked areas. Nickel bonds the grit and the wheel blank. [24]

Electroplated wheels have some advantages over other grinding wheels, for example, running ability for high speeds and removal rates. In addition, wheels don't need dressing or truing. As showed in the Figure 4. the wheel consists of electroplated nickel layer that bonds the single layer of abrasives to the steel core. The lifecycle depends on the single abrasive layer. [25]

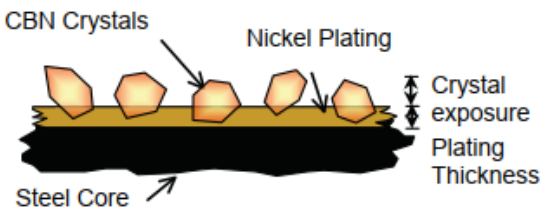

Figure 4. *Cross-section of an electroplated CBN wheel. [25]*

2.3.3 Al_2O_3 grinding wheel

Aluminium oxide (synthetic or natural = corundum [17]) wheel is used to grind for example ferrous materials (steel). Grains can be either blocky or sharp and this depends on the purity and preparation of the abrasives. Blocky grains are used for heavy stock removal due to high impact resistance. Micro-fracturing grains are more durable due to fact that the grains are kept sharp while minimizing both forces on the grains and grain's volume fracture lost. Heavy removal rates are needed when dealing with very tough grains and promoting micro-fractures. [16]

The crystal structure of the Al_2O_3 is hexagonal with a hard aluminium oxide phase of α-alumina. Large scale of variation in the Knoop hardness is determined by the hexagonal crystal structure, depending on purity and degree of crystallization. Synthetic aluminium oxides contain metallic oxides which can be found as impurities or purposefully added. Depending on the structure and chemical composition, the hardness value varies. These differences in structure and composition can be explained with different manufacturing methods. [17]

2.3.4 Comparison of CBN and Al_2O_3 grinding wheels

The samples that are being studied and measured in this thesis (20MnCrS5 steel) are ground with commonly utilized Aluminium oxide and CBN abrasives that were chosen due to their thermo-chemical stability. The thesis compares the achieved results of these wheels to determine the performance of the wheels for the grinding process. When energy partition is taken into account, CBN is clearly ahead. Energy partition of CBN is around 20% or a bit under while aluminium oxide has a lot higher energy partition of 60-70%. This means that CBN has significantly better thermal conductivity ranging from 240-1300 W/(m•K) compared to Al_2O_3 35 W/(m•K) [10], thus thermal damage is less likely to happen due to the lower grinding temperatures. With CBN, lower temperatures are achieved because of better energy partition, meaning less grinding heat enters to the workpiece. By comparing hardness of these materials one can see that CBN abrasives are two times harder than aluminium oxide. CBN abrasives have also better wear resistance which means that CBN abrasives have longer service life. Generally Aluminium oxide wheel is used in 120 m/s or slower wheel speeds and CBN is used in higher wheel speeds. [10]

Compared to Al_2O_3, atleast in theory, CBN could offer better surface quality, reduce the machining costs, hold the size better and increase the productivity. Due to hardness and

significantly higher thermal conductivity, CBN produces mechanically induced residual stresses with minimal thermally induced residual stress because of the low amount of heat involved. There are also studies where similar conditions using both wheels have created opposite residual stresses, CBN has produced compressive residual stress while Al_2O_3 produced tensile residual stress. [10]

2.4 Grinding induced surface layer transformations

Grinding induces surface layer transformations, affecting to the residual stress distribution and that way to other characteristics and parameters. In this chapter the factors affecting to the residual stress are introduced with a way to measure residual stresses.

2.4.1 Residual stress

Residual stresses are very important factor influencing the surface integrity of the ground sample. It is impossible to avoid residual stresses to generate. The residual stresses can be either positively or negatively affecting to the material, depending factors like stress distribution and magnitude. If residual stresses are not distributed properly in the sample, it can have huge effect on the sample's service life as well as its reliability in use. Normally residual stresses originate from mechanical processes where heat is involved. [10, 26]

Important parameters for mathematical model of stress creation are: cutting speed, depth of cut, feed rate, cutting forces (result of feed rate and depth of cut), samples mechanical properties and heat conductivity of the sample and grinding wheel. [2]

The goal is to produce carburized cases with tempered martensite and a bit of distributed, stabilized austenite. Gormley divides [2] grinding induced residual stresses into three types. Type I: holds abusive grinding possibly inducing crack or burn. Type II: generated heat has produced a tensile peak, though close to surface plastic deformation has slightly restored the balance. Type III: good grinding technique has been used and heat generation has been controlled well enough so that only surface work hardening is allowed to occur. This will also improve fatique resistance. Overall the most influential factor controlling residual stress is heat treating. [2]

The grinding related parameters affecting to the residual stress are introduced in the Table 2. The residual stresses are further explained throughout the chapters 2.4.1, 3 and 4. Since similar parameters are related for these topics to avoid repeating the same information.

Table 2. *Grinding related factors that affect to the residual stress values.*

Residual stress
grinding related factors
abrasive distribution [10]
porosity [10, 40]
dressing [10]
grinding speed [13]
wheel speed (cutting speed) [14]
work speed [14]
infeed [14]
wheel wear rate [41]
grade of hardness [43]

Grinding-induced residual stresses can be divided primarily to three different causes: localized thermal expansion/contraction (while grinding), plastic deformation (abrasive grinding wheel) and localized phase transformation-induced volume change. First two of these are the most common causes. Residual stresses are self-balancing stresses when all external factors and stimuli aren't affecting to the component. [10]

Grinding-induced residual stresses affect to the fatigue strength, service life and corrosion resistance. Thermally induced plastic deformation is responsible for forming tensile residual stresses to the ground sample. Surface residual stresses form in a way that the grinding direction has the least compressive stress which can be seen from the tests done for the samples regarding of this thesis. [10] This is also backed up by literature. For example, in the study by Shouguo et al. [27] the compressive residual stress were pointing out that the lowest compressive stress was in the direction of grinding. This is due to the mechanical effects that play major role in the formation of grinding-induced residual stresses since the grinding temperature stayed under 90ºC. In Figure 5. the grinding direction is marked with blue and perpendicular direction is marked with red. v_s is the wheel speed, v_w is the workpiece speed and a_p is the grinding depth. [27]

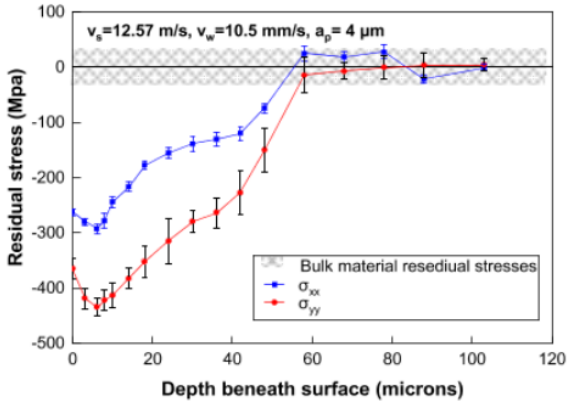

Figure 5. *Compressive stress distribution to the grinding (σ_{xx}) and perpendicular direction (σ_{yy}). [27]*

Typically in the mechanical abrasion, meaning plastic deformation to the material, surface residual stresses appear to be compressive. When thermally induced plastic deformation occurs, the residual stresses appear to be tensile on the surface of the ground sample. Depending on the density of the transformed phase compared to the original material, the residual stress varies. If the density is higher than the original, the residual stress is going to be tensile. This can be explained by the fact that on the subsurface new material retains its volume and on the surface it has tendency to shrink. On the other case, when the density is lower, the residual stress is compressive, due to the constriction of the original material for the new materials expansion. [10]

Mechanical interactions between abrasive grains and component are mainly caused through localized plastic flow, resulting mostly as compressive residual stresses. Tensile residual stress is caused by thermal-inducing phenomena due to grinding temperature and its gradient. Tensile residual stress comes to existence when thermally hotter material expands and is constrained due to the cooler subsurface material. This initiates compressive thermal stresses near the surface causing plastic flow in compression, assuming that the stresses are high enough. After grinding, subsequent cooling starts and development of tensile residual stresses begins. This initiates compressive residual stresses to develop deeper into the material in order to keep mechanical equilibrium. Magnitude of the compressive stresses is minor compared to tensile stresses. Compressive stresses are wanted and have favorable effect on the mechanical properties, while tensile stresses are unwanted and can have severe consequences for the material. If the grinding is abusive enough, most likely the possible cracks are induced to normal of the direction of grinding. To get the compressive residual stresses instead of unwanted tensile residual stresses, low removal rates needs to be used unless the grinding wheel

used is CBN. CBN grinding wheels have high thermal conductivity that lowers the energy partition to the ground piece. [19]

Tensile stresses can be avoided with low-temperature grinding under transition temperature through the grinding cycle. Tensile stresses occur while sample is contracted. Grind hardening happens when new material is formed. As said, transformation with volume reduction creates tensile stress. Quenching can be used as a way of creating compressive stress. In grind hardening, martensite is formed from what used to be ferrite and pearlite, the volume increases, thus creating compressive stress. [28] Increased temperature causes expansion constraint by bulk material. If the yield strength is surpassed by thermal stresses, the surface will be upset and tensile residual stresses will occur while subsequent cooling. Rapid heating and cooling cycle can induce formation of martensite in hardenable steels, creating compressive residual stress. Plastic deformation creates compressive residual stress if the smearing of the material is involved in the direction to the plane of the surface. [2]

Stress types

Stress types can be divided into residual and applied stresses. External force results as applied stress that manipulates direction and magnitude of magnetic easy axis. Nonuniform plastic deformation is behind the rise of residual stress which remains after the external force is removed. Residual stresses can be further divided into compressive and tensile stresses but also to macro- and microstresses. Macrostresses can be either introduced during mechanical processes or form locally around defects. Scale of the stress is sample scale. Microstresses form due to nonuniform deformation. Scale of microstresses is grains diameter. If the stresses exceed yield strength then plastic deformation happens, otherwise it is elastic deformation. Strain, ratio of variation of length to starting length, is used as a measurement scale for the amount of deformation. In elastic deformation the distance of consecutive atomic planes increases. After the applied stress is removed, the change is reversible and returns back to the state it was before stresses were introduced. In plastic deformation due to movement of dislocations atomic planes slip, permanent deformation happens that stays after the applied stress is removed. [29]

Measurement of residual stress with X-ray diffraction

Measurement of residual stresses is important in order to avoid the detrimental and unwanted effects of tensile residual stresses by controlling and measuring the residual stresses [26]. Measurement of residual stresses can be done using different methods. One way to determine these stresses is to measure the elastic strain [2].

Residual stresses are determined through measuring the elastic strain. The residual stresses can be calculated from the elastic strain results. The strain change is caused by removal of the material from the sample's surface. Elastic strain occurs, when there is mechanical force involved and the stress produced by the mechanical force is less than the yield strength. The elastic strain change is calculated and from these results the residual stress can be calculated. X-ray diffraction (XRD) measures the crystal dimension from the atomic lattice dimension that can be then related to the magnitude and direction of the stress (which can be applied or residual). XRD relies on the spacing changes of atomic planes in metallic structures due to elastic strains. XRD measures interplanar atomic spacing to calculate the total stress that is in the sample. [2] Residual stress alterations can be examined from the surface of the material as the grinding process may generate the mechanical force, thermal stresses and phase transformations. With XRD, estimation of the grinding burn status can be made. [30]

Microstresses are interesting error inducing source. Across single metal grain there is strain variation that is detected by XRD, effecting to the X-ray peak by broadening it. This broadening phenomena is completely different than the peak shifting that happens due to residual stresses. In XRD measurements more important than sharp resolution is the ability to measure repeatedly the position of the diffracted X-ray peak. [2]

Full width at half maximum (FWHM) is a measurement for the width of the diffraction peak used to illustrate plastic deformation, hardness, and microstresses. For the FWHM it is common that the value increases when the hardness increases. Visual example of FWHM calculation is illustrated in Figure 6. [31]

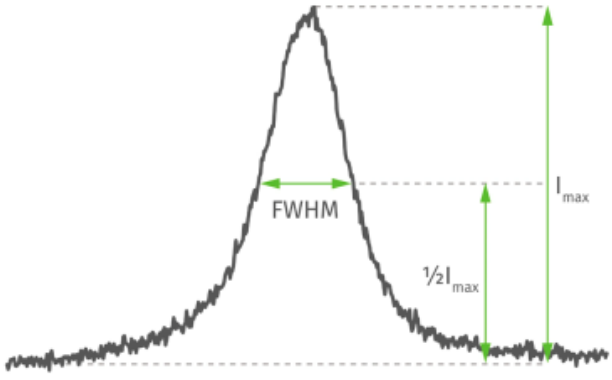

Figure 6. *Example of diffraction peak and defining of FWHM. [31]*

Residual stress in carburized steels

In Figure 7. can be seen typical diagrams for case-hardened steels. Longitudinal residual stress, carbon content and distribution of hardness are presented in the Figure 7. [2]

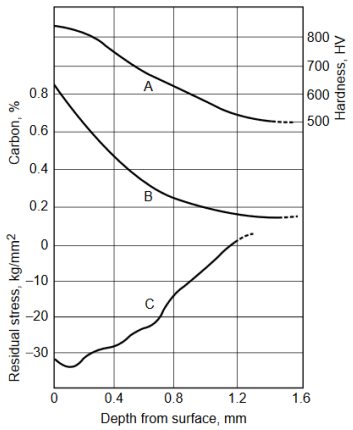

Figure 7. *Typical diagram for case-hardened steels. A= distribution of hardness, B= carbon content and C= longitudinal residual stress. [2]*

Analysis of residual stresses is a demanding task even though methods have been developing since the 30's. This is due to physical-mechanical processes which impact both mechanical and heat stresses with structural changes. Residual stresses can be divided into macrostresses and microstresses. Microstresses can be found in crystalline grain while macrostresses are microstresses on finite base. Residual macrostresses are calculated by measuring metal grain lattices atomic plane distance changes. Macrostresses vary continuously over the body in order of dimensions while microstresses in microstructural elements show up with variating patterns and magnitudes. External forces are the core reason for creating these stresses. [2]

2.4.2 Grinding burn

Grinding process demands high amount of energy to remove material and all of this energy is considered to be dissipated into the grinding zone. This is the area where grinding wheel interacts with the sample. These high temperatures may lead to thermal damage known as grinding burn. There are different kind of possibilities how this thermal damage can effect to the sample, for example burning, tempering, rehardening, formation of tensile residual stresses or cracks. [19]

Grinding burn is a thermally induced damage on the material surface that can be produced during grinding. Examples of the reasons why the grinding burn can happen are grinding wheel wear (rate), too high work speed and poor dressing. [6, 10, 14, 30] When the grinding wheel goes through enough consecutive grinding cycles and ultimately wears, transformation of grain geometry may eventually elevate the heat content [6]. High work speed can in some situations lead to higher risk of grinding burn, due to increase of grinding force and temperature [14]. The first grinding pass could occur such way that the grinding in higher end of tolerance parts of the workpiece is aggressive and can result as a grinding burn [32]. Poor dressing increases the temperature in the grinding wheel-workpiece contact area exposing the material to grinding burns [10]. Grinding burns are produced due to high temperatures that go higher than the tempering or austenitizing temperature of the material that is ground. This may induce microstructural changes and reduction in compressive residual stresses that were gained from the heat treatments. This will affect to the ground material's wear and fatigue performance. For the residual stresses that occur after grinding process the reason could be either thermal phase transformations or plastic, thermal and mechanical deformation as cooperative action. [11]

Grinding force and temperature are related with surface integrity. Grinding force can cause surface hardening and compressive residual stress while being able to plastically deform metal. Grinding temperature can change metallurgical structure of the material, cause tensile residual stress and grinding burn while enabling cracks on the materials surface. Primary reason for tensile stresses are thermal stresses. [12] Elevated temperature in grinding zone is due to the fact that majority of the grinding energy converts to heat. The temperature rise under grinding stresses accelerates the wear and thermal damage in both, grinding wheel and ground sample. [33] Local overheating causes local changes in microstructure during mechanical processing. Tempered martensite is produced in tempered zones as visualized in figure 8 a). [34] When temperature is between austenization and normal tempering range, by applying slow quenching, over-tempered martensite forms. Retempering burn creates tensile stress and lowers the hardness on the surface. [35] Temper damage requires temperatures to increase above tempering temperature to appear. Softening and reduce of wear resistance are consequences of this type of thermal damage. [28]

In the rehardened zones quenched martensite and retained austenite are produced with higher hardness and tensile or compressive residual stress. This is usually surrounded by the tempered zones. Example of this is shown in Figure 8 b). [34] When temperature is over austenization temperature, untempered martensite (UTM) forms on the surface

of the material when rapid quenching is applied. This outer layer is harder and prone to corrosion than deeper in the workpiece. This changes the integrity of the surface and is known as rehardening burn. [35]

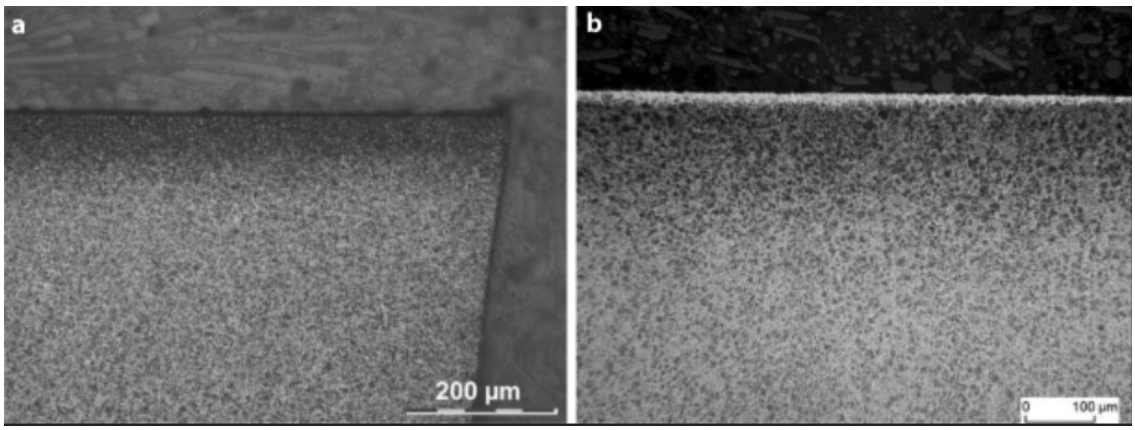

Figure 8. *Image of a) tempered zone and b) rehardened zone. [34]*

Rehardening damage appears when the grinding temperature goes over 850 ºC. Hard and brittle martensitic white layer forms to the surface of the material. This layer is still wear resistant though the fatigue experienced in service breaks the hard particles from the surface causing direct damage while maintaining the possibility for further damage in the form of cutting by the wear particles. Under the surface layer, a softened layer is produced due to lower rise of temperature. Under this softened layer material structure was not affected by the temperature. This is shown in Figure 9. [28]

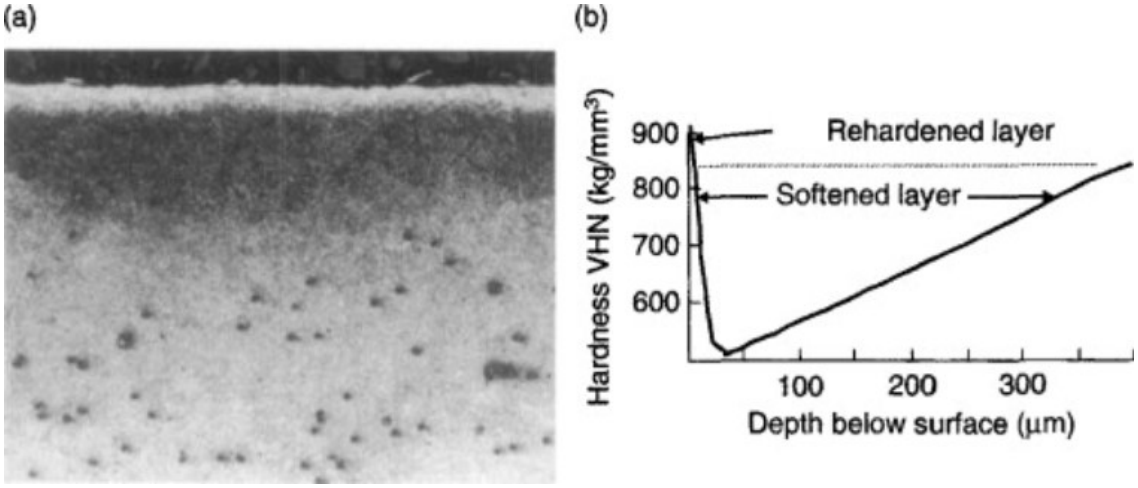

Figure 9. *(a) Presents the rehardening damage, hard and brittle layer in the surface (white), softened layer in the middle (darker) and the unaffected area below softened layer. (b) The rehardening damage with the variations in hardness values. [28]*

Tempering (softening) is a transformation of hardened steel that can occur due to temperature increase above tempering temperature during grinding. Tempering happens due to carbon diffusion that is dependent from time and temperature. It occurs near the surface of the workpiece. [19] Tempering process of the quenched steel goes as follows; During tempering, there are factors that can cause volume change. Contraction is created when carbide separates from the martensite and the α-phases concentration in carbon decreases, while expansion is caused by the transferring of the retained austenite. Typically this leads to decreased volume due to the fact that contraction has more dominant role. [2]

Same thing as tempering, rehardening is a transformation of hardened steel due to unreasonable high temperatures during grinding which leads to brittle martensite. This requires high temperature and long enough time so that reaustenization can happen. Rehardening decreases probability of tempering which means that the materials hardness has increased. The larger the grinding depth, less tensile proportion there is on the finished sample surface. [19]

Thermally induced residual stresses are expected only at low specific grinding powers. When mechanical loads are the reason for the workpieces surface plastic deformation, the compressive stresses spike up. When the specific grinding power is increased, mechanical loads reduces and thermal load increases with the temperature in wheel-workpiece contact. [10] Mechanical force mainly produces compressive residual stress which is wanted property in most of the cases. High thermal output mainly produces tensile residual stress which is unwanted property and considered harmful. [19] State of stress below the surface depends on the grinding parameters. With higher grinding speed, subsurface layer obtains better consistency of residual stresses while lowering the grinding depth, leading to better finish that can be obtained on the surface of the material. Cutting and tool geometry parameters can significantly generate compressive stresses with chamfer or tool round. [13]

2.5 Inspection methods for grinding burn detection

In order to grind material away, high input of energy is required. Almost all of the generated energy converts to heat in the grinding zone. This increase of temperature can cause thermal damage to the ground workpiece which can occur as grinding burn, tempering, rehardening, unwanted residual stresses and/or phase transformations. [17] Since the thermal damage can be detrimental to workpiece, it is important to use quality control after grinding processes and inspect the products. During this chapter, few of the

most common inspection and quality control methods are introduced. These methods are commonly used to inspect the material residual stresses and possible grinding burns. The most commonly used is Nital etching. This is influenced by the fact that the method is standardized. For example bigger industrial companies require that the testing method used is Nital etching due to standards. As a backup so to say, relying method that is standardized and taking no risks with unfamiliar method. So after short introduction, couple of the methods are showcased how inspection and quality control is implemented in real situations.

2.5.1 Nital etching

Nital etching (or surface tempered etching [34]) is a destructive testing method that is most commonly used method of grinding burn detection at the moment. Basic idea behind Nital etching is that the steel has different sensitivities to the etchant due to various microstructures and hardness. This leads to different colors present on the surface of the sample. Depending what colors are present, the grinding burn can be determined by visually investigating the surface. Tempering grinding burn can be seen as black color, due to sorbite microstructure which is responsible of the color change. With quenching burn, microstructure is mostly martensite with a smaller amount of other structures as well, this can be seen as white with black outer coloring. Due to standards that regulate the classification based on coloring, darker color means serious grinding burn while lighter color indicates minor burn. [29,34]

The need to find other methods to replace Nital etching can be seen by its challenges. The method is difficult to post handle and automate. The component inspected with Nital etching requires determination if the etched samples are usable and nevertheless, Nital etching does not work for new steel alloys. One of the reasons that Nital etching is popular is the fact it is a standardized method. [30]

This was taken from a theory based source, published earlier this year. Despite the claims that Nital etched inspected parts are not usable after the inspection doesn’t ably in industrial scene. The discussions during visits in different companies that regularly used etching as their quality inspection method stated differing answers. From destroying the components (usable or not) etched to using them without any treatment after etching (if no defects were found). Using the components that had no defects afterwards was actually quite popular opinion. These opinions were based on the facts that the method is standardized and the material removal is insignificant. [32]

2.5.2 Acoustic emission

Acoustic emission (AE) is produced by rapid release of strain energy starting the irreversible changes that cause the transient elastic waves within the material. Commonly AE is used under mechanical loading so it suits for grinding monitoring. Sensors are mounted to the surface of the component to document the propagation of the transient elastic waves. To detect grinding burns, signals are taken prior and after the grinding to see the contrast between the characteristics. The changes can be used to predict and prevent the grinding burns. More often multi-sensor signal system is used to detect grinding burns due to the influence of grinding parameters to the AE results. Root-mean-square of Barkhausen noise voltage signal (RMS), peak of FFT (fast Fourier transform) and deviation of AE signal's are magnetoelastic parameters used with AE to detect grinding burns. Signal processing has taken into account processing methods like wavelet analysis and wavelet packet analysis concerning time and frequency domain. This is done due to AE signals nonlinear time-varying characteristics. Wavelet transform is frequency analysing method that has the ability in time and frequency domains to denote local signal characteristics. Due to these abilities AE can provide a representation of grinding burn. [30]

AE is a good way of monitoring and identifying the appearance of grinding burns. AE sensors offer unique advantages like easy installation, high sensitivity and abilities to cancel out the interfering signals to get detection from small signals as well. Having said that, pinpointing grinding burns is challenging when there are many signal sources which create noise, making the detection of grinding burns challenging due to the difficulty of separating the signals. [30]

2.5.3 XRD for residual stress measurements

At the moment XRD is the most commonly used NDT method for testing residual stresses. XRD can be used for crystalline materials as a residual stress measuring tool, detecting material failure, verifying calculations and controlling the quality. [30]

When the metal is either under residual stresses or applied stresses the appearing elastic strain causes changes in the spacing of the atomic planes in the crystal structure. Meaning that XRD is capable of determining inter-planar atomic spacing. Study by Song et al. presents [30] residual stress distributions of the teeth surfaces that were compared with the respect to distance from the surface with and without grinding burn in the axial

and radial directions. XRD measurements were done to examine the stress variations of the subsurface and longitudinal surface near the produced grinding burn. [30]

Advantages using XRD as residual stress measuring device are accuracy and extensive analysis. On the other hand limiting factors are cost, complex operations, penetration distance in metals and geometry of the sample. For the measurements sample surface needs to have space for collimator, and this limits the use in production purposes. [30]

2.5.4 Eddy current

Eddy current is one electromagnetic method that is used for conductive materials to detect and characterize defects on the surface and near surface. The structure and stress state affects to the magnetic permeability and electrical conductivity. With ferromagnetic materials the effect of magnetic permeability is significantly higher than the electrical conductivity. Grinding burn is responsible for the increase of magnetic permeability while also being responsible of stress state and structural changes in ferromagnetic materials. [30]

The principle of eddy current testing (ECT) with ferromagnetic materials is as follows: coil with alternating current moves closer to the ferromagnetic material. Eddy current is produced on the surface by the alternating magnetic field. With the coil's magnetic field, alternating eddy current produces magnetic field that is then coupled due to mutual inductance. This induced eddy current is affected by defects in its amplitude and phase. These changes alter the magnetic coupling that is then detected in the coil impedance. [30]

ECT detection method for electrically conductive materials offers advantages like low cost, short measurement times and contact free testing. Limiting factors are low sensitivity and the results are not easy to understand. ECT results can also be quite easily disturbed, with that in mind, this method can be used as a quality control system while additional development is needed to create larger application range where ECT could be used. [30]

2.5.5 Metallography

After quenching and tempering, the microstructure of steel is tempered martensite and retained austenite. This changes when grinding burn develops. Metallographic methods are used to detect qualitative changes in the microstructure to find possible grinding

burns. Analyzing is done either with optical or electron microscopy. The method is destructive. Results depend on the one who does the observations and his or hers experience, making this not the most reliable method. On top of that, preparation of the samples is complex work. [30]

Song et al. created [30] a classification system for grinding burns based on the microstructure. Based on the subsurface layer microstructures the grinding burn types were; unburnt layer of tempered martensite, tempered troostite or sorbite burn and quenching martensite rehardening burn. [30]

2.6 Recent studies with the common inspection methods

Nital etching and XRD were the methods selected to be introduced in a study and real situation- environment. Nital etching was chosen due to the fact that it is standardized and XRD since it is one of the most used NDT methods and relative to this thesis.

2.6.1 Nital etching study

In the study by Seidel et al. [34], the defects can be seen after etching so that the bright areas demonstrate rehardened zones and tempered zones are seen as grey-brown. Study included laser manufactured defects on reference blocks instead of grinding burn due to fact that generating reproducible grinding burns is extremely challenging. Study also debated if the laser produced defects could simulate the actual grinding burns. Due to the transformation of energy to frictional energy taking the most amount of power from the process, it was justified to assume that predominating factor is the thermal influence in the generation of grinding burn. [34]

Study also made lot of material characterization (hardness, metallographic, residual stresses) in order to find out that the properties of the laser produced defect were comparable to the real ones. In total, 15 laboratories tested 29 samples with significant deviation in the results. Although all the rehardened and heavily tempered zones were detected 100%, the labelling of the right answer in the identification stage was done correctly only 84%. For the light tempered zones the detection was done 72% and labelled correctly only 46%. Some of these deviations in values are expected to be result of circumstances and skill set of operators. Mainly the reason was etching bath. [34]

Reference blocks were used to evaluate the condition of the etching bath. Specified reference blocks are used with one rehardened zone and ten varying depth zones of tempered zones. Material that was used to manufacture the reference blocks was case hardened 20MoCr5 steel. ISO 14104 standard for the test was used. Testing was done so

that fresh etching bath was used and reference block was in the condition that met the requirements set by ISO 14104. After 113 samples, it was tested again and this time another reference block was etched. Now reference block was non-uniform and dark meaning that the bath needed to be changed. The first reference block sets the normal. Even though the color would meet the requirements of ISO 14104 the amount of visible tempered defects and reharden defect sets another limitation. If less than the amount of those defects are visible on the reference block than in the original reference block, then the bath needs to be changed as well. [34]

2.6.2 XRD study

In the study by Bang-Ping et al. [36] X-ray diffraction was used to measure the residual stress values. In the study AISI 1045 steel was going through simulation burn that was caused by laser surface treatment (LST). Study had been made to further improve the knowledge of surface grinding since the grinding process is in a relevant part of the modern manufacturing process. In the experimental part of the study the simulation of the grinding burn was produced by laser surface treatment. This laser irradiation simulated the heat that is produced during grinding with the phase transformations that affected to the surface integrity and mechanical properties similar fashion than surface grinding process actually would produce. XRD was used to detect and classify the grinding burns. The parameters of the laser used were: wavelength of 1.07 μm, adjustable power up to 300 W with a ranging pulse duration from 0.5 to 6 ms and pulse frequency ranging between 1 to 50 Hz. The motion velocity was 0.2 mm/s and diameter of the laser spot was 1.5 mm. Thermal damage could have been varied by changing frequency and duration of the pulse. Since the study generated intentionally generated grinding burn there was microstructural changes in the invisible and visible burn area. The base material was ferrite and pearlite. In the invisible burn area phases that were present were ferrite, pearlite and martensite. Visible area consisted of martensite. The hardness for the base material was Rockwell C hardness (HRC) 34-36, for the invisible burn area 39-41 and for the visible burn area 45-48. The surface hardness change was phase transformation-induced and clear when comparison was done between base and visible burn area. This indicated that the temperature rise induced by LST changed the mechanical property as well. Before the introduction of the burn, the residual stresses were measured to be compressive residual stress in this study -120 MPa (x-axial) and -110 MPa (y-axial). After laser irradiation the new residual stress test revealed that in the visible burn area the residual stresses were tensile, 320 MPa (x-axial) and 295 MPa (y-axial). This means that

residual stress had turned from compressive to tensile ones. Thus, the mechanical properties have weakened and surface was more prone to crack initiation. [36]

3. BARKHAUSEN NOISE

Barkhausen noise is a micromagnetic technique for ferromagnetic materials where applied varying magnetic field is used to magnetize the material and monitor the signal influenced by material properties. Material condition and properties are determined by measuring and analysing the signals. [29] Magnetic Barkhausen noise (MBN) is based on domain wall interactions in magnetized ferromagnetic materials with microstructural defects and it is detected as fluctuating magnetization. MBN jumps are interactions between pinning sites (dislocations and other defects) and domain walls. [37]

Technique is non-destructive and evaluates the microstructural state and stresses of the studied material. The method can be divided into low frequency and high frequency magnetic Barkhausen emission (MBE). High frequency measurements are done with external magnetic excitation more than 10 Hz and the signal analysis can be done in the signal frequency range of 2-1000 kHz. Low frequency measurements are done with external magnetic excitation less than 1 Hz and the signal analysis can be done in the signal frequency range of 0.1-100 kHz. Skin depth (maximum depth that signal can still be detected on the surface) is deeper with lower frequency measurements than high due to attenuation of the higher frequency signal and effects of magnetic field penetration. [38] Typically the power spectrums are frequencies higher than 1kHz. High –frequency MBN is dependent on sensor positioning (local), while larger volumes are magnetized with low-frequency excitation field. MBN's high –frequency content means that it is natural measurement method for near-surface, limited to penetration of 0.01 and 1 mm. Measurement uncertainties can be divided into two categorize: experimental technique and domain walls inherent statistical behavior induced. [29]

Advantages of BN are that the information is collected from the surface layer (information obtaining depth), fast measurements with ability to measure complex geometries and the machine is easy to move around meaning good portability. [38]

Evolution and structure of the magnetic domain under magnetization are affected by multiple parameters. Examples of influencing factors are surface condition, carbon content, microstructure, residual stress and domain wall pinning sites. These multiple variables produce a complex signal. During interpretation, all parameters that can affect the wanted value needs to be taken into consideration. At the moment there is only one standard concerning MBN grinding burn detection due to the high amount of variables

that limit the establishment of acceptance criteria. Main reasons are differences in measuring system and in complexity of the MBN data. [29]

MBN can be used indirectly to measure and monitor ferromagnetic materials due to the fact that MBN is sensitive to domain structure changes. Magnetic properties of steel and MBN correlations associate with the changes that happen in magnetic domain structure. Response that MBN gives is domain structure interactions with pinning sites, their density, grain size etc. MBN results from abrupt localized changes that happen in ferromagnetic material during magnetization. These changes generate high-frequency signals that peak in coercive point amplitude. MBN can be used to study microstructure and stresses. With development of models incorporating specific parameters, it would open a possibility to widen the potential diagnostic applications for MBN. [29]

Limiting factor is the capability to only test ferromagnetic materials. Measurement is sensitive to a variety of other parameters, any single parameter can affect to the result and it is difficult to isolate any specific parameters. Measuring surface may need preparation since coatings and corrosion can affect to the results. For the measurements, the initialization step is faster and more convenient compared to some of the other measuring methods. Only preparation of surface is required to reduce lift-off and signal attenuation. [29]

Hysteresis curve

Irreversible steps appear during magnetization cycle of a ferromagnetic material while the material is under applied field. Transitions are not smooth due to the discontinuous jumps that are the result of localized irreversible changes in the domain structure and is observed as Barkhausen noise. Figure 10. [39] is an example of a hysteresis curve. [29]

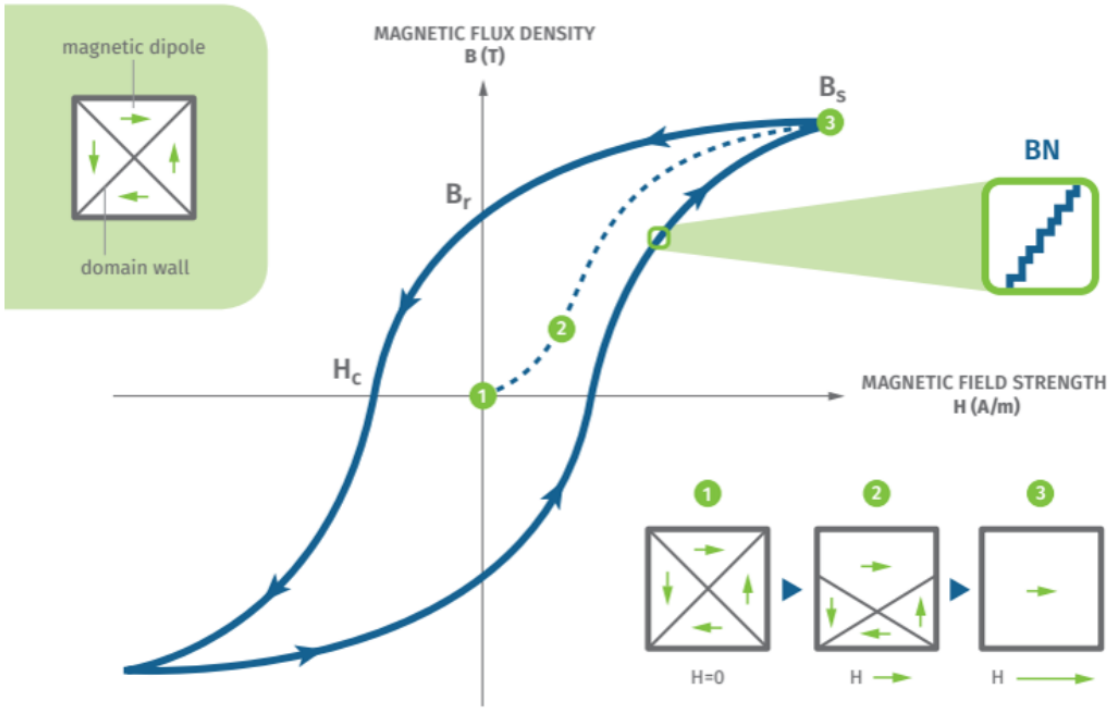

Figure 10. *Hysteresis curve. [39]*

When starting from the demagnetized state (1) and applying magnetic field, those domains that are orientated more suitably start to increase in volume due to domain wall movement (2). This is still reversible since only the weakest pinned domain walls can move. When increasing the applied magnetic field the domain walls can irreversible jump due to magnetic field overcoming the pinning and causing Barkhausen noise. To get over these imperfections, energy is needed and this energy spend is the reason for irreversible jumps in the hysteresis loop. The energy used is the reason for the sudden changes in the magnetization of the material. These sudden changes induce electrical pulses that generate the noise known as Barkhausen noise. Getting higher up in the hysteresis curve means that external field is stronger to overcome domain wall pinning. In the lower field area, 180º domain walls are contributing more to the process while 90º domain walls participate at higher field values. When closing saturation, the domain walls are aligned in same direction than the applied field (3). Once the material is magnetized it retains its magnetization in some degree when the applied magnetic field is removed due to remains of magnetic flux (B_r), meaning that some of the magnetic domains are not able to return back to original alignment state, unless component is demagnetized. When increasing magnetic field in to the opposite direction, H_c is the point where domains are able to return to the original alignments removing the residual magnetism (demagnetization). In the Figure 10. irreversible jumps are illustrated in the magnified image (BN).

When the applied magnetic field is reversed, in the saturation the alignment is into the other direction. [28, 34, 39]

Domain configuration

Ferrite structure is a body-centered cubic (bcc) and it has incompletely filled 3d orbitals in a subshell that stays at room temperature in ferromagnetical order. The 3d-shell electrons that are responsible of the ferromagnetism, contribute slightly towards the electrical conductivity that originates from 4s shell. If the magnetic moments overcome the thermal energies, exchanging interaction with neighbouring atoms will align them to form domains. [29]

Domains are magnetized to the directions of grains in local crystallography and to saturation. Domain wall is the boundary that separates close domains from each other. Walls can be either 180º or 90º depending from the angle of the domain's magnetization saturation vectors that are next to each other. [29]

Demagnetized magnetic moments align themselves to the direction of magnetic easy axis. For ferrite in this case, easy axis are [100], [010] and [001]. This happens to minimize the energy and leads to formation of domain walls. Exchange energy is the origin of the ferromagnetism, which rises due to interactions between spins of atoms next to each other. [29]

Barkhausen noise can be created when the sample is magnetized with applied magnetic field, narrowing the samples to ferromagnetic materials. Ferromagnetic materials are combination of domains and domain walls that are separating the domains from each other. Domains maintain random orientation when magnetization is zero. [35]

Barkhausen noise models

Two models are used as a way to describe the constant applied stress effecting to Barkhausen noise. The Sablik stress model suggests that in the direction of the external magnetic field the hysteresis curve's slope increases while tensile stress increases. This means that typically tensile stress enhances the magnetization of the material. There are some steels that reach the peak amplitude and continuation of increasing tensile stress just decreases magnetization, opposite to what was introduced. Barkhausen noise response is modified by these effects. [29]

The other model is Flux-closed magnetic object model (MO) which associates Barkhausen emissions observed with 180º domain wall movement in MO. Model takes into account how tensile/compressive stress applied increases/decreases the relative volume

of 180º to 90º domains in order to name the MO. Model is based on domain structures flux-closed-correlated regions. Interaction between regions and nearby domain structures happens through formation of moments. [29]

Magnetic circuit hysteresis

With flux-controlled system, to provide additional parameters for measurements, hysteresis loops can be extracted. Effective coercivity and permeability are parameters that hysteresis loop can provide. Effective coercivity and permeability are basically combined results from the sample and electromagnet response. Variations in these values from sample to sample modifies the magnetic response permitting relative measurement. [29]

Commonly, MBN can be used in two categories: evaluation of microstructure and residual stress detection. Due to lack of standards and calibrations MBN usage is hindered as inspection method. The advantage is the residual stress detection coupled with XRD in the industrial scene, due to cost effective inspection. MBN could be used to detect residual stresses with the use of calibration samples, to identify easy magnetization direction and creep damage. For quality control side of MBN, it is used to inspect case hardening quality, grinding burns and weldings. [29]

The sensitivity of the BN for the domain structure during magnetization means that BN is also sensitive for example grain size, residual and applied stresses, microstructure and carbon content. Micromagnetic techniques can be used to characterize properties like hardness, tensile and yield strength. Limiting factors include skin-depth which effects limits the surface measurements. [29]

With Barkhausen noise, different grinding burns can be reliably detected due to fact that Barkhausen noise responds to hardness and stress changes. Barkhausen noise signal amplitude increases with soft sample and decreases with hard. Compressive residual stresses decrease and tensile residual stresses increase the intensity of Barkhausen noise. Through measuring the intensity of the Barkhausen noise, the direction of the stresses can be determined as well as the amount of residual stresses. [35]

3.1 Grinding wheel characteristics and their influence on Barkhausen noise

Grinding wheel selection and wheel parameters used in grinding process affect to the outcome of the grinding. In this thesis two different grinding wheels were used to ground the samples, Al_2O_3 and CBN. Measurements are done in order to see what kind of dif-

ferences can be seen from the end result. The collected information will be used to determine which one is the better wheel for the manufacturing process, or do both wheels give similar results. In order to be able to answer this, first the literature review must be done to understand the materials and parameters that needs to be taken into account. Next chapters are reviewing the wheels and parameters from the standpoint of theory, what is known and how the end result should look like. Later on the thesis, results of the measurements and analyzes are presented to see how the actual measurements can be compared to the literature.

3.1.1 Grinding parameters affecting to the BN results

Barkhausen noise is a method that is not yet standardized. This is based on the fact that so many parameters can affect to the results and it is difficult to pinpoint only one parameter in the calculations. Once the analysing starts, every single parameter that has an effect to the results needs to be taken account.

The affecting parameters are mentioned in the Table 3. More detailed introduction to these parameters and how the affects can be seen is showcased in the chapter.

Table 3. *Parameters affecting BN response of ground surface.*

Parameters affecting to BN response
grinding depth [13]
abrasive distribution [10]
porosity [10, 40]
residual stress [10, 40]
dressing [10]
wheel speed [14]
work speed [14]
infeed rate [14]
wheel wear rate [6]
thermal damage [19, 28, 33]
cooling [2, 10]

Abrasive distribution means the distribution of the grains. In the grinding wheel with carefully planned positions of the grains versus random pattern, this distribution offers significantly less variation on the ground surface, less grinding power and grinding forces. [10]

Porosity allows the cooling liquid run through the contact areas of the sample and the grinding wheel. Making it easier for the chip to move away from the grinding zone, thus decreasing grinding force and temperature. [10] High wheel porosity reduces loading. With high porosity, the thermal and mechanical load's decrease increases the control of grinding-induced residual stresses. Higher porosity means higher wear rate but improved grinding fluid intake to grinding contact. Higher wear rate can be compensated by using higher grinding speeds. This is done to solve wheel loading problems. [10, 40]

Higher residual stresses can be obtained with high amount of cutting edges and fine-dressed wheel than with less active cutting edges and coarse-dressed wheel. With continuous dressing, the grinding temperature can be reduced considerably. [10]

Dressing is one of the requirements for efficient cutting with reduced temperature and grinding forces. Today, the most used dressing method is mechanically done dressing with diamond abrasive tools to recover grinding capabilities and worn grinding wheel geometry. Continuous dressing significantly lowers the grinding temperatures and enables restriction of tensile residual stress to the surface layer ~10 micrometers deep. [10] Tool cleaning can be used to lower the possible rise of RMS values with good machined chip removal. The critical specific energy can be lowered by 33% and 100% increase can be detected with critical specific energy removal rate while grinding superalloy Inconel718. [10]

With higher grinding speed, subsurface layer obtains better consistency of residual stresses. While lowering the grinding depth (the amount of material removed from the surface), it leads to better finish that can be obtained on the surface of the material. Ultra-high-grinding speed provides more reliability and service life than high-speed grinding due to lower tensile residual stresses on the surface of the material. Residual stresses below the surface decrease more evenly than the residual stresses produced by high-speed grinding. Using ultra-high-speed grinding, better surface quality can be achieved in addition of compressive or lower tensile stress. These effects are presented in the Figure 11. [13]

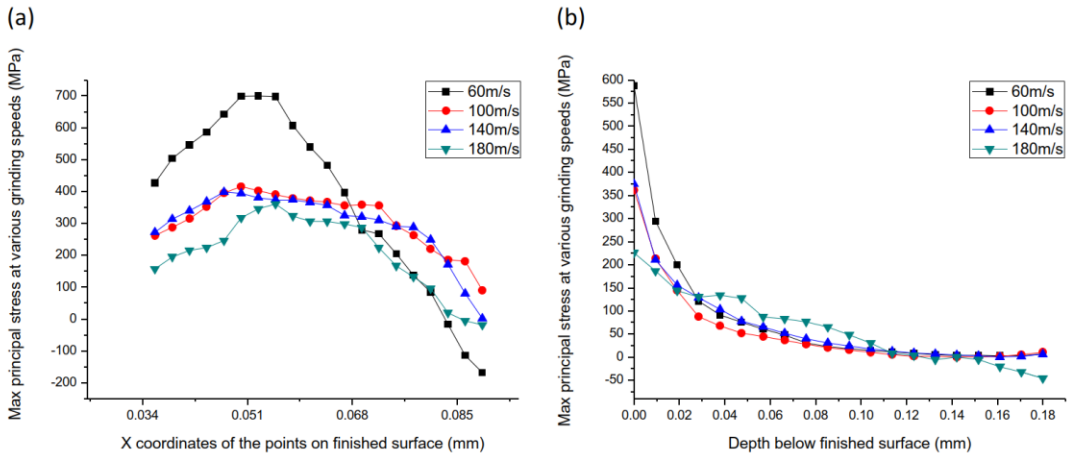

Figure 11. *Different speeds effect to the residual stresses. [13]*

Influence of the cutting speed (wheel speed) is discussed as follows. Forces are quite low while the wheel - workpiece contact length stays small. Although the overall forces are low, for a single cutting edge the force is high, this is because of the low amount of cutting edges actively engaging simultaneously. To decrease the total grinding forces, cutting speed should be increased with constant feed rate in order to reduce the chip length and thickness. What needs to be taken into account in this scenario is that while total forces decrease, increase of cutting speed, will increase the thermal stress of both workpiece and tool. [14]

Influence of feed rate (work speed) can be seen as follows. Feed rate has a substantial effect to the time of a machining process. Increase of feed rate leads to increase in both thermal stress and grinding forces due to increase of chip thickness and chip length. [14]

Influence of infeed is as follows. Together with feed rate these two parameters determine the time needed for the grinding process. Increase of infeed increases the amount of active cutting edges lowering the surface roughness while increasing the thermal stress and grinding forces. [14]

Influence of interrupted cut, meaning the impact and alternating forces the wheel is under, when the grinding is up and down grinding. This effect needs to be counteracted with right choices of bond and wheel material to endure the added wear. Bond's job is to keep the grains in place while the grains need to endure the grinding conditions. Surface quality suffering and wheel wear increase are due to happen if bond selection fails. [14] Wheel bonds are a bonding material and structure of the abrasive wheel to hold the grains in the place. For example, vitrified bond is usually used with CBN superabrasive. In hardness, vitrified bond goes to middle of the pack, other two main classes of wheel bonds are organic and metal bond wheels. Main advantage is that vitrified wheel can

produce forms for grinding various profiles when the wheel is trued. When the wheel becomes too dull, truing allows the wheel to be re-sharpened. [16]

Wheel wear rate affects to the BN response when the already developed wheel wear starts to generate increasing amount of heat due to intensifying friction between wheel and workpiece in the contact area. This friction and increase of heat are happening since the contact area gets progressively larger diminishing the escape routes for produced chips. [6] Wheel wear rate effect can be seen by measuring the amount of heat at the grinding zone. The wheel wears and through consecutive grinding cycles this leads to transformation of grain geometry that eventually can be seen as higher content of heat. Eventually workpiece contact occurs and higher heat penetrates deeper in to the workpiece inducing softening, thicker heat affected zone (HAZ) and higher BN, ladder being due to increase of tensile stresses. [41]

In the study by Shouguo et al. it was determined [27] that higher grinding speed equals higher compressive residual stress in the surface of the material. This was tested with 3J33 maraging steel and ground with electroplated CBN wheel. When grinding speed was changed from 5.03 to 12.57 m/s the overall increase of compressive residual stress was -58 MPa. Other test with maximum compressive stress was backing up the first one since the value of the test with Vs=5.03 m/s was -240 MPa and with the increase to Vs=12.57 m/s the value increased to -292 MPa. The reason for this was the increase of the chip flow rate, meaning that the thermal energy left the grinding contact area faster, reducing the thermal affect and simultaneously increasing the effect of mechanical loading. Mechanical loading as a main factor creates more compressive residual stress to the prone area. [27]

3.1.2 Wheel characteristics

Grinding wheels are a big part of grinding and in order to get the best end result, there are characteristics that require understanding. Wheel characteristics have multiple ways of affecting to the grinding outcome. In order to get the best possible grinding result, these are the factors that need to be taken account.

For a cooling process, usually wet grinding is preferred over dry grinding due to ability to carry away thermal energy from the contact zone while also removing friction. With cooling, reduced temperature and preferable residual stresses are achieved. With cooling fluid, energy partition can be significantly lower than with minimum quantity lubrication (MQL) or dry grinding. [10]

Grains, bond bridges and pores together create the structure of the abrasive layer. The behavioral characteristics of the grinding wheel are determined by the grains and bond bridges combined strength and proportions. Wheel specifications consist of abrasive type, structure, grade, bond type and grain size. Grain size determines the surface roughness since the roughness is dependent on the used grain type. With coarse grit the roughness increases due to the dependence of the grit dimension and surface roughness. Fine grit is stronger and offers lower roughness. It was noticed that while the grain size decreased, the amplitude of BN signal decreased. [16, 42]

Grade of hardness means the hardness of the grinding wheel or in other words, it means how securily the binder holds the grains. This shouldn't be confused to hardness of the abrasive used in the wheel. The higher amount of binder produces harder wheel. The harder the wheel the later the letter is in the alphabets. [43]

Wheel and workpiece materials are affecting to the energy partition. Depending on what kind of wheel, type of grinding is used and overall conditions, the values of energy partition can vary significantly. For example conventional abrasive wheel with shallow cut gives answers of 60-85% while with creep feed grinding and porous aluminium oxide wheel, energy partition values can go as low as 3-7% (This depends on parameters, such as, type of the grinding, fluid conditions etc.). [19]

Wheel bonding material

The bonding agent keeps the grinding wheels abrasive particles in place. The grade and hardness are severely affected by the bond percentage in the grinding wheel. With higher percentage and bond strength, the better the hardness of the wheel shall be. The harder the wheel is that much better it retains its cutting grains while softer wheels loose the grains faster. If the selection of the grinding wheel has been too hard for the case in hand, the dulled grains are held by the bond and no new grains will expose to be new cutting edges. The bond is also responsible of the safety of the grinding process at running speed by holding the wheel together under centrifugal force. [22]

Grain size selection

Soft and ductile material to be ground means that the grain size of the wheel should be coarser. Higher the amount of material needed to be removed, the coarser the grain size should be. Finer finish requires finer grain size. Grinding wheel should be evermore softer when the hardness of the material increases. If the contact of the wheel and the material is larger, softer wheel should be used and vice versa. When work speed relation

to wheel speed gets higher, the harder the grade should be while the grinding should be less aggressive. Grain spacing should be wider when the material is more ductile and softer. When finer finish is required, the denser should the grain spacing be. Medium grain spacing should be used in cylindrical and tool grinding. [22]

3.1.3 Recent studies of Barkhausen noise as a tool in the quality control/inspection process

Experimental study by Thanedar et al. [15] features Barkhausen noise analysis (BNA) as one of the methods to analyse the effects of grinding parameters on integrity of the ground surfaces. The study was done in three parts, starting with screening experiments to narrow the parameters to most influencial regarding BNA and hardness. Gathered information is then used with the response surface methodology and finally ending up with validation experiments. Cylindrical plunge grinding was used, where the workpiece is under constant heat flow causing thermal damages with eventual dimensional errors. Ground surface was assessed using BNA. Vitrifield CBN was used to ground micro alloy steel 38MnVS6. In order to create this experiment, process parameters that were changed and kept constant needed to be decided. Changing parameters were work and wheel speed with the spark-out time and infeed. Spark-out is the time that the radial movement of the wheel is stopped to remove the releasing elastic deformation [44]. Constant parameters were material of the crankshaft, temperature, cutting oil, grinding operation, grinding wheel and dressing conditions of the wheel. During the study, finishing and spark-out time were considered to be analysed and the first phase (roughing) of the cylindrical plunge grinding was ignored. Experiment consisted of radial stock finishing of 0.5 mm companied by the spark-out time. Experiment started with induction hardening and tempering the crankshafts. After this the length of the components were checked so the possible growth would not cause any wheel damage. [15]

The grinding was then carried by using the varying parameters following the response surface methodology design. Once the components were ground they were sent to metallurgical quality control (MQC) lab so that the residual stresses could be measured and Barkhausen noise analysis could be done. The measurement parameters were temperature dependent but since the measurement of temperature is difficult during grinding Thanedar et al. defined [15] the study to be emphasized towards the end effects of this temperature change with the measurements of BNA and surface integrity. [15]

Crank-scan 200 was the machine used in the measurements of BNA. Sensor was run over the face surfaces, radial and diameter surfaces to gather the BN levels all over the

crankshaft. If the components were ground properly, the profile that was gathered with the scan should look like flat with low magnitude signal levels. Meaning that the component had uniform metallurgical properties and compressive residual stress surface. In case the component had defects the scan shows high magnitude peaks. Ability to detect these grinding burns are dependant of mechanical properties of the material and applied frequency. [15]

In the results the increase of the wheel speed also increased the BNA value 12% due to the increased heat in the grinding zone. Increase of the work speed on the other hand lowered BNA value 25% due to the shorter duration the grains were in contact with the component, thus lowering the temperature. Infeed was stated as statistically insignificant parameter with very minimal increase of BNA value. The response surface method - based analysis was used to find statistically significant parameters with the end result of wheel speed, work speed and spark-out time. [15]

Further analysis of the BNA interactions was made. Using contour plots visualization was made to show what kind of adjustments should be done to obtain low BNA value. Images of these contour plots are shown in Figure 12. To obtain low BNA value, higher work speed should be used with low grinding speeds. The interactions of spark-out time and wheel speed implemented that with moderate speeds and high spark-out times minimum BNA value would be achieved. [15]

Based on these results work speed was the most influential parameter changing the value of BNA and achieving the minimum value. With a prediction that the cause of this was due to the heat dissipation controlling into the component. [15]

Final step of validating the results was to find out the error percentage in the prediction of the BNA. Predicted values were plotted against the actual experimental values to see if this model could be used to predict BNA values in grinding with same conditions. The study ended up with the result that the accuracy was good enough for model to be used to predict BNA decently. [15]

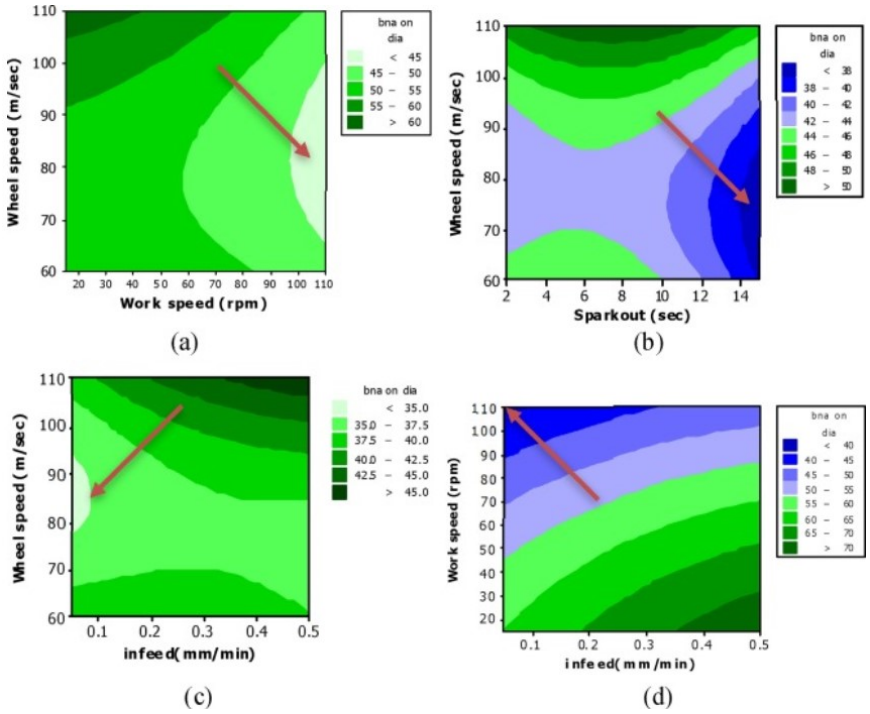

Figure 12. *Examples of contour plots. [15]*

Study done by Cillikova et al. [41] focused on the 100Cr6 bearing steel with hardness of 62 HRC. Study covered surface damage through impact of the grinding conditions, focussing to wheel wear. The bearing steel rings used in this study to produce wheel wear were manufactured to have same measurements. Three batches of rings were used for the experiments. Re-dressing of the grinding wheel was done before each batch. Each ring was measured with BN from 8 different points. The BN values in this case meant the effective RMS value. Microhardness tests were done. Sectioned rings were prepared for the metallography observation in order to reveal microstructure transformations. Observations were done from the matching positions corresponding BN measurement positions. Residual stress measurement was done using mechanical method that implemented both etching and simultaneous ring deformation measuring. [41]

In order to investigate surface integrity – BN correlation many varying quality surfaces and corresponding BN values were required. Low BN emission was obtained when the surface had low magnitude of tensile stresses, fine precipitates and high dislocation density (the nearly untouched surface layer, wet grinding). Higher BN emission was obtained when wheel wear increased, the volume of heat increased. This eventually caused grinding burns to the samples (dry grinding). [41]

Due to continuos grinding cycles, the progressive wheel wear started to develop, causing transformation in the geometry of the grains. This was followed by generation of higher

heat to the grinding wheel-workpiece contact area. This influences so that the temperature penetrates deeper to the component. This increases the thickness of HAZ with clearer indications of thermal softening while also increasing BN emission. Increase of BN emission (thermally induced) meant decreasing dislocation density, with coarser precipitates and tensile stresses. This also lowered the microhardness. In the study, increase of BN was directly related to synergy effects of stress and microstructure, which was demonstrated with a figure of increasing BN relation to increasing wear. Reduced flow of coolant increased the wear faster than constant flow. Study showed that lack of coolant increased the wear rate and dulled the wheels fast. Although the wear rate was slower while the wheel was still sharp. Thus, results showed that risk for a grinding burn was higher when the wear of the wheel was more developed in condition where failure of coolant had happened. [41]

In dry grinding cycle the abrupt increase of BN happened due to before mentioned temperature increase in contact zone and deeper penetration of temperatures. The results showed significant decrease in subsurface hardness and increased thickness of HAZ after dry grinding cycles. Thus indicating the increasing BN values while thermal softening increased. The growth of BN values starts to decrease when the temperatures went over austenitizing temperature in the contact area. This caused self-cooling effect and rehardening that started to appear to the surface (white layer). Decrease of BN was due to BN emission rate being driven by the ratio (thickness) of White layer (WL) and HAZ. [41]

Sublayers, that have thermally softened, contributed to the BN signals on the free surface overruling weak BN emission of WL when WL thickness was thin. When WL thickness increased, BN started to decrease. This was influenced by poor BN of WL and limited sensing depth of BN. [41]

In the study [41], correlation was discovered between magnitude of tensile stresses and the thickness where the tensile stresses occurred with the values of BN and thickness of HAZ. Disclaimer was made at the end of the study that while claiming this was reliable monitoring system based on the BN emissions to monitor thermal damage this was only confirmed for this 62 HRC hardness steel and other steels would require more research. [41]

4. ISSUES AFFECTING TO THE GRINDING OUTCOME AND TO THE SURFACE CHARACTERISTICS

Grinding is a process that can have major effect to the surface characteristics and overall the outcome of the grinding process. In this chapter the parameters affecting to the outcome of the grinding as well as the surface characteristics are showcased. In the Table 4. the parameters are introduced and throughout the chapter explained more in detail.

Table 4. *Parameters for the grinding outcome and surface characteristics.*

Parameters affecting grinding outcome and surface characteristics
wheel [19, 43]
Workpiece [19]
Cutting and tool geometry [13, 41]
grinding power [2]
mechanical force [10]
thermal damage [19, 28, 33]
grain size [43]

One of the main challenges in grinding processes is the possible occurrence of thermal damage. Thermal damage affects to different qualities of material and weakens them reducing the overall estimated lifetime. To maximize the benefits of materials to their fullest potential, some issues need to be controlled and monitored during the grinding process to limit the possibility of thermal damage. Tensile residual stress is thermally induced, compressive residual stress through mechanical interactions. Energy partition, meaning the fraction of total grinding energy that is converted as heat to the workpiece, is an important parameter to calculate. [19]

The correctly chosen grinding abrasive grain type is important factor determining surface quality. Fine grain produces higher quality finish versus coarse grain that can remove material in higher rate but offer less quality to surface finish. Other parameters of the grinding wheel affect also the surface quality not just the grain size. Grade and bonding material are examples of these other wheel related parameters. [43]

Grinding power increase also increases the tensile residual stress contribution to the stress balance of before mentioned three factors: plastic deformation, temperature increase and rapid heating and cooling cycle [2]. There are three different types of grinding-induced formation methods for residual stresses. Localized thermal expansion, plastic deformation and localized phase transformation –induced volume change. The reasons are in grinding-induced stresses. Mechanical-plastic deformation and thermal-plastic deformation play major role in residual stress formation of ground samples. Residual stress state depends interactions of both, mechanical and thermal. [10]

Cutting speed decreases while depth of residual stresses decreases. Although while cutting speed increases, both cutting and feed force decrease. In the study by Shouguo et al. [27] workpiece speed keeps surface residual stresses σ_s and maximum compressive residual stresses $\sigma_{comp,max}$ in stable state, regardless of speed changes in area of 10.5-18.35 mm/s. Using lower speeds 5.25-10.5 mm/s there is clear decrease in measured values for σ_s and $\sigma_{comp,max}$. This happens due to fact that increasing work speed also increases grinding temperature. [27]

5. EXPERIMENTAL: MATERIALS AND METHODS

The material of the samples used during the thesis is introduced in this chapter. The composition of the sample materials and tactical measurements are showcased. Naming of the samples is also made to ensure easier following of the results later on the thesis. Preparations of the samples for the measurements are also explained to offer closer look to the parameters and reasoning behind some decisions made on the preparation of the samples for certain measurements. This also provides opportunity to repeat or carry on the measurements with a possibility of using same parameters with different grinding wheels or wheel speeds to further continue the study.

5.1 Samples

The Master's thesis includes an experimental part in which differently ground samples were studied. All the cylinder-like samples were manufactured from the same material 20MnCrS5 steel with diameter of 45 mm and height of 35 mm. Chemical composition is displayed in Table 5. based on standard EN 10277-4-2008 [45]. All the samples were carburized case hardened with oil quenching. Effective case depth was around 0.8 mm (verified by the non-ground samples) and total case depth of hardening was between 1.2-1.5 mm. During the thesis, overall 27 ground samples were studied with additional five intentionally generated grinding burn samples and three non-ground samples. In the Table 6. all the samples are named and the name corresponds the ground off layer (mm). The sample 0.1A in batch B 181 was used as a comparison sample versus the 0.1 sample and is the bottom surface of the 0.1 sample.

Table 5. *Chemical composition of the 20MnCrS5 steel. [45]*

C	Si	Mn	P	S	Cr
0.17-0.22	**≤0.4**	**1.1-1.4**	**≤0.025**	**0.02-0.04**	**1-1.3**

Table 6. *Ground sample markings: Pre-determined ground off layer (mm) for each batch.*

Al_2O_3 (mm)	B 126 (mm)	B 181 (mm)
0.1	0.1	0.1(A)
0.2	0.2	0.1
0.3	0.3	0.2
0.4	0.4	0.3
0.5	0.5	0.4
0.6	0.6	0.5
0.7	0.7	0.6
0.9	0.9	0.7
1.1	1.1	0.9
-	-	1.1

Nine of the 27 normally ground samples were ground in Newcastle University Design Unit (UK) and the rest of the samples (18) were ground at Tampere; Hiontatyö Tuomainen. The grinding was done so that from these three individual sample sets of nine, each was ground to a different case depth. The range was 0.1-0.7 mm, 0.9 mm and 1.1 mm. In order to make the sample surface even the other side of the samples were also ground to gain better stability for the grinding. Similar parameters were used in both places: infeed rate was 0.01 mm with wheel speed of 28 m/s and table speed of 15 m/min. Diamond dressing was used if needed. The infeed rate was set in both places so that grinding process removed 0.01 mm of material from sample surfaces with each grinding pass. Example of one sample can be seen in Figure 13. Sample is already ground (with Al_2O_3) and marked for the XRD testing. Figure 14. illustrates the surface grinding that was done at Hiontatyö Tuomainen.

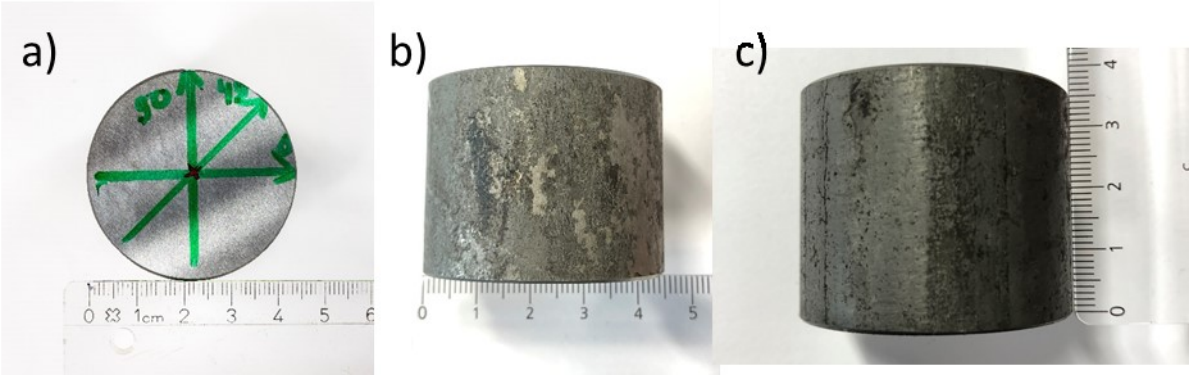

Figure 13. *Picture of the sample from the a) ground surface and b) and c) from the side with dimensions.*

Despite the maximum infeed flow of cooling mixture and low rate of infeed, sparkles can still be seen during grinding process (Figure 14.).

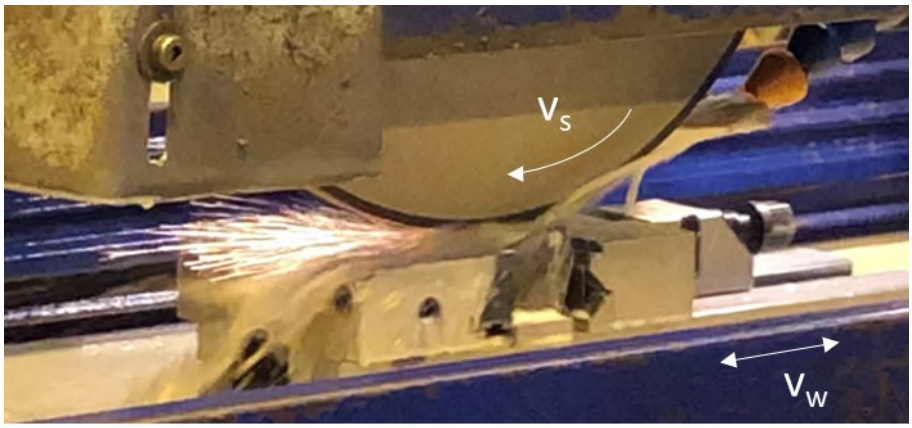

Figure 14. *Grinding at Hiontatyö Tuomainen with CBN B181 wheel. v_s is the wheel speed and v_w is the table speed.*

The intentionally caused grinding burn samples Newcastle 1, 2 and 3 were ground at Newcastle University Design unit and samples TUT6 and TUT8 were ground in Tampere at Hiontatyö Tuomainen.

Newcastle samples are shortened to N1, N2 and N3. In the Figure 15 a). the samples are shown, sample 1 is N1, sample 2 is N2 and sample 3 is N3. In same Figure (15 b).) the TUT samples TUT6 and TUT8 are shown. In the Table 7. the shortened names used to describe the grinding burn samples.

Table 7. *Intentionally generated grinding burn samples.*

N1	TUT6
N2	TUT8
N3	-

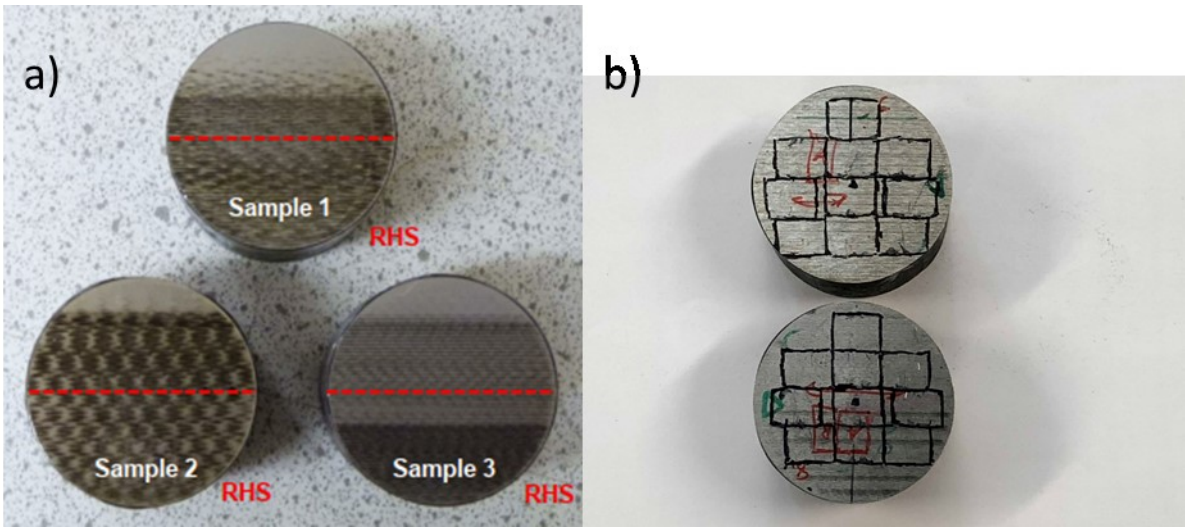

Figure 15. *Picture of the a) N samples (provided by Newcastle University) and b) the sample TUT6 (on top) and the sample TUT8 (below).*

5.1.1 Samples ground with Al_2O_3 wheel

The first sample set was ground in Newcastle University Design Unit, Newcastle (UK), using Al_2O_3 grinding wheel. The sample set is referred as batch Al_2O_3 during this thesis. Details of the grinding wheel, manufactured by Norton, were included in the specs of the grinding wheel: 95A46KVX. 95 was the manufacturers symbol indicating inclusively the abrasive that was used, A stands for the abrasive used (Al_2O_3), 46 is the grain size (300-400 µm) (medium) [46] (with this specific wheel 0.355 mm [47], confirmed also by partnering collaborator [32]), K stands for the grade (medium), V means the bond type used (vitrified) and finally X is manufacturer's private marking, indicating exactly what the wheel in use is. The used Al_2O_3 grinding wheel is presented in Figure 16.

The selected grain size of Al_2O_3 wheel is usually larger than the CBN's for the same grinding operation. [23]

Figure 16. *Al_2O_3 grinding wheel, image provided by Newcastle University.*

5.1.2 Samples ground with CBN wheels

Two other sample sets were ground in Tampere at Hiontatyö Tuomainen by using CBN grinding wheels manufactured by Ilyich Abrasive Company. These sample sets are referred as B126 and B181 during this thesis. In total 18 samples were ground at Hiontatyö Tuomainen, nine with B126 and nine with B181 grinding wheel.

Details of the grinding wheels are LKV50 B126 S2 C100 KS10 and LKV50 B181 S2 C100 KS10. LKV50 stands for the abrasive material, B126 and B181 both mean grain sizes, B126 (106-125 µm) results in as medium surface finish and B181 (150-180 µm) leaves the surface finish rougher but is considered to same medium category as B126 [46]. The parameters for both CBN wheels are: diameter 350 mm, height 20 mm and innerhole diameter 127 mm. There were some complications when grinding with B181 (informed by Hiontatyö Tuomainen) so it was assumed to be damaged or something was wrong as its quality wasn't satisfying. There were clear signs of waviness (informed by Hiontatyö Tuomainen) after the grinding process implementing damage and imperfections in the B181 grinding wheel. Also the first sample 0.1 mm was ground from both sides so the measurements was done from both sides of the sample. The bottom of that sample is known as 0.1A. The used CBN B126 grinding wheel is presented in Figure 17.

The selected grain size of CBN is usually smaller than the Al_2O_3's for the same grinding operation. [23]

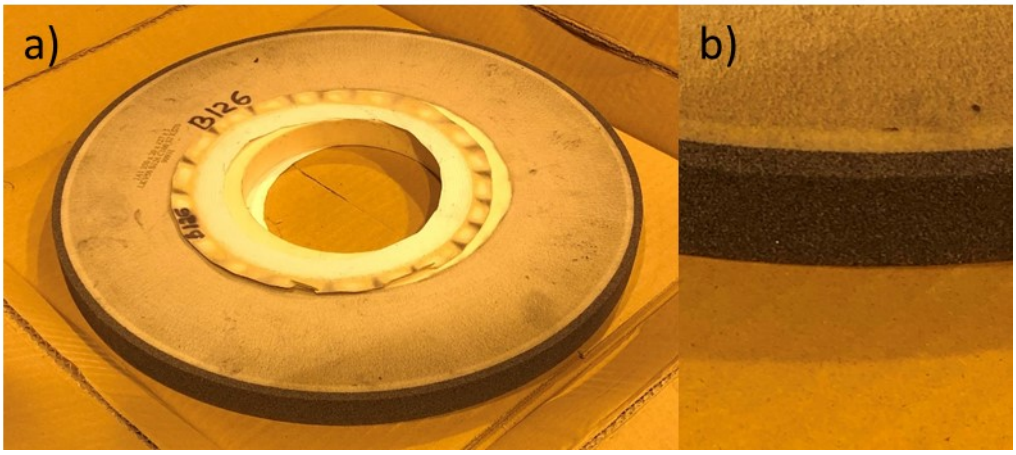

Figure 17. *CBN B126 grinding wheel used in Hiontatyö Tuomainen. a) Whole grinding wheel and b) closer take from the grinding surface.*

5.2 Preparation of the samples and equipment used in the measurements

In this chapter the non-destructive and destructive testing measurement preparation for the batches is explained and the used equipment are mentioned. Explanation covers the measurement process itself as well as the marking of the materials, used directions and possible corrections that are required during testing.

5.2.1 X-ray diffraction measurements

Measurement locations

The XRD for residual stress measurements were done first to the Al_2O_3 batch. The direction of the grinding couldn't be seen from the surface so the center point of each of the samples was first marked and straight line was drawn through the center point to get a starting direction, marked as 90. This was done with a green marker. Using this as the 90 degree direction the samples were measured. Measuring was done to three directions: 0, 45 and 90. After each samples center residual stress values were measured, actual directions were figured out from the collected data by using earlier measurements done regarding this project. In the earlier measurements the lowest compressive residual stress was in the grinding direction. Using this as a reference point, the directions were easy to organize based on the data from the measurements, example of this is shown in Figure 18 a). A circular paper cast was created with compass to ease the process of marking the outer measuring points of the samples (Figure 18 b).). The circular paper cast had a diameter of 25 mm. This allowed to quickly mark the points that were 10 mm off the borders. By creating a cast with crossing lines, it was possible to effortlessly mark the outer measuring points for each sample.

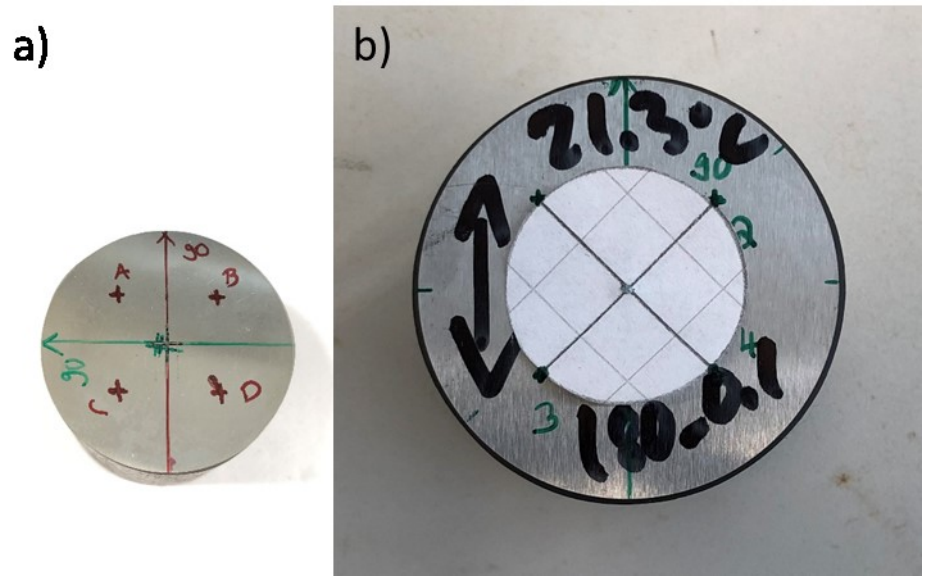

Figure 18. *a) Corrected grinding direction (red marker) based on the earlier experimental measurements and guessed grinding direction (green marker) and b) the self-crafted tool to measure the distances of the outer points A-D.*

The same four outer point measurement sequence was done to each sample after the actual grinding direction was drawn to the surface of the sample with a red marker, based on the estimation testing results. Marking has been done so that the 90 marked the direction of the grinding. For the measuring of the residual stresses from the samples, Modified Chi method (commonly used XRD technique) was used [48]. XTRONIC-software was used to gather the data from the XRD measurements done with XSTRESS 3000.

The used parameters for XRD measurements were as follows. Diffraction peak for ferrite with lattice plane (211) with a diffraction angle of 156.4º was used. The tube was Cr. The measurement consisted of five tilts, with a tilt angle from -45.0 to 45.0 and three rotations (0, 45 and 90) with a rotation angle from 0 to 90. Used X-ray voltage (kV) was 30 and X-ray current (mA) was 6.7.Measuring mode was Modified Chi.

For the batch B126 and B181 same measurement parameters were used. From the surface of these CBN ground batches the grinding direction was easy to see. Otherwise the preparation was the same and so was the measurements after marking, only exception was from the batch B181 sample 0.1 mm. From this sample both sides were measured and the marking on the top was 1-4 and on the bottom it was 5-8 instead of A-H. Example of the marked CBN ground sample in Figure 19.

Figure 19. *Marked sample B181 0.7 mm.*

XRD was used in the destructive testing later on with electropolytical polishing device Movipol-5 to create residual stress depth profile from a non-ground sample. During this measurement process the same point was measured while between the measurements the material was polished off in order to get residual stress depth profile.

XRD was also used to study the five intentionally caused grinding burn. The samples were ground so that the surface had visible grinding burn. After initial examination with Barkhausen noise the samples were tested with XRD. The middle points of the BN measuring areas were used for XRD studies (Figure 21.) to ensure comparison possibility with other samples.

Austenite content was also measured from the non-ground sample surface since the surface gave low compressive residual stresses that increased fast near the surface layers. This measurement was taken from the 0.09 mm depth from the surface by using XRD austenite content measurement.

5.2.2 Barkhausen noise measurements

Before Barkhausen noise measurements, the Al_2O_3 batch was tested with Residumeter II model EMUD2K to see if there was any residual magnetism. Residual magnetism was found in the samples and using MicroScan software the illustration of the burst outcome was collected. Residual magnetism was seen due to the fact that hysteresis loop was not placed in the middle and the sequential bursts were different sizes as seen in Figure 20 a). The samples were demagnetized and normal MicroScan result is shown after demagnetizing in Figure 20 b). After first set of X-ray testing there were two samples that had different direction marked as the direction of grinding than should have been. Using

the data, the direction was remarked with blue marker to indicate the right grinding direction.

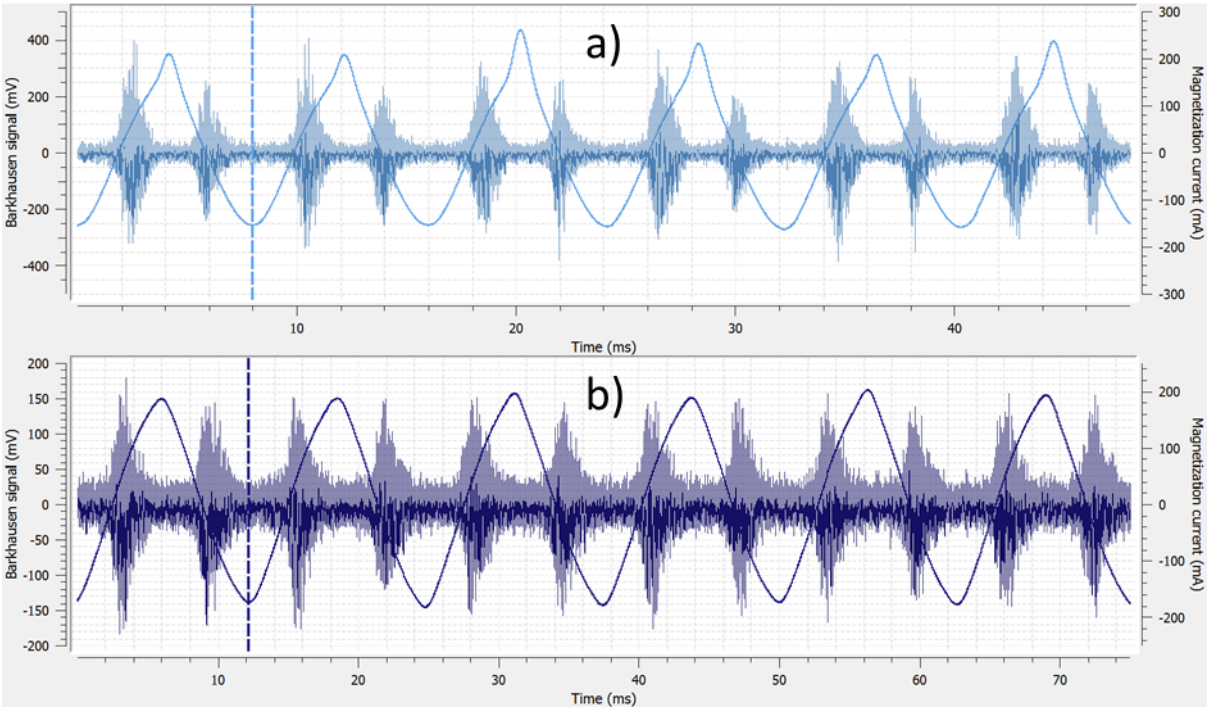

Figure 20. *MicroScan results a) residual magnetism in the material and b) demagnetized.*

There was no need to use Residumeter II model EMUD2K to see if there were any residual magnetization left due to fact that the batches B126 and B181 were demagnetized in the workshop Tuomainen and the samples weren't exposed to anything that would have magnetized them before arriving to TUT. Hiontatyö Tuomainen informed us that there were some problems with the B181, most likely some kind of flaw that may have affected to the grinding. This is discussed when reviewing the results.

The Barkhausen noise studies were done by using Rollscan 350. When measuring, the sensor magnetizes and demagnetizes the sample in cycles, picks up the Barkhausen noise signal and transfers it to Rollscan software. Rollscan analyzes and processes the signal. [35] Measurements were done with sensor S6387 and using measurement parameters of 80 Hz (frequency) and 7 vpp (voltage). Sensor type was S1-16-13-01 and the specification was 20x20 case for flat surfaces. The measurements were done three times per sample and four times if the results varied significantly. If the fourth measurement was needed the measurement with the most deviation was removed. The measurements were done to both directions, grinding and perpendicular. MicroScan –software

was used to gather and analyze the collected data. After collecting the data it was copied to excel where the averages were calculated from the collected data. After calculating the averages, different charts could be made to make the observation of the values easier. Every batch was measured similarly, only exception was the 0.1 mm sample from the batch B181 that was also measured from the other side and taken into account in the following calculations.

Later on the project three samples were ground in Newcastle University so that the visible grinding burns were visible in the surface of the samples. Also two samples which were ground to achieve intentional grinding burn at Hiontatyö Tuomainen earlier during this project were examined. The samples were named N1, N2 and N3 also TUT6 and TUT8. The same Rollscan 350 was used but the sensor was changed to S1-18-13-01 type, S4740 to measure the Barkhausen noise in different parts of the samples. This sensor was smaller than the S6387, helping to position and measure the areas more precisely. Measurement parameters of 125 Hz and 6 vpp were used for the measurements. MicroScan was used for collecting the data. Table 8. shows the parameters used to generate the Newcastle grinding burn samples with Al_2O_3. For the grinding, Al_2O_3 wheel was used with the wheel speed of 28 m/s.

Table 8. *Used parameters for the grinding burn generation.*

Sample	Depth of cut (mm)	feed rate (m/min)	Total removal of material (mm)
N1	0.138	18	0.266
N2	0.168	13	0.216
N3	0.138	8	0.164

The TUT6 and TUT8 samples were both ground with CBN B126 wheel, with the wheel speed of 35 m/s and feed rate of 10 m/min. Both had 0.6 mm taken away from the surface, for TUT6 it was done with three grinding passes and for TUT8 with six grinding passes. Before grinding samples were tempered.

Trials to generate the grinding burn were tested with the N1 sample with increasing the depth of cut (feed rate stayed at 18m/min during trials) until visual grinding burn was observed. Once the depth of cut was found the feed rate was changed for the other two samples, N1 and N3 were ground with same depth of cut (0.138 mm) and sample N2 with a bit higher (0.168 mm) depth of cut.

The measurement points were selected in three different planes using the visible burn levels as a guideline. Before actual testing, few test measurements were done in order to see what places should be measured to gain comprehensive results. The points were marked and the measurement direction for the perpendicular direction was decided to do from the right hand corner from the middle points and closest to the edge from the side points. Only exception was N1 which lower side points perpendicular measurements were taken from the inner side. The measurements were done so that the darker most visible burns were named the lower part and the less visible burn part was in the upper part of each sample. Figure 21. shows sample N3 and the sample point selection. The points are named so that the top layer is A, second layer is B, third layer is C and the bottom layer is D. Numbering goes from left to right and for example A1 is the top block and C2 is the middle block in the layer where the three measurement areas are not touching each other's sides. Similarly A1 is 1, B1 is 2 etc. in the upcoming measurements. From the marked areas one measurement was taken in both directions.

These sample points were also utilized in further studies with XRD mentioned in the previous chapter.

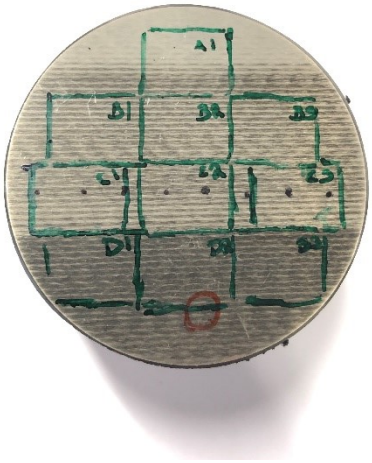

Figure 21. *Sample N3 marked and ready to be measured.*

5.2.3 Case depth studies with PCCaseDepth

Case depth determination with PCCaseDepth

PCCaseDepth is a software created by Stresstech Oy for case depth studies. It utilizes ratio of magnetizing voltage sweep slopes method in the case depth measurements. In order to work it needs sensor to collect the data and BN analyser with the network connection to transfer the data to the software. [49]

To start the actual measurements, measurement parameters have to be specified. This can be done from the session settings. Parameters to define are low and high frequencies combined with minimum and maximum voltage, step voltage and sweep direction. [49] Whole parameter list of sessions settings is shown in Figure 22.

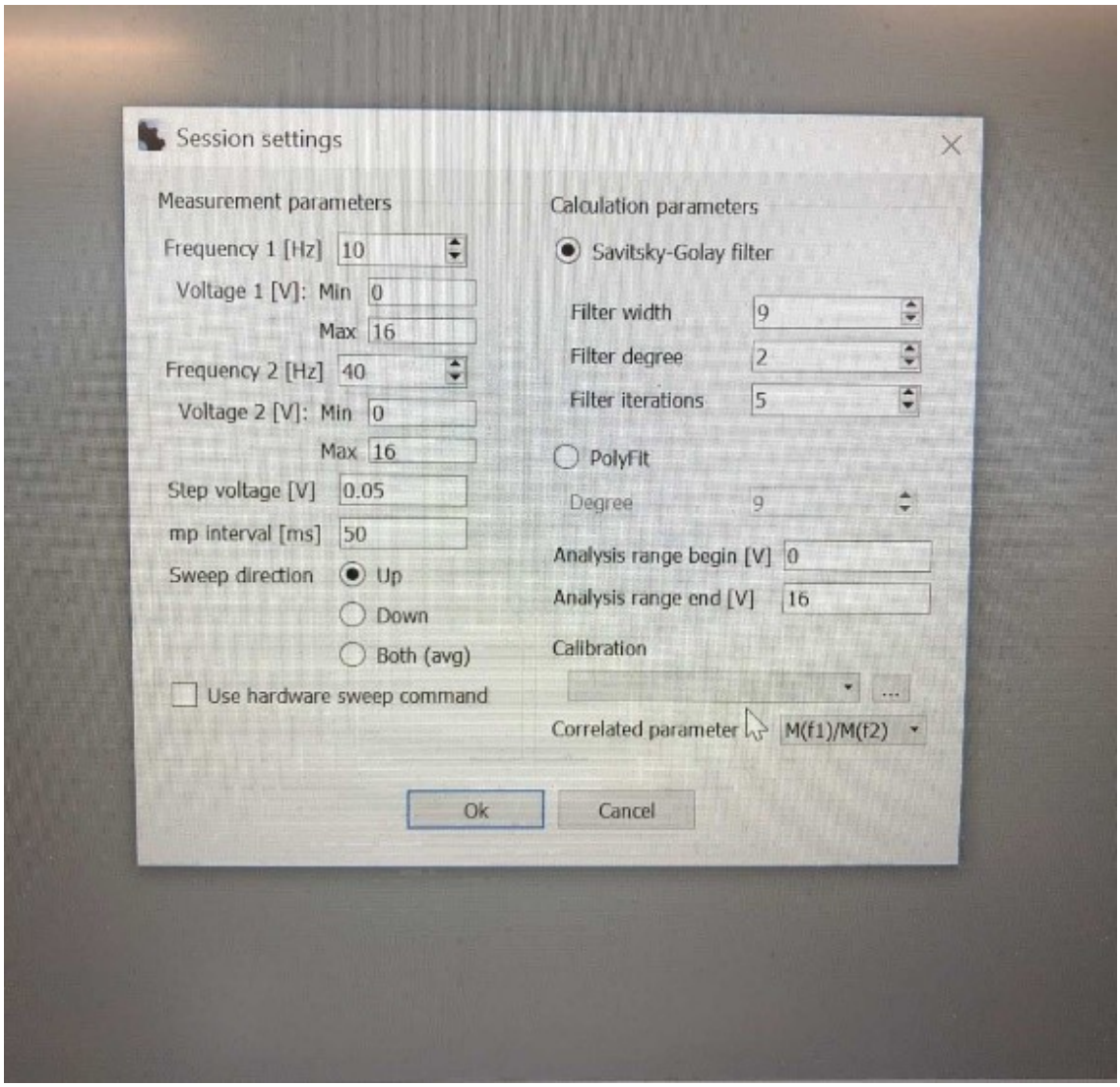

Figure 22. *Measurement and calculation parameters of PCCaseDepth session settings. Picture taken from the Stresstech PCCaseDepth software.*

On the right side of the Figure 22. are the smoothing and calculation settings. Since the Barkhausen signal is noisy, filtering and smoothing are used to ease the analysing process. Two possible options for this are Savitsky-Golay and PolyFit. [49]

From the calculation settings the beginning and ending points of the analysis range can be decided. This is useful when the measurements don't require going up to 16 V or there is no need to start from 0 V. [49]

Case depth measurements

The case depth measurements were done using Rollscan 350 with the same sensor (S6387) than in one of the previous set of tests. The PCCaseDepth software was used as the analyzing tool for the gathered data. Frequencies for the examination were 20 Hz and 125 Hz and analyzing voltage range was from 0 to 16 V. Sweep direction was up and step voltage was 0.05 V with mp interval of 50 ms. The measurement was run twice for each sample, one time for the grinding direction and once for the perpendicular direction for both frequencies. Collected data was copied to excel where it showed as x- and y-values for each sample for both directions (grinding and perpendicular) and frequencies (20 and 125 Hz) individually. This data was organized and send to D.Sc. A. Sorsa, who used algorithms to calculate the slope and peak positions for every sample including both directions and frequencies.

Every batch was measured similarly, only exception was the 0.1 mm sample from the batch B181 that was also measured from the other side and taken into account in the following calculations. Next step was to do same measurements with frequencies of 10 and 40 Hz. This was done to get better grasp on the lower frequency results. Again the data was handed out after the measurements to D.Sc. A. Sorsa, who used his algorithms to calculate the slope and peak positions for every sample. After the calculations the results were organized as graphs to have better vision to be able to interpret the results. Conclusion are discussed later on the thesis in the results chapter.

5.2.4 Surface roughness studies

For the contact surface roughness R_a measurements, Mitutoyo SJ-301 stylus measuring device was used. Normally ground samples were measured three times, once from the center line and once from each side of the middle line. This measurement was repeated for every sample and in both directions. Due to the fact that the machine was extremely

sensitive fluctuation can be seen in the results. The measurement machine was extremely sensitive since the magnitude of measurements was 10^{-6} cm. Due to this sensitivity possible measurement fluctuation could have happen due to either because of the measurement condition or the measurer. One possibility also is that the markings that had been done to the surface of the samples to aid in other measurements could have also affected to the measurements. This was biggest concern in the middle line measurements due to fact that in all samples the middle line was marked with a marker.

There was fluctuation in the results, especially for B181 batch, possibly the effects of the issue that was detected in the grinding wheel. The markings in the samples might have also been affecting to the results. More about this in the results chapter and further studies.

In addition, the surface roughness measurements were done with Alicona InfiniteFocus optical profilometry, obtainable roughness data presented in Figure 23. The measurement area can be adjusted so that the user can decide where and what size the area used in the measurement will be. When the area's x- and y- coordinates stay the same, by moving z-axel to two different positions, 3D surface model could be created. Examples of surfaces observed with optical profilometry are shown in the Figure 42. Images can be used to measure surface roughness values or average height of the measured area. With the optical profilometry, the images were taken from the surface, area that had the least amount of marker in order to avoid possible deviation to the results.

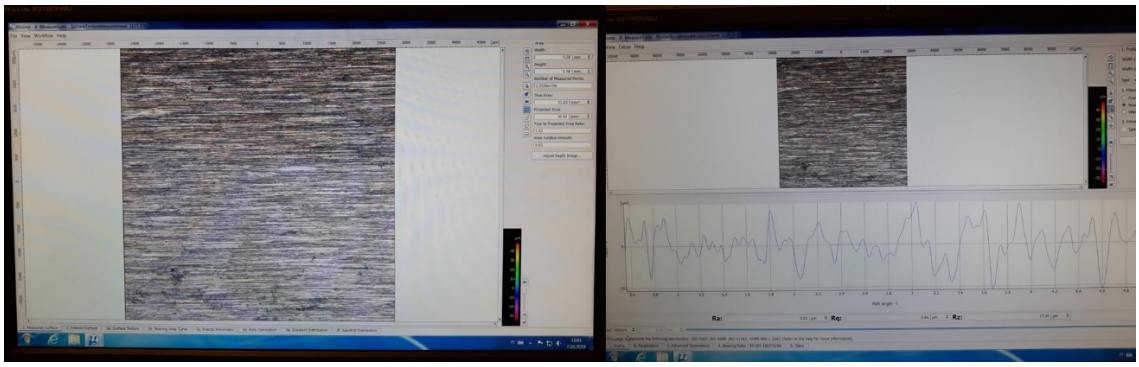

Figure 23. *Visual examples of obtained roughness data by using Alicona InfiniteFocus optical profilometry.*

The measurements have been done so that the R_a values were calculated from the perpendicular direction to the grinding direction. Method has standards but these measurements were done before acknowledging the fact that the measurements should have

been done with a different magnification multiplayer to fit the standards. The measurements were done with the 2,5x magnification when these should have been done with at least 10x magnification in order to follow the standard.

From the images, optical profilometer was able to measure the surface roughness values as well as different height related values. The true projected area ratio, meaning the actual surface area divided by the surface area could be also measured. The values that have been observed and analyzed from the measurements are S_a (average height of the area), true projected area ratio, R_a (average roughness), R_t (maximum peak to valley height of roughness profile), R_z (mean peak to valley height of roughness profile) and R_q (RMS roughness).

5.2.5 Residual stress depth profile

Residual stress depth profile was done using XSTRESS 3000 (XRD) for the residual stress measurements, software Xtronic was used to collect the data and Struers Movipol-5 to do the electropolishing for the material removal.

Residual stress depth profile was done by using Struers Movipol-5 electropolishing machine and Mitutoyo Absolute gauge for measuring the polished depth. Polishing parameters were: A2 (polishing liquid) 45 V, 45s/polishing sequence and flow of 10. The first measurement was taken from the sample before the first round of electropolishing. Electropolishing was done at the beginning so that the polished depth was very small in order to get better grasp on the layer beneath the surface of the sample's residual stress depth profile. The measurements were done from the center of the sample.

Step by step process of this three station measurement cycle was: electropolishing, measuring the depth and then either continue polishing until the next wanted measuring depth was achieved or XRD measurement. The time that the measuring takes is heavily depended on the one who does the measuring, since the experience on the electropolishing defines how effectively one can remove material. Also reading the depth from the measuring device can vary even with the slightest of positioning error on the measuring table, making the measurement process more depended on the one measuring.

Since ethanol is used after electropolishing to clean up the area, other ways of marking the measuring direction needed to be used than the marker lines across the surface since ethanol removes the markings. In this case for the mount that was used under the sample, the outline of the half sample was drawn. After drawing (basically a half circle) three spikes were marked to both, sample and the mount. When the spikes lined up, the

sample was easy to place in the same orientation for each measurement after polishing. Even though these markings were not in the area where the ethanol would likely spread on. Last modification for the sample was small scratched line to the lower part of the sample to mark the grinding direction, just in case the marker markings for some reason would have worn off before the end of the residual stress depth profile measurement. The center of the sample, where the residual stress depth profile measurements were done, was isolated by using circular plastic ring and scotch tape. This was done to prevent other areas of the sample to react with the A2 and to ease the electropolishing process by preventing air to leak in the vacuum of polishing process.

5.2.6 Microstructural observation

Microstructural observations were done by using Nikon Eclipse MA 100 optical microscope. In order to get to the point of observation, the non-ground sample required some preparation steps to be in condition for observation. The sample was cut to get a good representation of the surface profile (perpendicular direction). Then it was mounted and polished. After the surface was ground and polished, Nital etching was used to reveal the microstructure. Microstructure images were taken with different magnifications in order to see the microstructural changes (for example transition between case and core). Images were taken in such a manner that it was possible to recreate larger representation of the surface by using multiple images.

After the permission from the collaborators from the FUNBARK project was received, the destructive phase for measurements started with the preparation of the samples for the optical microstructure observation. From each batch, those samples giving the most interesting measurement results were chosen to be prepared. From Al_2O_3 batch samples with ground off layers 0.1, 0.6 and 1.1 mm were chosen, similarly from the B126 batch same samples were chosen. The reason for the 0.1 sample was the retained austenite layer thickness observed from the non-ground sample. The reason behind the choice of sample 0.6 was that it was showing off as a point were RMS value either increased or decreased depending on the measurement. The sample 1.1 mm was chosen due to the RMS avg – ground off diagram since the value decreased instead of rising in the 1.1 mm. The selection ended up being the same for the batch B181 in order to keep the results comparable.

The decision to prepare all the samples was made based on the results. Showing deviating values in the case depth comparison.

The preparation started with cutting the samples with Struers Discotom-10 by using 60A25 cutting wheel. In the Figure 24. the sample cutting plan is visually reconstructed. Same cutting plan was used for each sample and the side that was taken and mounted was on the B and D side of the sample. Example of this is in Figure 24. The piece was then cut to square in order to fit it into a mount in the way that the side that was in the middle line pointed down in order it to be the surface of the mount.

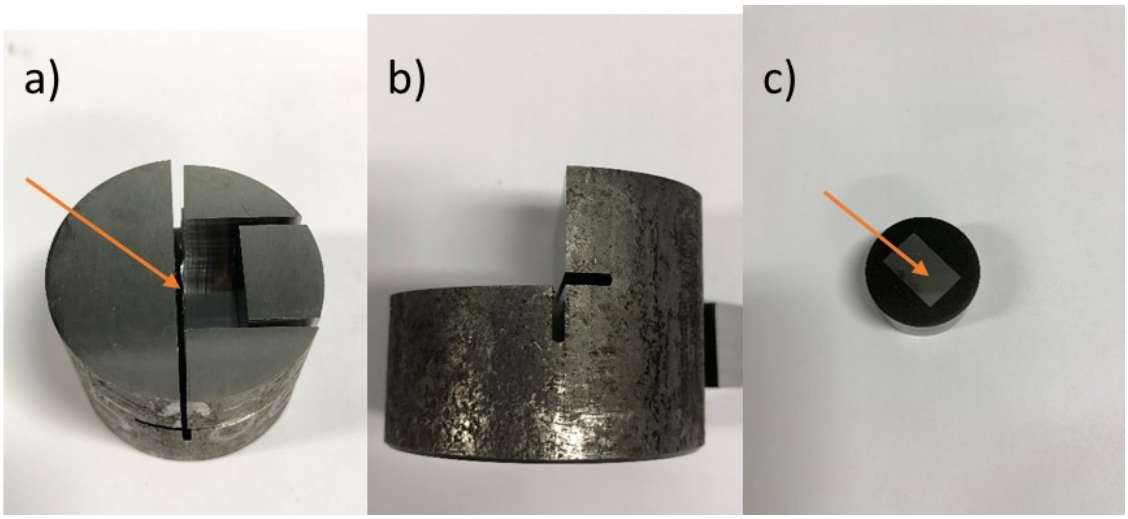

Figure 24. *Demonstration of the surface that is under study. a) B-D side on the right, b) depth of the cutting process and c) mounted sample B-D side up (mounted side is pointed by arrows in a) and c).*

Struers CitoPress-10 was used to mount the cut pieces. Polyfast was used as the mounting resin (20 ml). First preheating at 0 bar, 80 ºC for 3 minutes was used before heating at 250 bar, 180 ºC for 3.5 minutes. Cooling process was executed with high water usage for 2 minutes. This process was repeated for each of the samples before moving to the polishing process to produce high enough surface quality to be able to use optical microscope after etching to observe the samples.

For the polishing process Struers Tegramin-30 was used. The program that was used was premade to produce SEM ready samples. First five polishing cycles were done by using SiC foils (surface) with finer grain each cycle. Every cycle was 1 min with 25 N force and water. The rotation speed of the wheel was for the first four cycles 300 rpm but decreased to 150 rpm for the last cycle. The rotation speed of the samples was 150 rpm for all of the five cycles while rotating to the same direction as the grinding paper. Last two polishing operations were done with 3 mm and 1 mm extremely fine grain size papers. The force was dropped to 20 N for the 3 mm and to 15 N for the 1 mm wheel. The last two used surfaces were Dac and Nap. Both took 6 min with requirement of feeding

Dac3 (2nd to last cycle) and Nap-B1 (last cycle) solutions (no water!) every 30 seconds in order to keep the process lubricated.

After the sample preparation process was over, the samples were checked with microscope that there were no scratches. When samples were approved, the etching was done by using Nital 4% in order to be able to see microstructure of the surface.

Intentionally caused grinding burn samples were also prepared for the microstructural observation later on in order to see and confirm very likely grinding burns. The preparation (cutting) was done a bit differently since the samples had two to three distinctly different areas based on the level of grinding burn. As is showcased in Figure 25. The areas 4, 7 and 10 are same that was mentioned earlier. This was done to identify differences in microstructure between visually different burning marked areas.

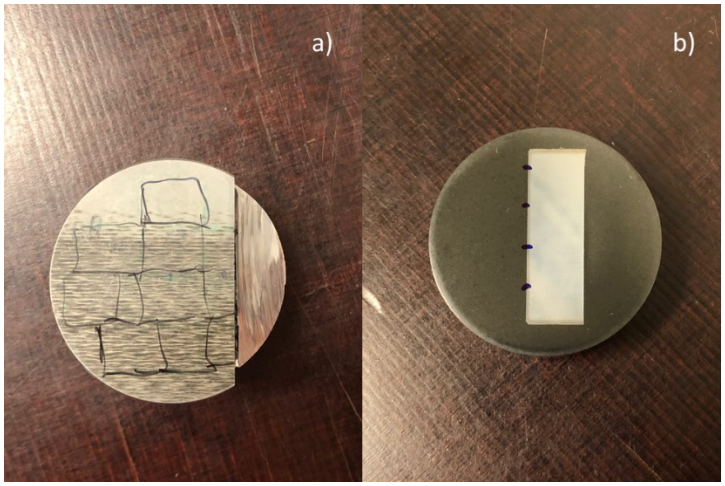

Figure 25. *a) Samples are cut so that 3 different areas can be seen 4, 7 and 10 and b) example of mounted sample for measurements.*

5.2.7 Hardness measurements

Cross-sectional hardness profile was done to the non-ground sample first. After the Nital 4% etching the sample was pressed with 1 kg weight in order to calculate Vickers hardness. Following the same line and steady intervals measurements were done to figure out the hardness depth profile. This was measured so that confirmation for effective and total case depth could be achieved. Choice of the testing method was depended on the hardening process used. CHD measures the distance from the surface to the hardness limit, point where the hardness reaches the HV value determined by the hardening process. The effective case depth is based on the HV1 test method where the 550 HV is the hardness limit. [8]

After other measurements, the most interesting samples (depths) were chosen to be studied with destructive testing methods. This included the hardness measurements for the chosen samples. The samples that were prepared for destructive testing and there for hardness profiles were also made from the chosen samples. The chosen samples as mentioned in the previous chapter were 0.1, 0.6 and 1.1. The hardness profiles were made by using Struers Duramin-A300 and software ecos 5.00.00. For the samples 0.1 and 0.6 (Al_2O_3, B126 and B181) the measurement distances were 0.15, 0.3, 0.5, 0.75, 1, 1.25 and 1.5 mm from the surface. For the 1.1 samples the measurements were done from 6 measuring points with distance of 0.25 mm between each measuring point. These distance selections were made based on the phases seen in the material during other measurements to guarantee enough distance between the measuring points. This was also determined by the testing round with the first two samples measured Al_2O_3 0.1 and 0.6.

Later on the decision to do hardness profiles from the rest of the samples between 0.1 mm up to 0.7 mm was made in order to see the variations in case depth values (effective and total). Same measurement distances were used as was used with samples 0.1 and 0.6.

Hardness measurements were also decided to be done to the intentionally caused grinding burn samples (N1, N2, N3, TUT6 and TUT8). The measurements were taken from the already marked areas (Figure 21.) for the BN measurements of these samples. With Struers Duramin-A300 near the center points of each marked area the hardness measurements were taken around the center point. Minimum of five measurements were taken from each marked area.

Later on microhardness measurements were also done by using Matsuzawa MMT-X7 with 40x objective, 300 g weight and 10 s dwelling time (HV0.3). This measurement was done to the intentionally caused grinding burn samples to further study the surface hardness levels and to confirm the type of the thermal damage in the samples.

6. RESULTS AND DISCUSSION

For this chapter the collected data is transformed to a presentable form (diagrams) and interpreted. Every measurement that was done towards this thesis is at least mentioned during the process of going through the results. There were loads of data and the most informative results are presented both visually and in writing.

6.1 Overall results

The first examination done to the normally ground batches was general visual inspection that did not reveal any grinding burns. The examination was continued with nondestructive testing methods. The final inspection methods were destructive for which some of the most interesting (with highest deviation) were prepared. All of the measurement processes have been explained earlier in chapter 5, in this chapter the results of all the measurements are going to be presented. In the order of the studies done for the sample batches, first the results for Al_2O_3 batch measurements are presented and right after that comes the results for the B126 and B181 batches.

The individual results for Newcastle University and Hiontatyö Tuomainen ground samples were analyzed at first before comparison. In order to make the result inspection more convenient, the comparison of the results is presented right after individual batch results. Conclusions of the differences/similarities that grinding wheels Al_2O_3 and CBN have are made based on the data.

6.1.1 Residual stress results

XRD residual stress measurement was the first test method used for the 20MnCrS5 samples. XRD was used to figure out what kind of residual stresses were present in the material and what were the values after the initial carburizing case hardening and oil quenching process. The measurements were done to three directions: 0, 45 and 90 degrees. 90 degrees was selected to be the grinding direction, meaning that 0 degrees was the perpendicular direction. From this point on 90 degrees is known as the direction of grinding. First round of measurements was taken from the center points of the ground surfaces. In the figures the results are presented for each direction. As can be seen from the Figures 26 and 27., residual stresses are the smallest in the direction of grinding and the highest compressive residual stress was into the perpendicular direction. In the study by Shouguo et al. [27] the results of the compressive residual stress were pointing out

that lowest compressive stress is in the direction of grinding. This is due to the mechanical effects that play major role in the formation of grinding-induced residual stresses since the grinding temperature stayed under 90 ºC. [27] Grit geometry is determined by the grit shape, therefore affecting to the rake angle, since the grits are randomly placed on the grinding wheel the grit rake angle can vary significantly even more than +45- -60º. Negative angle is not wanted since that leads to higher cutting force than with positive angles. Using low grinding velocity this is more obvious, but with higher grinding velocities the negative effect of negative rake angle is minimized. Figure 26. clearly shows the closing gap between the negative and positive rake angle when grinding velocity is increased. [50]

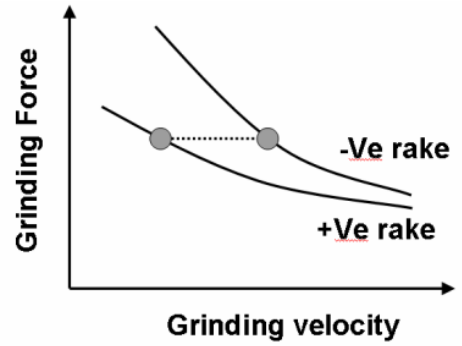

Figure 26. *The influence of the grinding velocity to negative rake angle and grinding force. [50]*

Other possible explanation idea found in the literature is that plastic deformation distribution differences over the ground surface while being effected by different constraint under grinding in parallel and perpendicular direction. [51]

XRD results

Examination revealed that the residual stress stays compressive until the whole layer is ground off. This can be seen from the measurement data received with XTRONIC-software where the results were compressive residual stress up to the 1.1 mm ground off. While the ground off depth increases and gets closer to effective case depth and total case depth, the compressive residual values decreases. When going closer to the total case depth of 1.2 mm (non-ground sample hardness depth profile), maximum case depth, the value of compressive residual stress is the smallest. The residual stress value is smallest to the direction of the grinding as theory and earlier studies suggest. The compressive residual value increases until 0.5 mm before starting to decrease. Residual

stress – ground off Figure 27. showcases the residual stress development through Al_2O_3 samples.

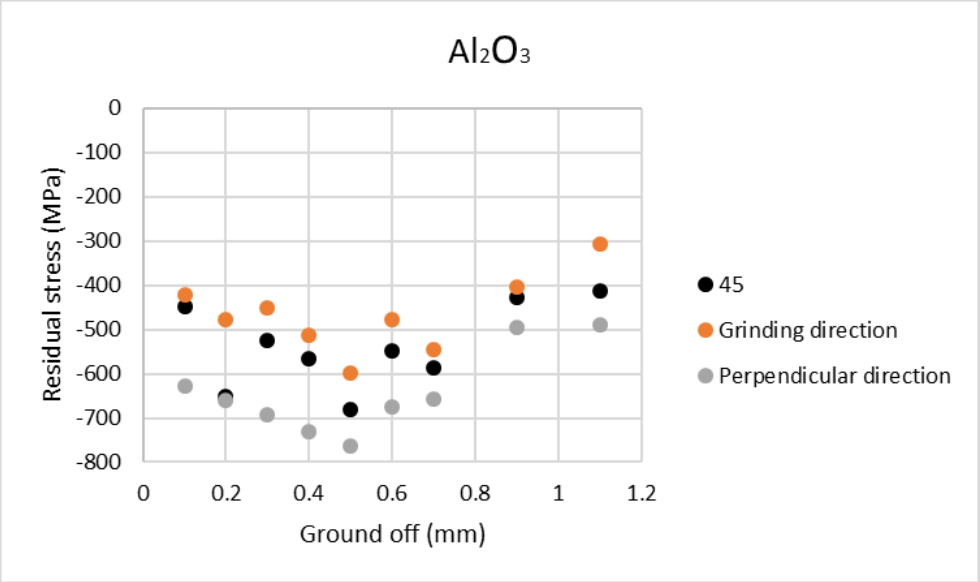

Figure 27. *Residual stress – Ground off.*

In the Figure 28 a). data was gathered with XTRONIC from the XRD measurements of samples ground with CBN B126 grinding wheel. The measurements show that the compressive residual stress was weakest in the direction of the grinding. In samples 0.1 to 0.5 mm compressive stress increased and rest of the samples decreased in similar pattern forming almost a “V”. The increase of compressive residual stress was steep, the low residual stress near the surface could be due to decarburization since it would lower the carbon content in the surface of the material and thus make it softer and influencing to the overall stress state. It needs to be pointed that surface stresses were measured from the ferrite phase, not from austenite phase. Due to this softer layer, lower residual stress value in the samples with less ground off could be seen. Decrease of compressive residual stress started to be rapid after sample 0.7 mm. After further studies, larger layer of retained austenite was detected in the B181 0.1 mm sample surface so instead of decarburization the retained austenite layer was the more likely reason to the low residual stress values since retained austenite layer was visible and martensite is harder phase than austenite.

The workshop Hiontatyö Tuomainen informed us that they noticed that B181 wheel had some issues. Hopefully the data reveals what was wrong with the grinding wheel. In Figure 28 b). the data that was gathered is presented from the 9 samples ground with CBN B181 grinding wheel. The measurements showed that the compressive residual

stress was the weakest in the direction of the grinding. First seven samples were following similar pattern quite well, but with the last two samples (0.9 and 1.1 mm) the compressive residual stress levels decreased significantly and fast. There is a possibility this is caused by the issue informed by the grinding operator or other explanation could be that material was ground more than asked. Later on other results will reveal that this was due to effective case depth being around 0.8 mm depth.

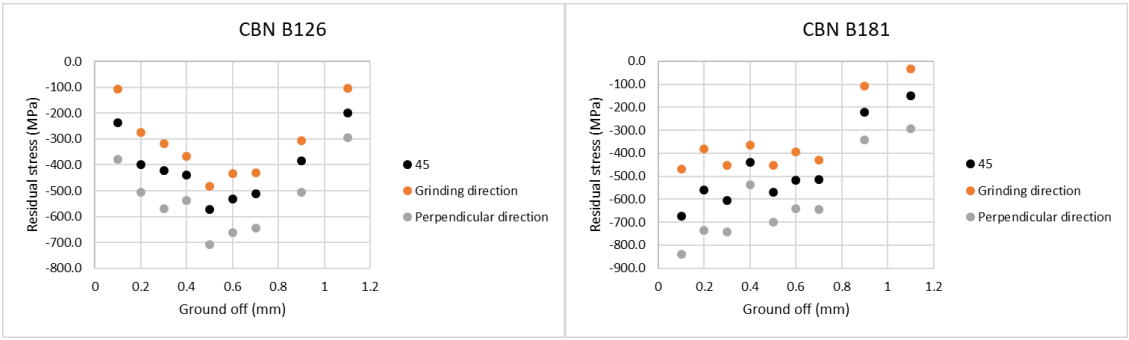

Figure 28. *Residual stress – Ground off CBN a) B126 and b) B181.*

Residual stress – ground off diagrams revealed the similar trend in every ground batch of samples. Every batch had fast change in the compressive residual stress value regardless of the grinding wheel after 0.7 mm. Only difference was that for CBN ground sample sets the value drops clearly lower than in Al_2O_3 ground sample set. From the Figure 1. It can be seen that the increase of compressive residual stress is typical curve behavior [2]. Similar behavior was seen in Al_2O_3 and CBN B126 ground samples. This would indicate that in CBN B181 the mentioned issues with the grinding wheel may have effected to the behavior of the measured results. In typical carburization, residual stress gradient is formed as can be seen from Figure 1.[2] which is also visible in the Figures 26 and 27 a). For the sample batches, this behavior in the Al_2O_3 and CBN B126 ground samples was quite clear.

In Al_2O_3 ground batch graph fluctuation can be seen in the first samples until 0.7 sample, similarly with the CBN B181 although the values have higher deviation. In CBN B126 the first five samples increase of compressive residual stress occurred before starting to decrease.

In the Figure 29. the FWHM XRD measurement was plotted with ground off layer. Profile went as it should and no deviation was seen compared to the different measurement

directions. All the directions, grinding direction, 45º and perpendicular direction values have very similar values. Most likely this correlates with the shape of hardness profile.

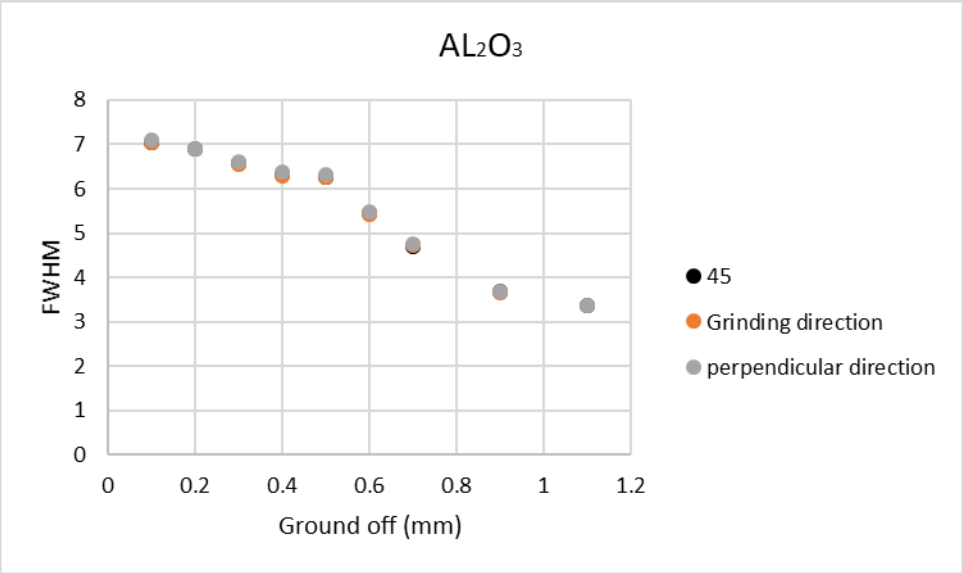

Figure 29. *Residual stress – Ground off.*

In the Figure 30 (a and b). the FWHM – ground off measurements are shown for B126 and B181. The profile goes as it should, without any deviation depending on the angle. Most likely this correlates with the shape of hardness profile. This meant that the value of FWHM decreased when the material got softer and compressive residual stress decreased.

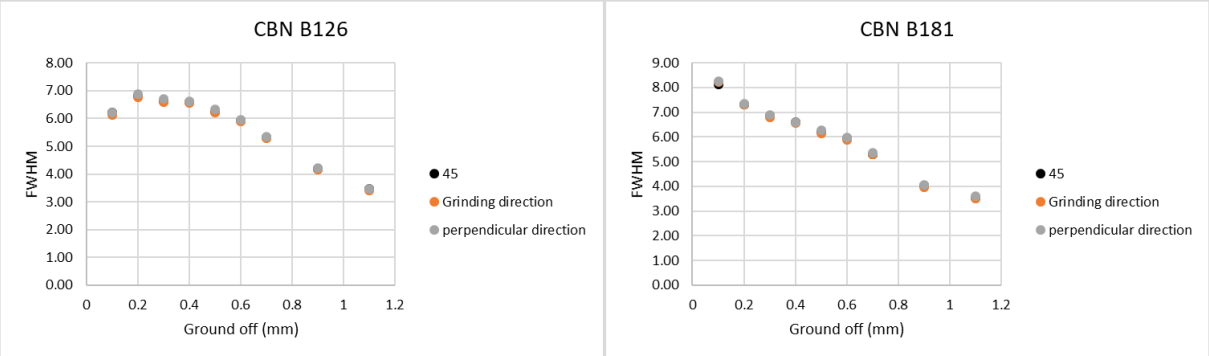

Figure 30. *FWHM – Ground off CBN a) B126 and b) B181.*

Same conclusions can be drawn from every batch, FWHM value decreased while removal of case hardened layer revealed the softer inner layers until the total case depth was removed to reveal the softer inner core.

Residual stress results outer measuring points

Residual stress measurements were carried out with four outer points (to the same directions what were used for the center measurements), similar distance away from the center. In Figure 31 (a, b, c and d). same residual stress – ground off -diagram was used to present the results. Every graph was made around one outer point, illustrated with letter A, B, C or D. Every point from all of the samples in a batch was in similar location so that the results can be compared. By looking at the Figure 31. it is clear that the surface residual stresses stays similar in the outer points. One result that can be seen to be as an outlier, is the 0.6 mm sample where the compressive stress value in 0º direction jumped lower than the 45º value. Otherwise the results are normal and compared to the center measurement, looking very similar and uniform.

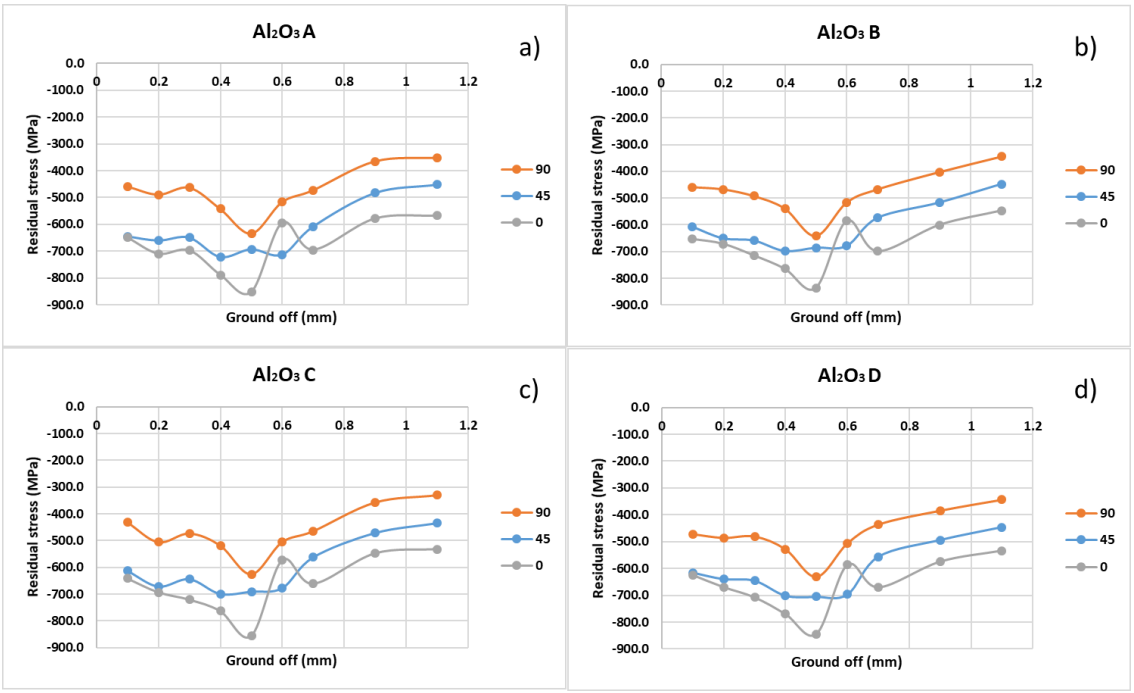

Figure 31. *Set of graphs of residual stress measurements from four different locations around the center of the samples ground with Al_2O_3. a) A, b) B, c) C and d) D point. Points are present in Figure 18 a).*

Residual stress measurements were carried with the same four outer points for batches B126 and B181, similar distance away from the center. In Figures 32 and 33 (a, b, c and d). the results are presented in the same residual stress – ground off figure like previously. Using letters similarly, results can be easily separated.

Figure 32. illustrates that the A, D and B, C are very similar. That can be explained with symmetry since the measuring locations A, D are basically same point only factor that

changes is the direction that the sample is looked at. If the sample is turned 180º the direction has not been influenced, only the viewing side for the direction of grinding.

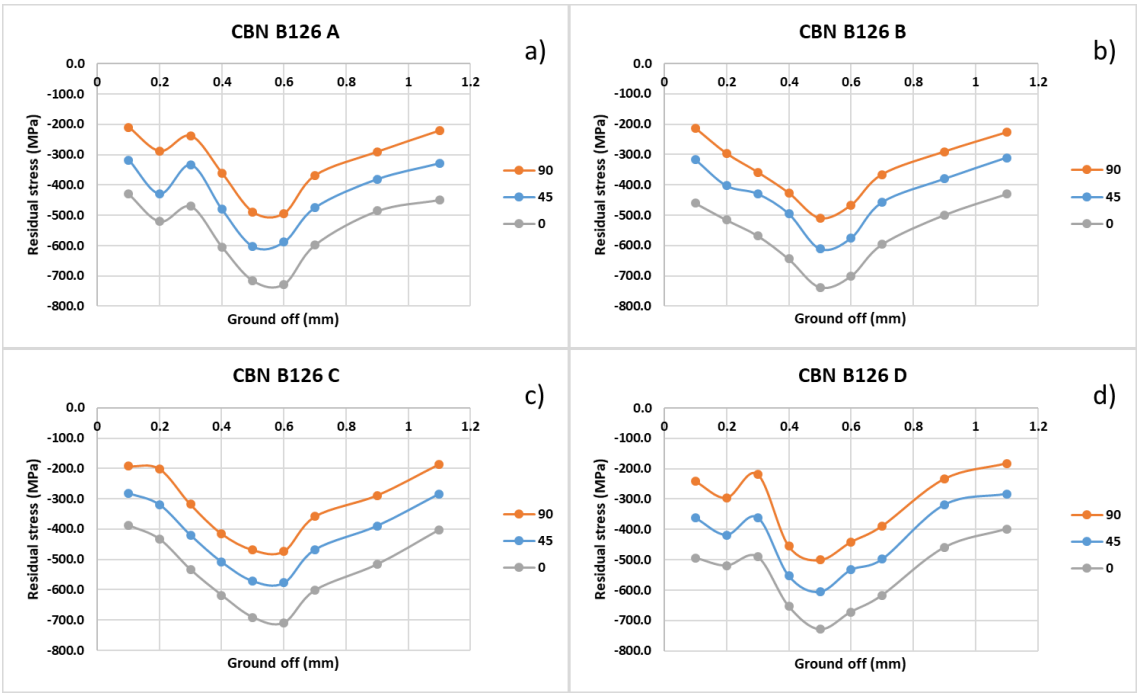

Figure 32. *Set of graphs of residual stress measurements from four different locations around the center of the samples ground with CBN B126. a) A, b) B, c) C and d) D point.*

Outer measuring points for B181 in Figure 33. are looking quite similar only bigger difference can be seen in the sample 0.2 mm. From sample 0.2 mm the deviation can be seen in the perpendicular direction where the value changes between ~ -590 and -710 MPa. Since this was the only larger deviation it was hard to verify that this would have been result of the mentioned issue with the B181 grinding wheel.

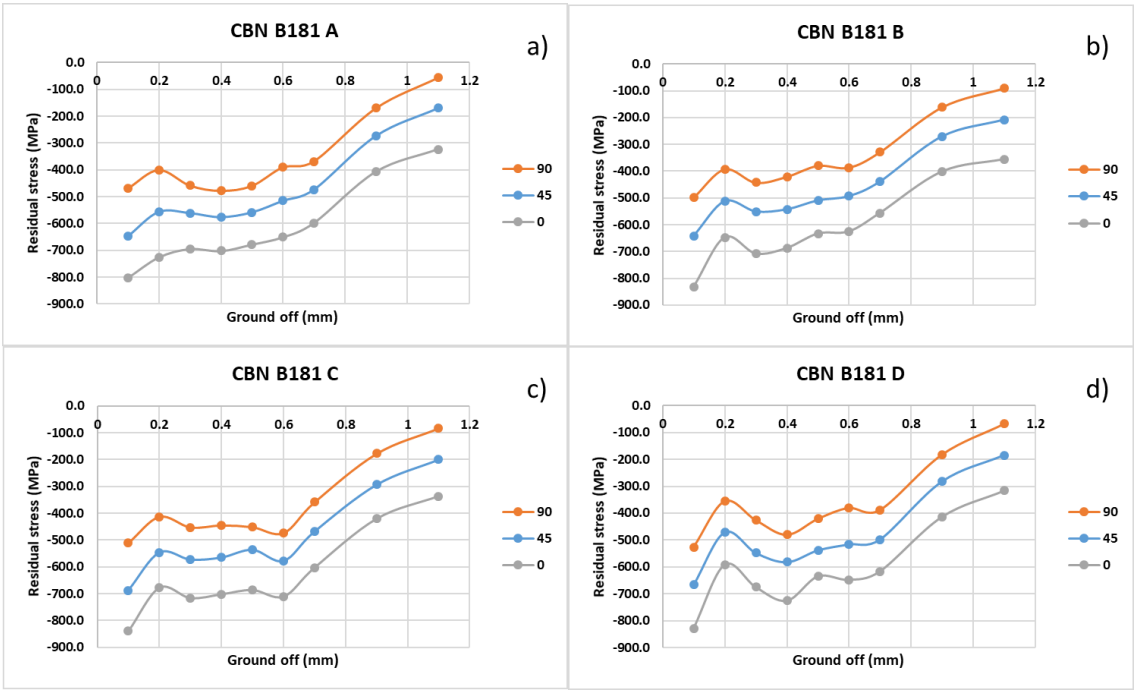

Figure 33. *Set of graphs of residual stress measurements from four different locations around the center of the samples ground with CBN B181. a) A, b) B, c) C and d) D point.*

6.1.2 Barkhausen noise results

Based on the Barkhausen studies with Rollscan 350 and sensor S6387 and using MicroScan software to collect the data, the following figures were created. Like in the earlier measurements, the 90 is the grinding direction and 0 is the perpendicular direction measurement. From the Figure 34. was noticeable that RMS values stay nearly constant until ground off layer reaches 0.6 mm. After this, for samples 0.7 and 0.9 RMS value rised rapidly and finally in the 1.1 sample the RMS curved back to lower value. RMS value stayed higher in the grinding direction in every sample. Low RMS indicates hard structure and this is due to the treatments done for the samples before grinding. After 0.6 mm something happens and in next samples compressive residual stress values drop fast. This tells that the material is softer near the total case depth which is a normal occurrence.

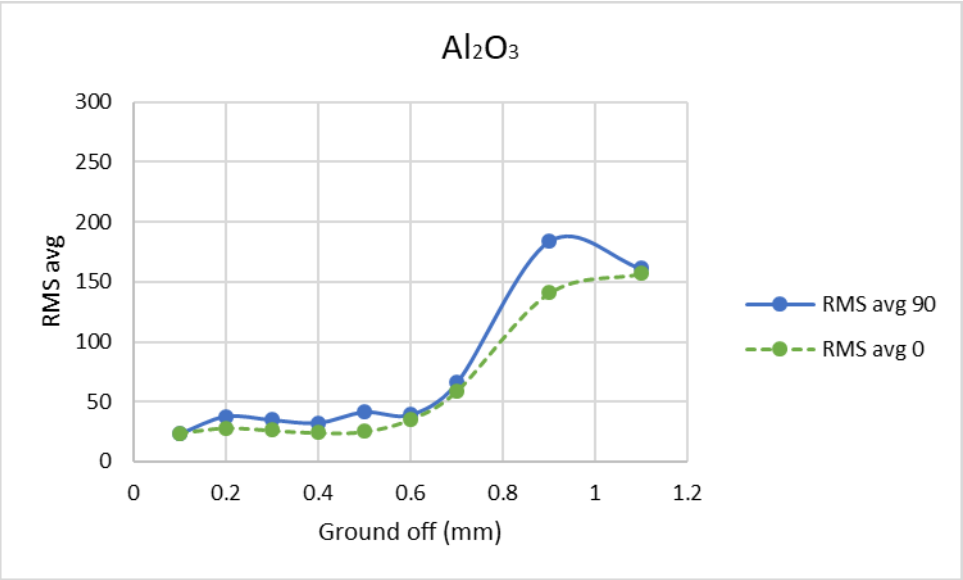

Figure 34. *RMS avg – Ground off for Al_2O_3 samples.*

From the Figure 35. it is noticed that until the sample 0.6 the RMS value stayed constant and after sample 0.6, the RMS value started to rise fast. Samples ground with B181 and B126 both have similar patterns, RMS value was higher in both batches into the grinding direction. CBN having higher RMS values and lower compressive residual stresses could be due to the issue informed to us with the grinding wheel but at this point of measuring and research, no deeper conclusions can be drawn from the RMS - ground off figure concerning possible defects in the grinding wheel B181.

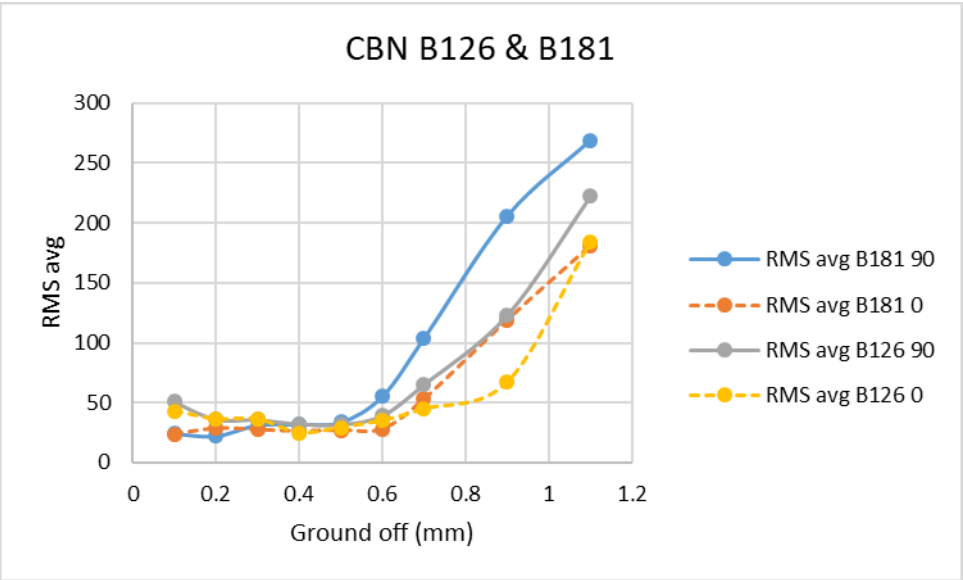

Figure 35. *RMS avg – Ground off for CBN B126 and B181.*

By comparing the RMS average – ground off diagrams of Al_2O_3, CBN B126 and B181, same kind of differences and similarities can be detected. In all of the ground sample batches the value stayed constant until the sample 0.6 mm. Based on the knowledge gathered from the theoretical studies, it is known that when compressive residual stress increases the RMS value decreases. Also when the hardness decreases the RMS value increases. Thus the constant values until 0.6 seen in the Figures 33 and 34. can be explained with these known facts. The combination of RMS lowering due to increase of compressive residual stress and RMS increasing due decrease of hardness due to case depth being ground off kept the value constant. [29, 35] After that the compressive residual stress started to decrease and deviation can be seen between the batches. Very similar behavior between B181 and Al_2O_3 batches can be seen until the last measurement where the RMS value further increased with B181 and started to decrease with Al_2O_3. Since the RMS value should increase when the sample gets softer, this might indicate that possibly higher surface roughness could cause the different behavior in the Al_2O_3 ground sample at 1.1 mm due to worse response to measurement.

The RMS – residual stress Figure 36. for the Al_2O_3 ground samples shows that the RMS values follows normal correlation of RMS – residual stress data. RMS value is small while the compressive residual stress value is high, following the correlation found in literature [52]. Since the RMS value was small and the compressive residual stress value was high, indications of carburized case depth layer being deep and the material being hard can be seen.

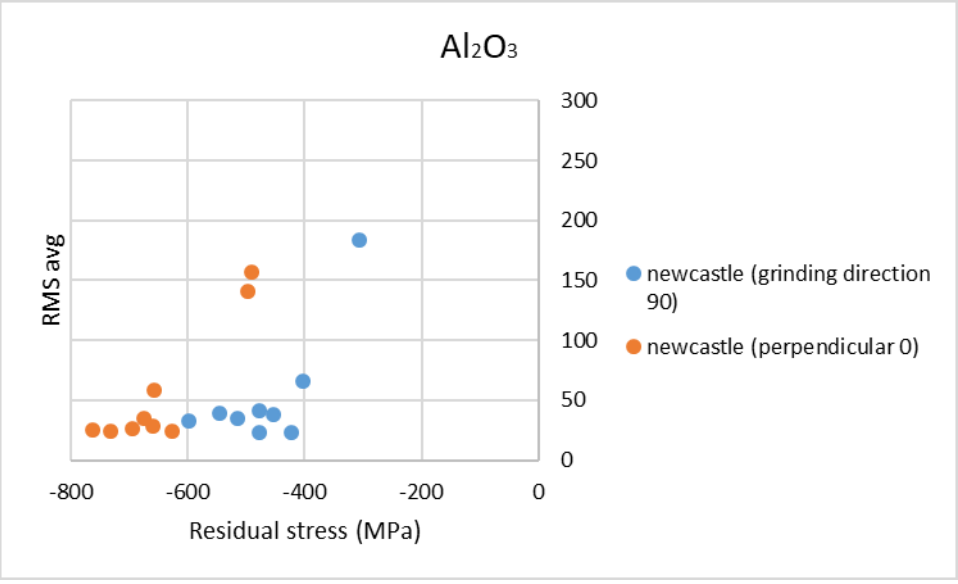

Figure 36. *RMS avg– Residual stress for Al_2O_3 samples.*

The RMS – residual stress Figure 37. for CBN B126 illustrates that the RMS values follow normal correlation of RMS – residual stress data. Some deviation can be seen in B126 into the grinding direction. Similarly CBN B181 values follow the normal correlation. The deviation noticed in the B126 can't be seen in the B181 ground samples. No signs of issues with the grinding wheel B181.

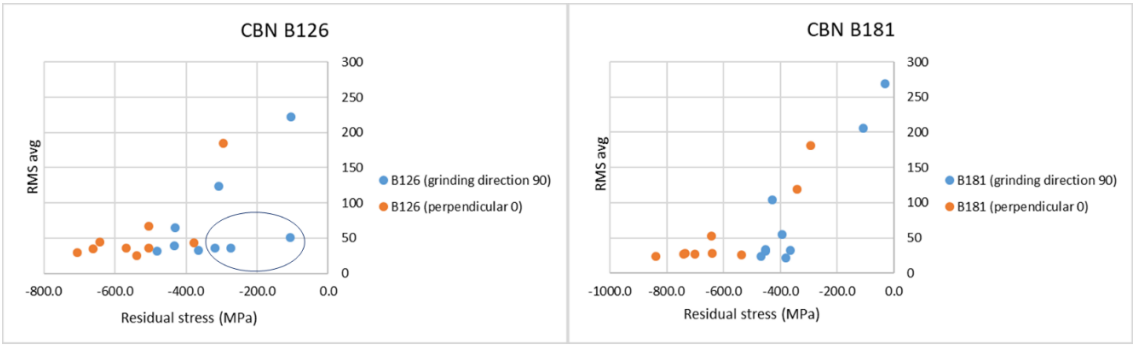

a) b)

Figure 37. *RMS avg – Residual stress for CBN a) B126 and b) B181.*

When comparing batches B126 and B181 to the values of Al_2O_3 batch, they are more compactly together in Al_2O_3. The deviation that can be seen in B126 batch could be due to the possibly deeper retained austenite layer in the surface of the first couple of samples. This might deviate the results since the compressive residual stress value at 0.1 mm and 0.2 mm samples was significantly lower than in either B181 or Al_2O_3. This oould be explained with the retained austenite layer since the layer is softer than martensite, layer before inner core material. Besides the RMS, also other features calculated from the Barkhausen noise signal with MicroScan software are studied.

BN Integral area – residual stress trend for the ground samples reveals similar behavior correlation with the residual stress as the RMS in the previous Figures 35 and 36 (a and b). Based on this, integral area behavior was similar than RMS. B126 had similar deviations as well.

BN FWHM – residual stress possibly correlates better with the residual stress than the RMS as presented in Figure 38. Very similar results can be seen for both directions.

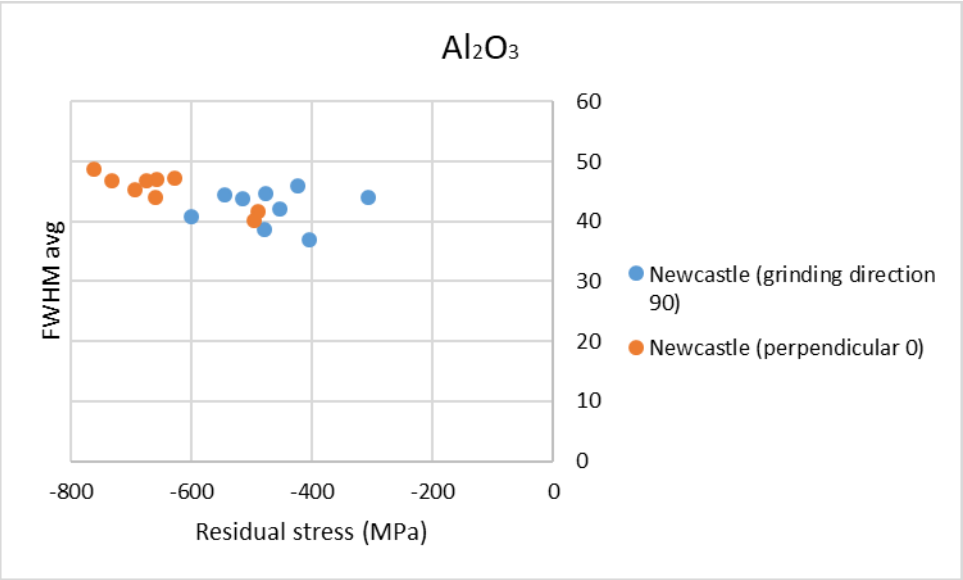

Figure 38. *FWHM – Residual stress for Al_2O_3 samples.*

BN FWHM – residual stress graph possibly correlates better with the residual stress than the RMS. This correlation is illustrated for both B126 and B181 in Figure 39 (a and b). Although B181 deviates a bit more.

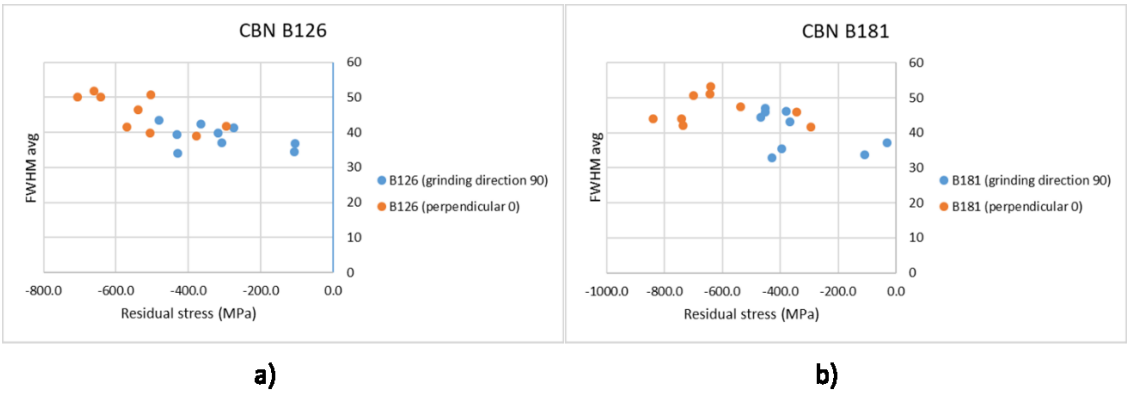

Figure 39. *FWHM avg – Residual stress for CBN a) B126 and b) B181.*

From the collected data can be seen that BN FWHM values increased with the increase of compressive residual stress and decreased when the compressive residual stress decreases. This correlation is clear in each batch, however, the deviation in the FWHM values is quite drastic. Since the measurements where repeated at least three times the values are quite consistent but if these where done with only one measurement, the results would vary a lot. In order to see the correlation, test must be done so that the values are taken as average of multiple measurements. The deviation that can be seen between the batches may be due to the high deviation in some of the samples measured.

Peak position average – residual stress graph measured with Barkhausen noise correlates well with the residual stress as presented in Figure 40. Higher value of peak position equals to higher compressive residual stress. Also, the deeper the material has been ground the peak position average gets smaller values. This can be explained with the softening material closer and after the effective case depth. Peak position generally correlates with the hardness [29].

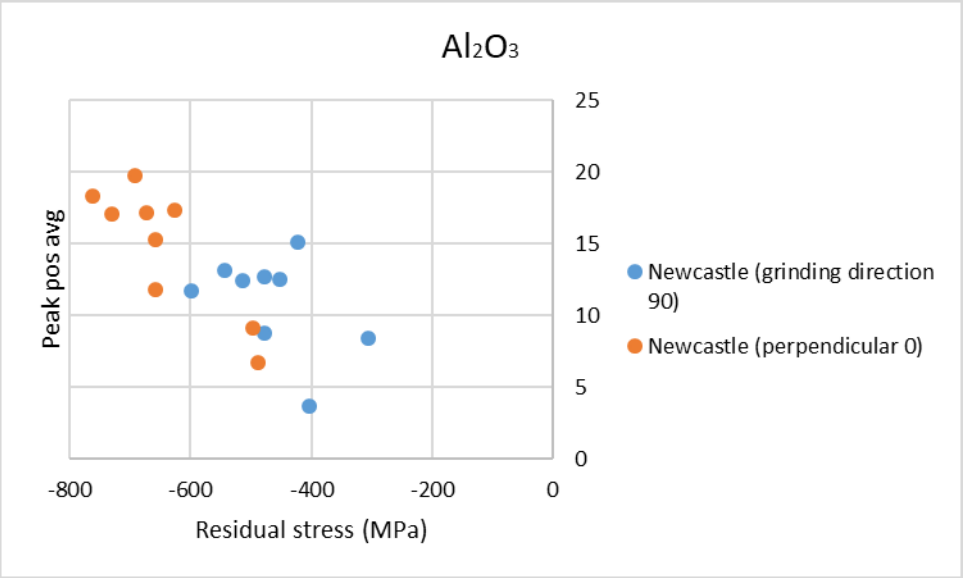

Figure 40. *Peak position avg – Residual stress for Al_2O_3.*

Peak position – residual stress Figure 41 (a and b), measured with Barkhausen noise correlates well with the residual stress. Some deviation can be seen in the CBN B181 wheel ground samples. This might again be caused by the issue mentioned by the grinding operator.

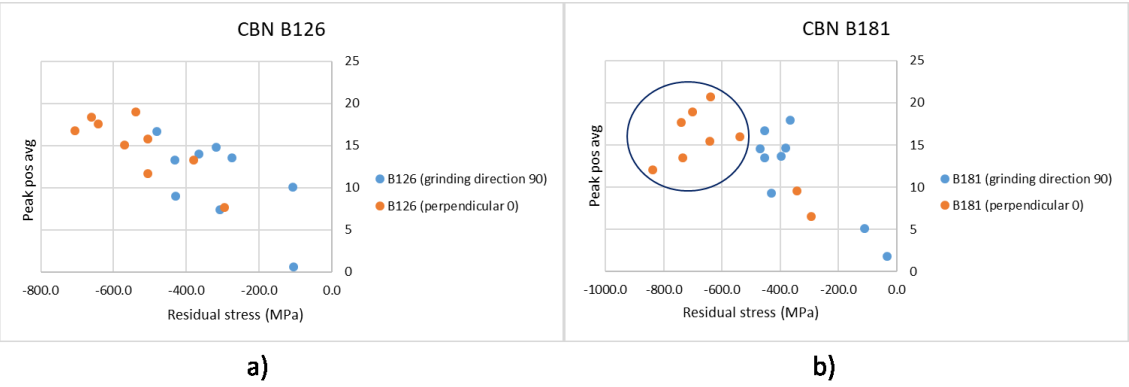

Figure 41. *Peak position avg – Residual stress for CBN a) B126 and b) B181.*

In all batches the peak position was higher into the perpendicular direction to the grinding. The peak position measurement in the diagrams is the average of three measurements and deviation could be seen in them. Meaning that the measurement results would likely differ from each other if another set of measurements would be done. Although the correlation would still be similar.

6.1.3 Surface roughness results

Alicona InfiniteFocus optical profilometry was also used to examine B126 and B181 sample's surface roughness. The measurements were not done according to standards. This was noticed late and the availability of the measurement device was limited. Due to this, some deviation can occur if roughness tests are repeated. Assumption is that the deviation is minimal.

The calculated parameters from the data for all samples: S_a, true projected area ratio, R_a, R_t, R_z and R_q. By comparing results between B126 and B181 grinding wheels, the difference that can be seen in true projected area ratio is small. The average for B126 was 1.03 and for B181 it was 1.02.This seems a bit odd since the lower the number is for the grinding wheel the better surface quality should be achieved. Even though these grinding wheels are close to each other's tolerances and the B181 had some issues it is possible that this can be counted as result variation. The surface roughness R_a averages were for B126: 4.08 µm and B181: 3.36 µm. Based on these results, B181 wheel has a better surface finish.

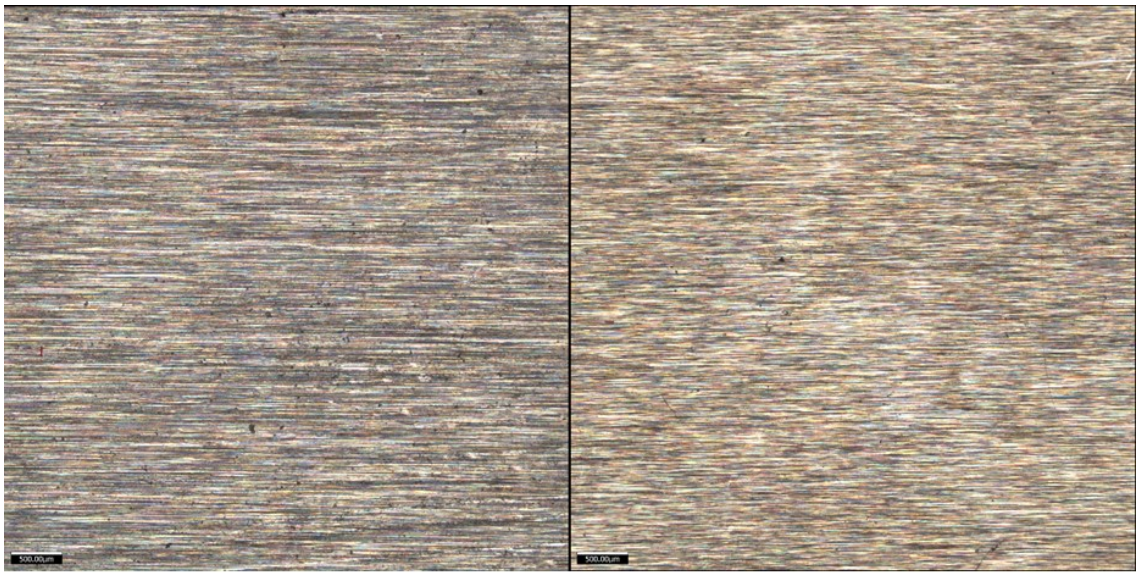

Figure 42. *Ground samples under Alicona optical profilometry. a) CBN B126 ground sample and b) Al_2O_3 ground sample.*

Average roughness R_a for Al_2O_3 ground samples was 6.039 µm and the true projected area ratio average was 1.061.

Figure 42. presents both differently ground samples captured with Alicona optical profilometry with a 2,5x magnification. From the average R_a values calculated for the sample batches, the worst surface quality based on the roughness was on the Al_2O_3 ground samples. The R_a average value of 6.04 µm was significantly higher than values for B126 (4.04 µm) and B181 (3.36 µm). Also the S_a value was higher, meaning that the value of true projected area ratio was also higher, backing up the R_a related conclusions about the surface quality differences between the CBN and Al_2O_3 ground batches. Interesting feature thought, for a naked eye, surface quality of the Al_2O_3 batch was better than neither of the CBN ground batches.

As mentioned in the sample introduction section of the thesis, the grinding wheel grain sizes vary from Al_2O_3 300-400 µm, B126 106-125 µm to B181 150-180 µm. By comparing the R_a values to grain sizes and looking at the theory, B126 should result as finer surface than B181 wheel. Since fine grit is stronger it should offer lower surface roughness [16]. As the Al_2O_3 has clearly the higher grit size (= bigger grains) it should have the worst quality surface of the batches. This raised a question, could this be due to mentioned issues with wheel B181 actually lowering surface roughness for some reason? Although it is important to take into the consideration that the measurements were taken from a small area and not quite following the standard since it was mentioned late.

6.1.4 PCCaseDepth results

In Figure 43 (a, b, c and d) are the results of slope of voltage sweep as a function of remaining case depth presented for both 20 Hz and 125 Hz for grinding and perpendicular direction. From the results can be seen that the calculated slope is higher in to the grinding direction. Also the effective case depth is visible since the values in each batch starts to rise when getting closer the effective case depth (around 0.8 mm) and after that rise is significantly faster. Similar patterns for the measured values can be seen between the 20 Hz and 125 Hz diagrams. Into the grinding direction interesting curvature can be seen between the 0.9 mm and 1.1 mm samples of Al_2O_3 batch (Newcastle). The curvature back to lower value is similar that can be seen in RMS avg – ground off graph for Al_2O_3 ground batch.

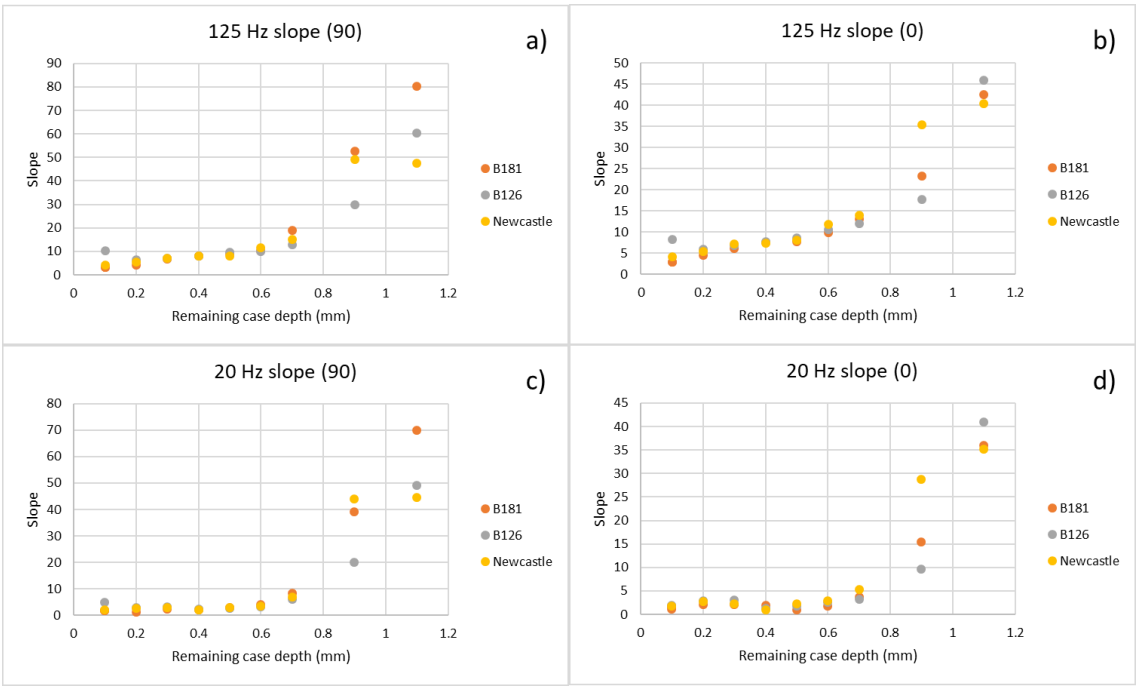

Figure 43. *Slope – ground off diagrams of measurements a) 125 Hz grinding direction b) 125 Hz perpendicular direction c) 20 Hz grinding direction and d) 20 Hz perpendicular direction.*

Before the knowledge that the effective case depth was around 0.8 mm these diagrams seemed to be not useful before the confirmation for the effective case depth was received the results are as expected. The results give clear indication that the effective case depth is around 0.8 mm since the slopes curvature increases significantly after around 0.7-0.9 mm.

6.1.5 Destructive testing results

In this chapter the results of material destructive test methods are shown and analyzed. Before going through the Al_2O_3 and CBN ground samples, destructive testing was done to one non-ground sample. From this sample a residual stress depth profile was made.

The first destructive testing method used was the electropolishing of the material surface in order to find out the residual stress depth profile of the non-ground surface. Figure 44. showcases the residual stress depth profile where the residual stress is presented as a function of depth below the surface.

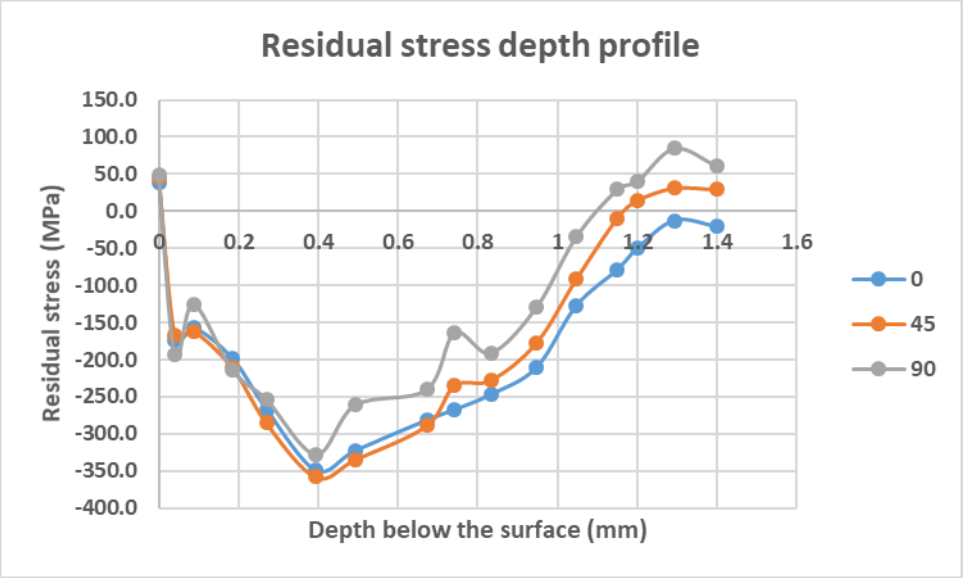

Figure 44. *Residual stress depth profile of the non-ground sample in directions 0, 45 and 90º.*

The uneven electropolishing of the material resulted in as a difficulty to get the material amount wanted polished off. The material was removed so that after few measurement depths the polishing happened lopsidedly, polishing the other half of the polished area much more aggressively. This made the approximation of the polishing cycles needed to get to the wanted depth difficult since the polishing could not be controlled. This can be seen from the Figure 44. The goal was to take measurements more frequently at the beginning, close to the surface and decrease the frequency of the measurements when getting deeper into the material. From the measuring depths in the x-axel, couple of bigger changes between the measuring depths can be seen. For example Figure 45. of the sample reveals the ridge that can be seen in the middle of the polished area instead of a cup shape (little bit of paper is in the polished area in order to give better contrast of

the shape). Due to the changing height and distribution of the polishing depth owing to uneven electropolishing, it was difficult to adjust the exact depths for the measurements.

Figure 45. *Polished non-ground sample (paper bits (examples of paper bits pointed out with arrows) used to showcase the depth and small hill at the bottom).*

The process of polishing was repeated mostly cycling two polishing runs and after that checking how deep the polished area was. The amount of runs depended how lopsided the polishing happened and how well the air was kept away from the polishing chamber. The more air bubbles were let in to the chamber during polishing, the less polishing happened per run. Since the total case depth of the samples (case hardened) was 1.2 mm (initial non-ground hardness depth profile) the residual stress depth profile was continued until 1.4 mm in order to see changes after the end of case hardened layer. Possible “error” or variation sources in this type of examination are the ability to keep the sample in the same orientation, measure the depth from the same spot and since the depth measuring device was on the Table 13. not to hit the table in order to keep the repeatable test results.

From the Figure 44. increase of compressive residual stress can be seen near the surface of the material before starting to decrease towards tensile residual stress after 0.4 mm. From the stress depth profile for the non-ground sample, FWHM – depth from the

surface was created, as seen in Figure 46. Again indicating that values follow the same pattern as they should, no deviation depending the angle.

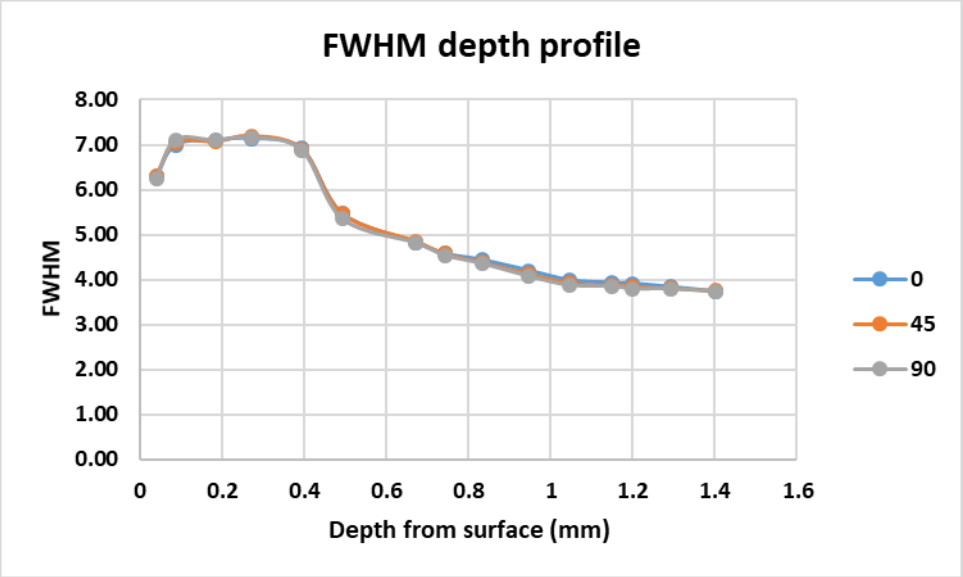

Figure 46. *FWHM – depth from surface for non-ground sample.*

Interesting point can be seen on the surface of the material before polishing. Values aren't compressive but tensile in the Figure 44. This is interesting since even with minimal polishing the values go compressive. Is there something in the surface that affects to the calculations or why does it show tensile instead of compressive? Is the surface finish too coarse before grinding that the surface shows as tensile stress? Or might there be a retained austenite layer influencing to the results? After further measurements most likely the reason is the retained austenite.

The XRD showed austenite content of the non-ground sample right under the surface (0.09 mm) to be 54.8 ± 4.2 %. Therefore, it is suggested that the deviation is caused by the high amount of retained austenite. The amount of austenite also confirms why the values in the different points on the surface of the samples, like 0.1, showed quite huge deviation on the residual stress measurements between the same layer's measuring points.

Hardness depth profile was done from the non-ground sample. The measurement was done with Struers Duramin with Vickers method. Determination of the case depth for the carburized sample was done by following the standard.

Before testing the non-ground sample was cut so that the sample's carburized top part could be mounted up for the cross-sectional hardness measurements. Starting from the

carburized end of the mounted sample, the hardness was measured as is presented in Figure 47. The measuring points actual distances from the surface were ensured by using Leica DM2500M optical microscope.

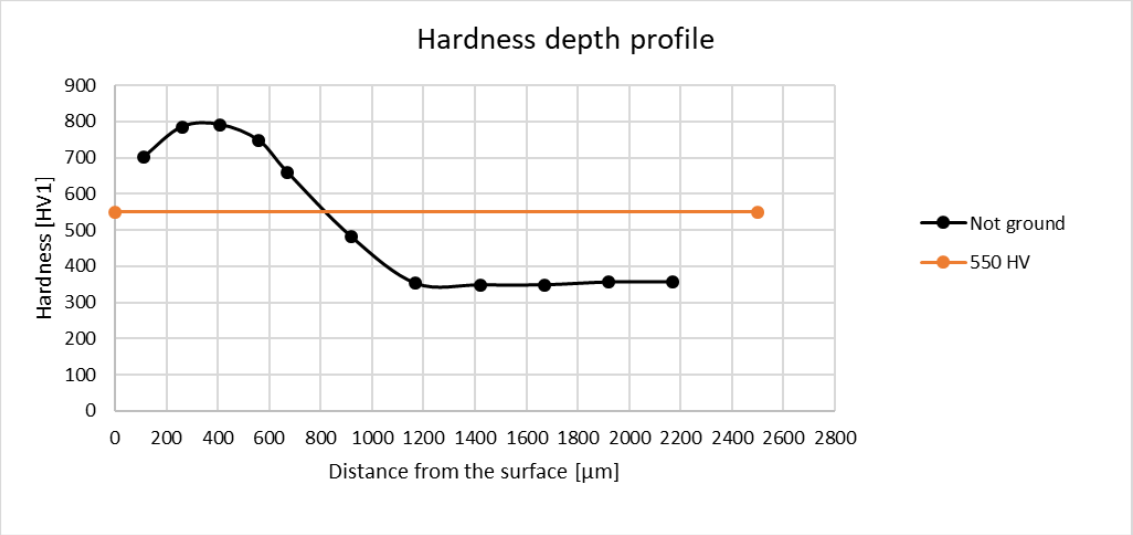

Figure 47. *Hardness depth profile taken from the non-ground sample.*

From the initial hardness depth profile it can be seen that the effective case depth was 0.8 mm. In the sample details total case depth of 1.2 mm has been informed. Depth of 1.2 mm was the point where the hardness has decreased to core hardness. 550 HV is the case depth limit for the carburized material, meaning that effective case depth is pointed to be where hardness drops to this value. Effective case depth of 0.8 mm explains few of the earlier results. Near surface decreased hardness was explained with the XRD austenite content measurement which revealed high amount of retained austenite near the surface.

The residual stress depth profile study that was done by using XRD and Struers Movipol-5 polishing machine, had a significant drop in compressive residual stress after 0.8 mm. This would explain the result since the effective case depth is only 0.8 mm anything after that is clearly softer. When the distance from the carburized case depth (=effective case depth) increases, the compressive residual stress decreases fast. Similarly this also explains both the RMS avg- ground off and residual stress- ground off graphs where rapid decrease of compressive residual stress can be seen after ~0.8 mm.

Hardness depth profile was also done to samples 0.1 up to 0.7 and for the intentionally caused grinding burn samples. The results for the remaining case depth and total case depth are shown in Tables 9 and 10.

Table 9. Remaining case depths for each sample based on the hardness depth profiles (550 HV).

Ground off (mm)	Remaining case depth (550 HV) Al_2O_3
0.1	0.53
0.2	0.46
0.3	0.46
0.4	0.41
0.5	0.32
0.6	0.15
0.7	0.08

Ground off (mm)	Remaining case depth (550 HV) CBN B126
0.1	0.36
0.2	0.67
0.3	0.62
0.4	0.32
0.5	0.25
0.6	0.14
0.7	0.1

Ground off (mm)	Remaining case depth (550 HV) CBN B181
0.1	0.82
0.2	0.66
0.3	0.53
0.4	0.35
0.5	0.25
0.6	0.11
0.7	-

N1	Remaining case depth (550 HV)
4	0.73
7	0.7
10	0.63

N2	Remaining case depth (550 HV)
4	0.75
7	0.75
10	0.82

N3	Remaining case depth (550 HV)
4	0.74
7	0.73
10	0.825

TUT6	Remaining case depth (550 HV)
4	0.77
7	0.66
10	0.78

TUT8	Remaining case depth (550 HV)
4	-
7	-
10	-

From the hardness depth profiles the remaining case depth was observed from the point where the hardness level (550 HV) met the hardness curve of the sample. The results deviated quite a lot. Most significant deviation can be seen in CBN B126 0.1 sample with a remaining case depth of 0.36. Also from the microstructure images difference of the CBN B126 compared to other 0.1 samples was clear. This may be due to deeper grinding than what was planned. If the 0.1 is omitted, the remaining case depths of CBN ground samples are similar. Al_2O_3 values on the other hand are inconsistent. Possible deviation might have happened in the samples during initial heat-treatment of the samples. Possibility of different temperatures, placement and exposing times could have lead the effective case depth to settle in different layer. This conclusion can be drawn from the deviation in the case depths of the non-ground samples.

Table 10. *Total case depths of the samples measured from the hardness depth profiles (Determined from the point where the hardness fluxuation stops).*

Ground off (mm)	Total case depth Al_2O_3 (mm)
0.1	1.2
0.2	1.2
0.3	1.25
0.4	1.3
0.5	1.5
0.6	1.4
0.7	1.45

Ground off (mm)	Total case depth CBN B126 (mm)
0.1	1.2
0.2	1.35
0.3	1.45
0.4	1.45
0.5	1.45
0.6	1.4
0.7	1.5

Ground off (mm)	Total case depth CBN B181 (mm)
0.1	1.25
0.2	1.5
0.3	1.4
0.4	1.5
0.5	1.5
0.6	1.45
0.7	1.5

N1	Total case depth (mm)
4	1.2
7	1.2
10	1.2

N2	Total case depth (mm)
4	1.2
7	1.15
10	1.2

N3	Total case depth (mm)
4	1.4
7	1.2
10	1.1

TUT6	Total case depth (mm)
4	1.35
7	1.35
10	1.2

TUT8	Total case depth (mm)
4	1.1
7	1.45
10	1.3

In the Table 10. are the total case depths of the samples including the ground off. Meaning that the intended ground off is added to the values in order to keep the total case depths easier to be compared. From the total case depths deviation can be seen. This could be due to the initial heat treatment process or due to possible mistakes in intended grinding depths of the samples.

By compiling these effective values with RMS average values taken from the surface of each sample (0.1-0.7), Figure 48. can be created to compare with the earlier results that included ground off instead of remaining case depth.

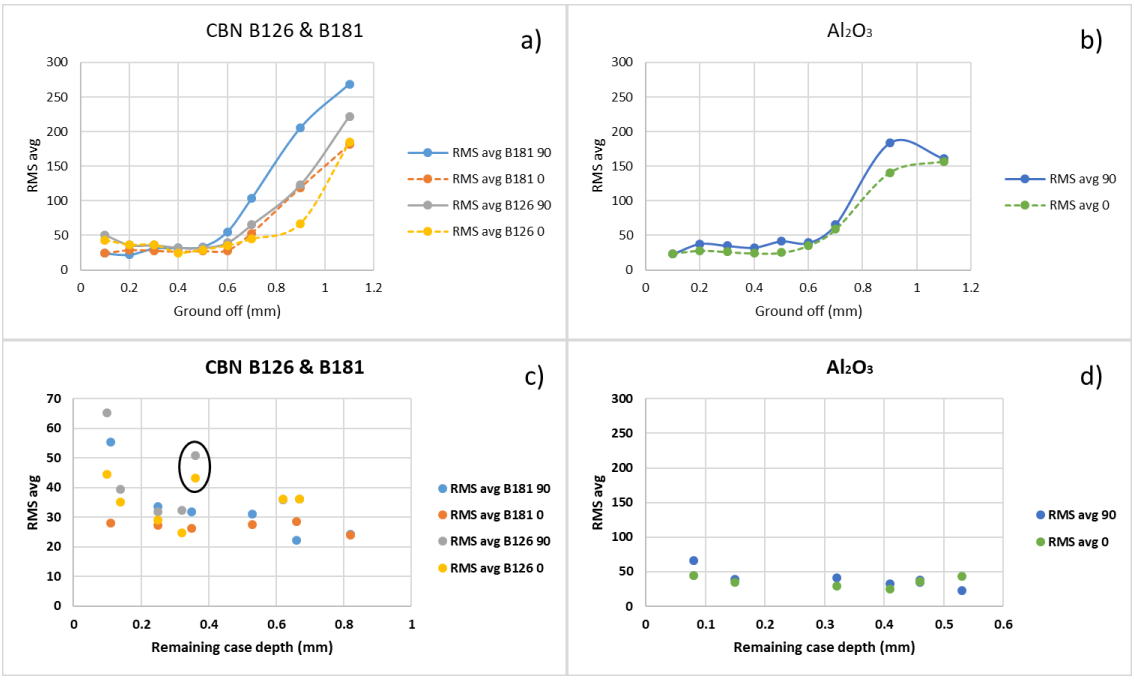

Figure 48. *a and b earlier RMS – ground off measurement results and c and d are the RMS – remaining case depth measurement results.*

By comparing these, decent correlation can be seen meaning that in most samples resulted depth followed in the lines of originally planned grinding depth. The effective case depth Figure 48 (c and d) are a mirror image of the ground off Figure 48 (a and b). The most significant deviation was in the B126 0.1 sample (circled) only stating 0.36 mm as the remaining case depth. This with the added originally planned grinding depth is 0.46 mm clearly lower than in the other samples ground with CBN B126.

This similar observation of shorter transition between case and core for B126 0.1 sample was also made with optical microscopy in the later measurements (next chapter).

In the Figures 49 and 50. can be seen the hardness – remaining case depth measurements. In the Figure 49. are the measurements only including the actual remaining case depth based on the hardness (HV1) measurements and in the Figure 50. the ground off has been added.

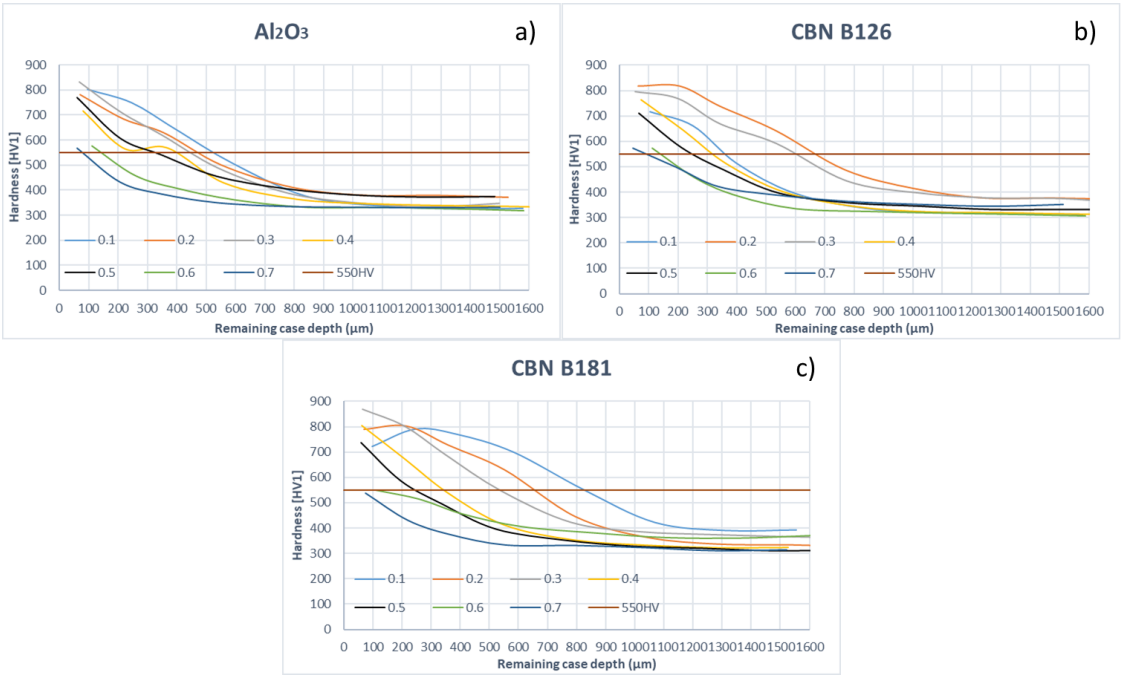

Figure 49. *Hardness remaining case depth measurements for the normally ground samples.*

In the Figure 49. The horizontal line is the hardness 550 HV indicating the remaining case depth of the sample in the point were the lines cross each other. Deviation can be seen from the results.

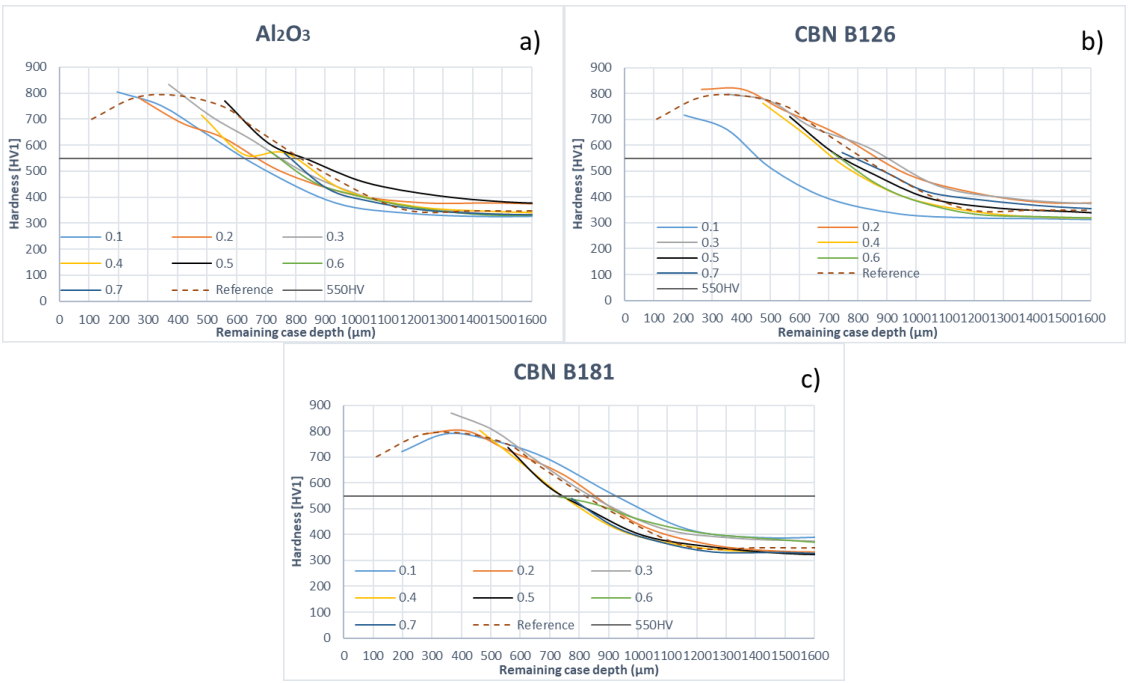

Figure 50. *Hardness remaining case depth measurements for the normally ground samples, ground off added.*

From the Figure 50. it is obvious that there is deviation. In the Figure 50. the sliced line presents the initial hardness depth profile for the non-ground sample. These deviations in the 550 HV line are too high to be happened in the sample preparation. Explanation therefore could be in the heat treatment process. To test the possibility of the error being in the heat treatment process, from two more non-ground samples the hardness depth profile was measured. In the Figure 51. are the non-ground sample hardness depth profiles.

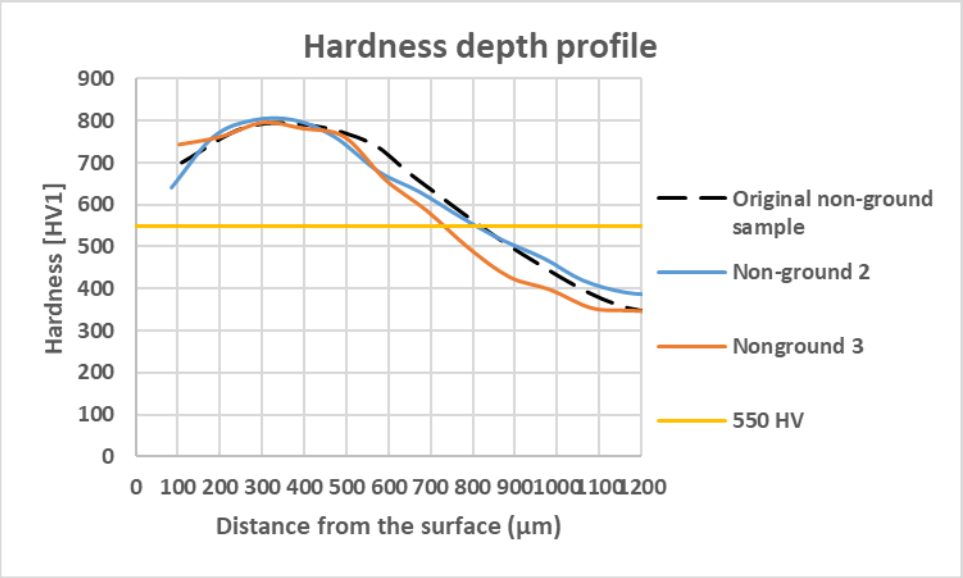

Figure 51. *Non-ground samples hardness depth profiles.*

The results clearly show deviation in the non-ground samples effective case depth, thus leading to conclusion that the original heating treatment process may have been the most likely cause for the differences in case depths measurements.

Optical observation of materials

Optical microscopy results for verifying remaining case depth values after grinding were taken with Nikon Eclipse MA 100. Figure 52. shows non-ground sample measured with Vickers hardness test. Next Figure 53. from a non-ground sample is introduced. From these images, taken with magnifications 5x and 10x, retained austenite can be seen on the surface layer (right side of the image). The retained austenite layer was not constant but instead its depth varied. Hardness measurements and optical observation backed up by XRD austenite content measurement near surface. This explains the deviation in the outer XRD point measurements in the samples surfaces, since the retained austenite

might be still on the surface and in some of the measurement points causing this deviation. After martensite layer, the core material layer starts.

Figure 52. *Vickers hardness test for the non-ground sample.*

Figure 53. *10x magnification of the non-ground sample.*

From the actual ground samples similar inspection was done. From each batch the samples giving the most interesting results were chosen to be prepared and examined. Therefore from each batch samples 0.1, 0.6 and 1.1 were chosen (reasons mentioned in the theory section). The images are in the row so that the interpretation and following of the results would be easier. In the figures black arrow indicates the martensite layer, the gray arrow initial material (20MnCrS5) and red arrow retained austenite layer. Later on decision to prepare all the samples was made.

First set of images consist of the sample 0.1 from each batch. Images have been taken with the magnification of 5x. In Figure 54 a). the sample from the batch Al_2O_3 is shown, in Figure 54 b). is the sample from the B126 batch and in Figure 54 c). is the B181 batch sample. Each of the figures green lines are drawn to determine the microstructural

changes (for example transition between the case and the core). These are presented in the Figure 54.

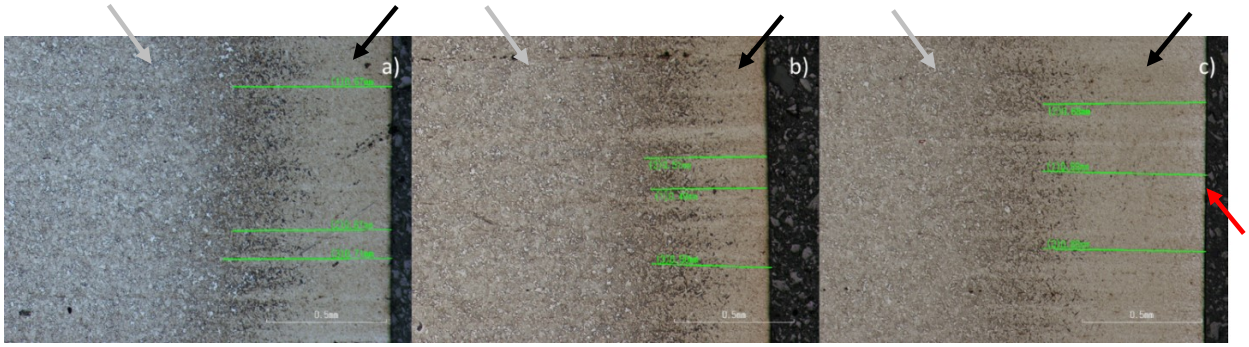

Figure 54. *Microstructural 5x image of a) Al_2O_3 0.1, b) B126 0.1 and c) B181 0.1. Martensite layer (black arrow), initial material (gray arrow) and retained austenite layer (red arrow).*

Each sample had a clear martensite layer. At least in the surface of the sample B181, a layer of retained austenite can be seen that most likely has caused the differentiating results based on the hardness measurements and optical observation backed up by XRD austenite content measurement near surface. This is due to fact that austenite is softer than martensite and since the layer thickness of the retained austenite seems to differ based on the earlier studies, it would create lower hardness on the near surface layers.

By comparing the microstructural transitions, variation can be seen. With Al_2O_3 the distance is roughly 0.68 mm. For the B126 the distance is 0.50 mm and for the B181 it is roughly 0.68 mm. For the B126 sample the measured distance was only 0.5 mm. This deviates from the Al_2O_3 and B181 samples and from the already measured distance. This raises couple of questions in the open, was this due to mistakenly grinding too much away or were the initial heat treatments to create the wanted case depth not homogeneous? No grinding burn indications were visible in any of the samples.

The next sample that was examined from each batch was sample 0.6. Images have been taken with the magnification of 5x as presented in the Figure 55 (a, b and c).

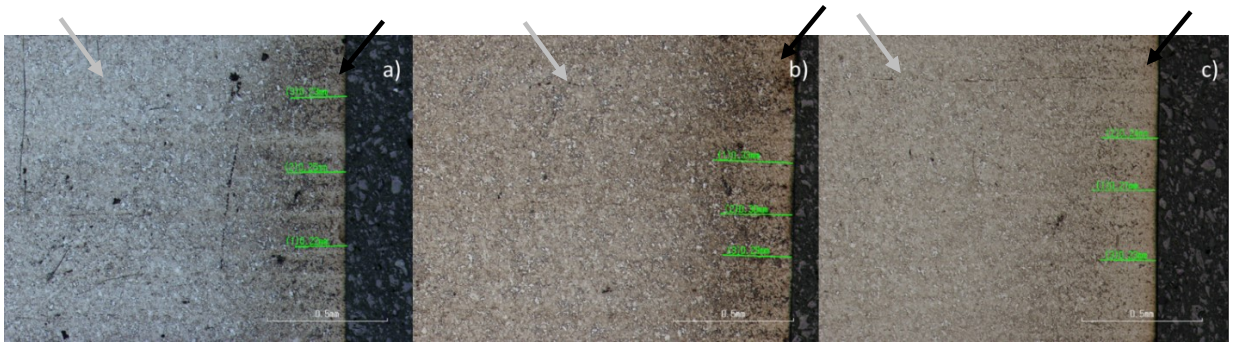

Figure 55. *Microstructural 5x image of a) Al_2O_3 0.6, b) B126 0.6 and c) B181 0.6. Martensite layer (black arrow), initial material (gray arrow).*

The retained austenite layer has disappeared from the surface as expected and the distance to the transition depth has narrowed. For the sample of batch B126 the distance is now around 0.3 mm. Similarly, sample from the batch B181 distance is 0.25 mm. The sample from batch Al_2O_3 gives the closest distance to transition depth with a distance of 0.23 mm. This would suggest and further back up the theory of too deep ground in sample 0.1 from B126 batch due to the fact that there was practically no deviation in the B126 0.6 sample compared to other 0.6 samples. No grinding burn indications visible in any of the samples.

Last sample from each batch was 1.1. These are illustrated in the Figure 56 (a, b and c). Images have been taken with the magnification of 10x.

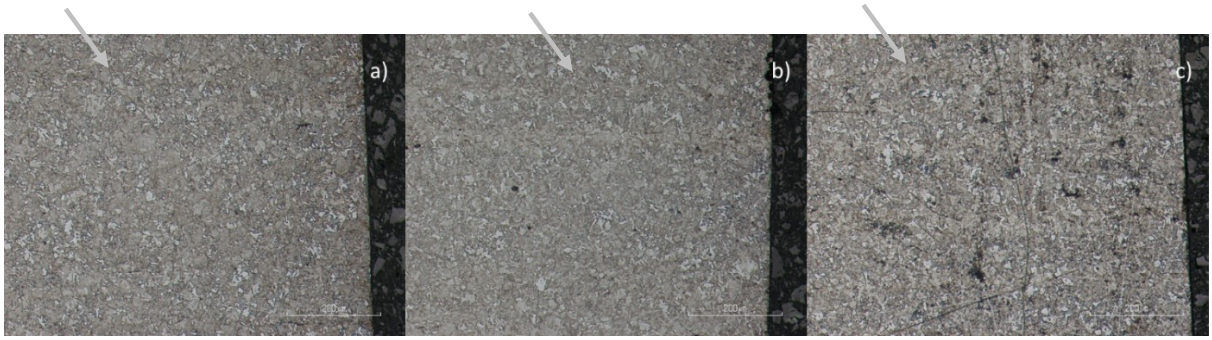

Figure 56. *Microstructural 10x image of a) Al_2O_3 1.1, b) B126 1.1 and c) B181 1.1. Initial material is indicated by gray arrow.*

Last sample from each batch was 1.1. As the images show there is no martensite case layer left anymore, the material is the original material before heat treatment. No differences in the quality nor any visible grinding burn indications in any of the samples.

The decision to cut the rest of the samples as well was made. Since the amount of the samples is quite considerable, the results of the other measurements are mentioned in

a table instead of figures. This is done to ease the interpretation of the results. Only the samples selected in the first place are also informed with figures, since the results pointed them originally out as most interesting ones. In the Table 11. all case-core transition distances are shown.

Table 11. *All of the case-core transition distances.*

Ground off (mm)	Al_2O_3	CBN B126	CBN B181
0.1	**0.68**	**0.5**	**0.68**
0.2	0.6	0.59	0.62
0.3	0.5	0.52	0.49
0.4	0.39	0.39	0.39
0.5	0.31	0.3	0.25
0.6	**0.23**	**0.3**	**0.25**
0.7	0.11	0.11	0.09
0.9	-	-	-
1.1	-	-	-

6.1.6 Results from intentional caused grinding burn samples

The samples that had intentionally caused grinding burns were examined by using Barkhausen noise. Few test measurements were done to see what kind of values and areas would be most beneficial to measure before the actual measurements. During this testing period it came clear that the BN RMS response was consistently higher to the grinding direction. Every point marked to the sample was measured once for the grinding direction and to the perpendicular direction. As mentioned in Barkhausen noise measurements - chapter, the measurements for the grinding direction were taken from the middle of the block. The measurements for the perpendicular direction were taken from the outer side of the corner blocks, except the sample N1 in which lower part of the blocks were measured from the inner side. Perpendicular direction of the middle blocks were measured from the right side of the blocks.

After measuring the samples and collecting the data to MicroScan, it was transferred to excel and edited to easier interpretation state, diagrams. From the diagrams it was easy to see that the RMS value into the direction of grinding is higher most of the time. This is showcased in the Figure 57 (a-e). Blue is the direction of the grinding (90) and orange is the perpendicular direction (0).

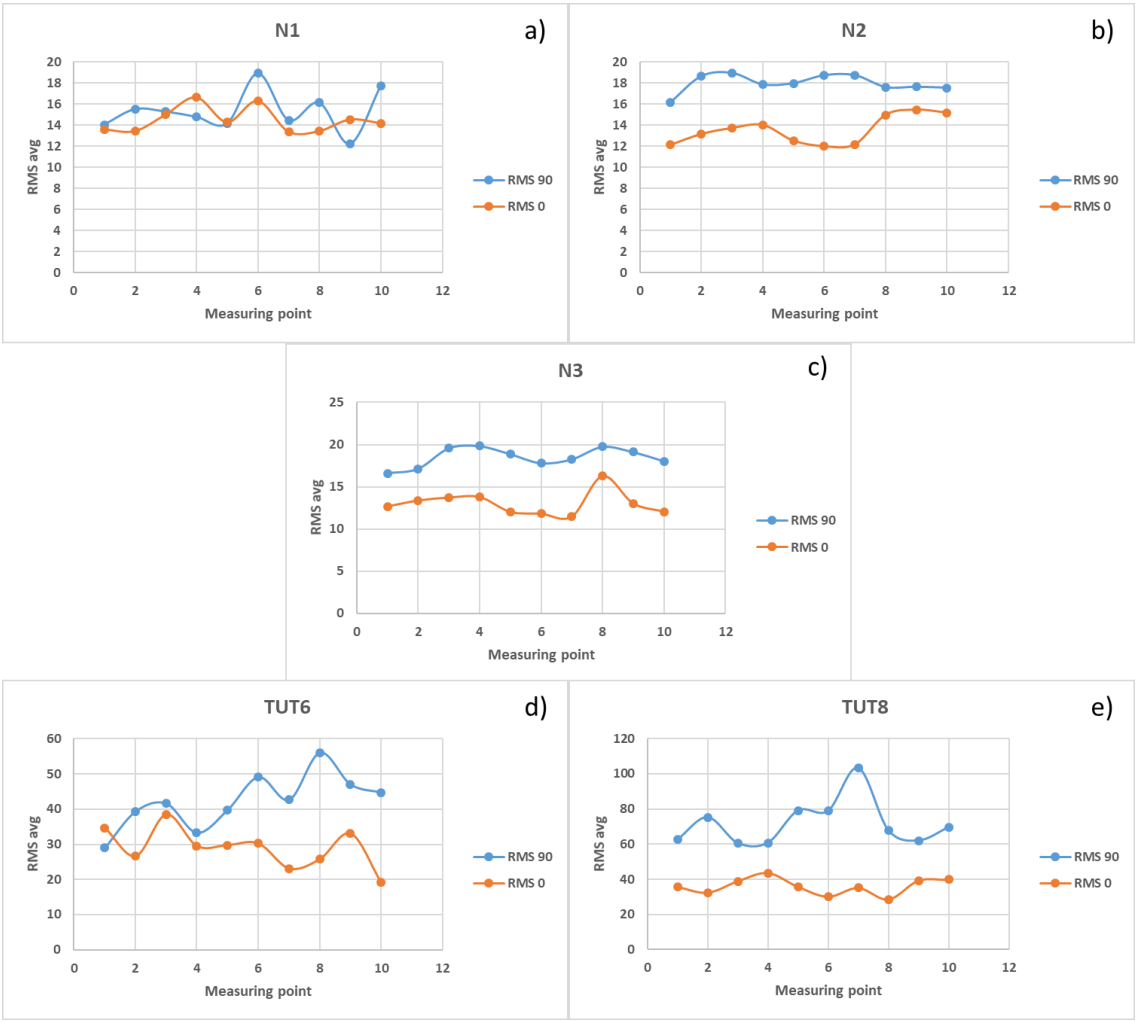

Figure 57. *RMS data for each of the grinding burn samples for both grinding and perpendicular direction. A, b and c ground with Al_2O_3 wheel and d and e ground with CBN wheel.*

From the Figure 57. it was obvious that in sample N1, the values deviated a lot and similar correlation can't be seen than in N2, N3 and TUT8 where the values for the grinding direction were seemingly higher compared to perpendicular values.

In a study by Thanedar et al. [15] observation was made, that the increase of the work speed decreases the temperature in grinding zone due to the less time abrasive grains spend in contact with the workpiece, decreasing also the BN response. [15] Based on this study the results are in order. The RMS values were higher in N3 sample which had the lower work speed compared to sample N1. Sample N2 was not counted to this comparison since the depth of cut also influences the BN response and it was different than the one that was used to ground samples N1 and N3.

There is also significant difference in the RMS values between N and TUT samples. The N samples stay mainly 10-20 RMS while TUT samples vary around 20-100 RMS. Based

on the look of the samples (Figure 15.) N samples should have been sustained more “damage” compared to TUT samples which are not even close to being visually in the same shape as the N samples. However, it should bear in mind that for the TUT samples the case depth was almost ground off.

Residual stress measurements were done to the N and TUT sample sets with XRD. From the residual stress standing point the compressive residual stress was significantly lower in N than TUT samples, even shifting to tensile residual stress in some measuring points of the grinding direction. The results of XRD measurements are presented in Figure 58. The measuring points are presented in Figure 21. There are total of 10 measuring points and starting from the top layers were named A, B, C and D. from left to right numbering goes 1, 2 and 3. In these graphs measuring point 1 corresponds measuring point A1, 2 measuring point B1 etc.

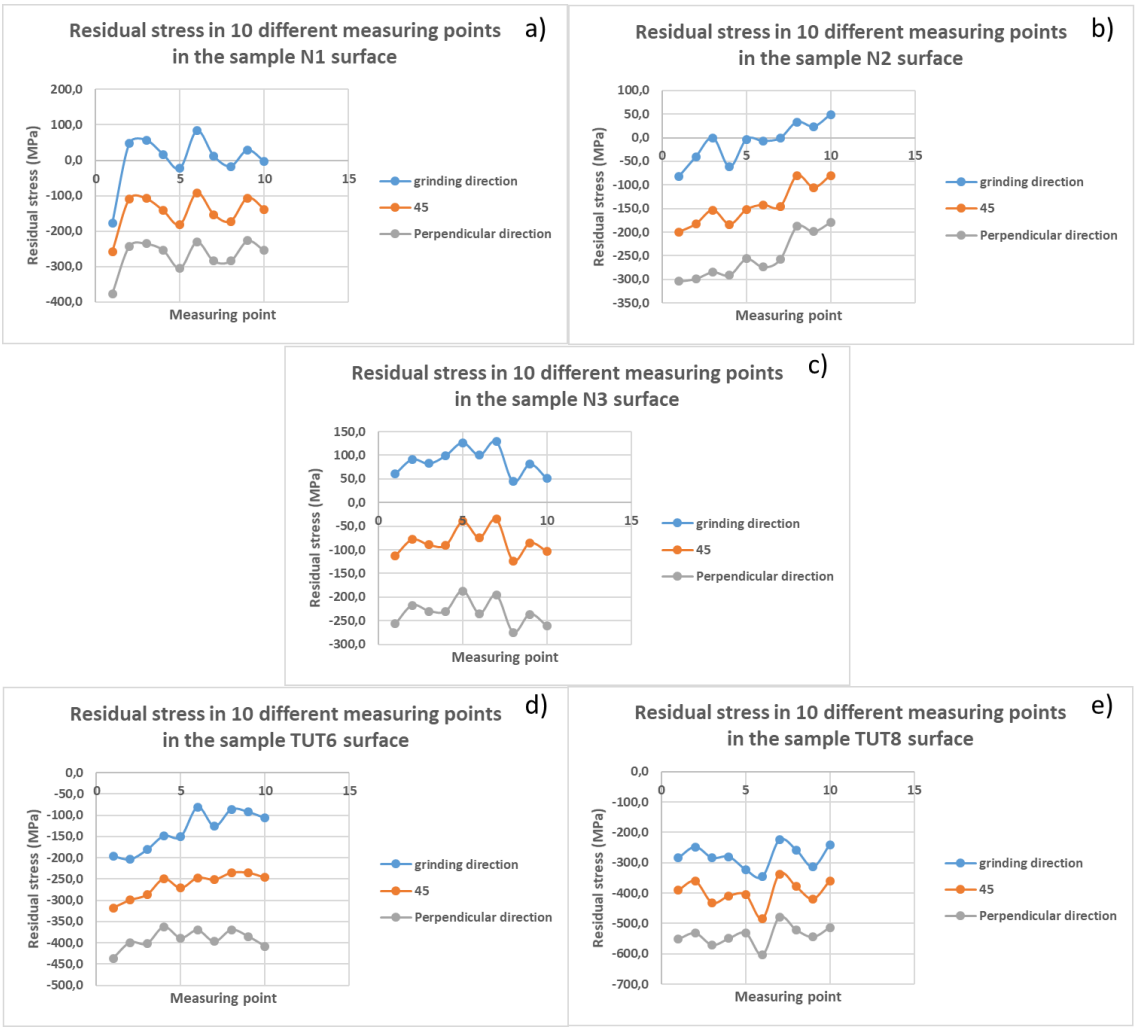

Figure 58. *Residual stresses in intentionally caused grinding burn samples a) N1, b) N2, c) N3, d) TUT6 and e) TUT8.*

Following the normal pattern as in the other residual stress measurements, residual stress was the least compressive to the direction of grinding. By comparing the results from the grinding wheel perspective, clearly more devastating damage has been happened with the N samples ground with Al_2O_3 wheel. The residual stress values shift from compressive to tensile in the grinding direction even though the values to perpendicular direction stayed compressive. In the CBN ground TUT samples the residual stress values stayed compressive in both directions. One of the reasons was the significantly higher thermal conductivity which allows the CBN wheel to be used in higher temperatures and more demanding conditions that are too much for a conventional grinding wheel such as Al_2O_3.

When comparing samples ground with the same wheel, differences can be seen between the samples. Al_2O_3 ground samples N1, N2 and N3 have clear deviations especially into the direction of grinding. This is due to the different grinding parameters used to ground the samples. From the Table 8. the parameters for the each grinding processes of the N samples can be seen. In Figure 15 a). all of the N samples are presented, from the visual standing point N2 which had highest depth of cut and looked to have the most severe visual grinding burn. Based on XRD results, the most severe grinding burn looks to be in sample N3 ground with parameters of 8 m/min feed rate and 0.138 mm depth of cut. Lower work speed increased the contact time of the grinding wheel grains which induced more heat to the contact area.

When comparing TUT6 and TUT8 samples it was obvious that TUT8 sample had higher compressive residual stresses in the surface of the material. This was likely due to the grinding process, the same amount of material was removed (0.6 mm) from the surface but TUT6 sample was ground with smaller depth of cuts than TUT8.

By comparing the normally ground samples to intentionally caused grinding burn samples the residual stresses have had more significant drop in Al_2O_3 samples than in CBN samples even though it seems that the overall load would have been higher in TUT6 and TUT8 rather than in N samples. This is due to better thermal conductivity of CBN. The conclusion can be drawn from the XRD results that CBN has significantly higher thermal conductivity than Al_2O_3 hence the grinding force and temperature had to been higher during grinding since the residual stress has shifted tensile. These need to be further studied by cutting the samples and etching them to be observed with optical microscopy to draw more conclusions.

The hardness measurements were done to the intentional burning samples. These measurements were taken around the middle point of each marked area, around the

area where the XRD measurements were also taken. Whilst the amount of measurements was high, only few of the marked areas for each sample batch were compared with each other with the average hardness. The chosen areas were 4, 7 and 10 (will be under microstructural observation later on) and these are illustrated in Table 12. In the hardness measurements deviation was seen, the highest differentiating results were left out of the average calculations.

Table 12. *HV1 hardness measurements from the intentional grinding burn samples, averages of areas 4, 7 and 10.*

N1	N2	N3	TUT6	TUT8	N1	N2	N3	TUT6	TUT8	N1	N2	N3	TUT6	TUT8
Area 4	Area 4	Area 4	Area 4	Area 4	Area 7	Area 7	Area 7	Area 7	Area 7	Area 10	Area 10	Area 10	Area 10	Area 10
621	637	636	554	491	693	651	639	589	430	605	636	683	583	483

The results of the BN and XRD measurements for the intentional grinding burn samples are showcased in Figure 59. From Figure 59. quite good correlation can be seen with RMS – residual stress data since the RMS value increased while compressive residual stress was smaller and changed to tensile residual stress in Al_2O_3 ground samples. When comparing the N samples results to the normally ground samples (Figure 36.) it was obvious that some degree of grinding burn was happened. This was noticeable since the total removal of the material was less than 0.3 mm (Table 8.) and the compressive residual stress has dropped in the perpendicular direction and even changed to tensile residual stress in the grinding direction. For the CBN ground TUT samples significant drop has happened with the compressive residual values but the stress has not changed to tensile residual stress like in N samples.

The TUT samples have clearly higher RMS values witch might suggest overtempering due to lower hardness values compared to the N samples values. XRD residual stress measurements also revealed that surface compressive residual stresses are quite evenly distributed in each sample. For the N samples the possibility could be reharden-ing. Based on the fact that RMS values stays low compared to normally ground once suggests that the surface might have hardened. Also residual stresses are low or even tensile and still the RMS values match normally ground. On the other hand retempering lowers the hardness value and since no clear hardness increase has happened compared to normally ground samples it can't be ruled out either. Further analysing using microstructural observation is needed to identify the type of thermal damage caused to the samples by the grinding process.

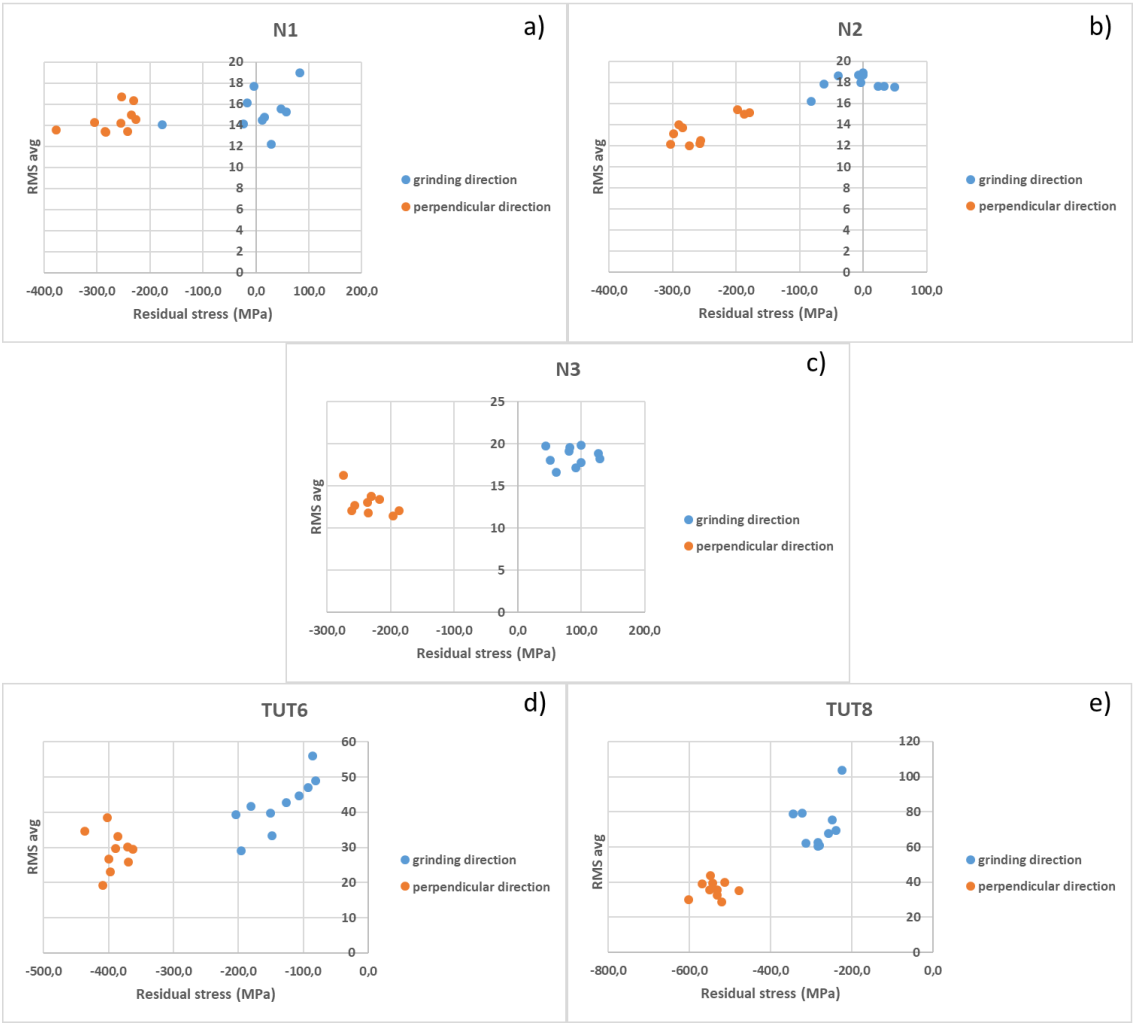

Figure 59. *RMS avg – residual stress results of the intentional grinding burn samples.*

Further microhardness studies for cross-sectional samples was done done by using Matsuzawa MMTR-X7. The results are presented in the Table 13. Example image of the measurements is showcased in Figure 60.

Table 13. *Microhardnesses of the intentionally caused grinding burn samples.*

	Hardness (HV0.3)														
area	4					7					10				
sample	N1	N2	N3	TUT6	TUT8	N1	N2	N3	TUT6	TUT8	N1	N2	N3	TUT6	TUT8
edge	681	717	617	589	**597**	673	705	657	533	351	577	669	666	550	**683**
1	715	752	723	572	369	706	753	723	506	-	698	717	722	575	391
2	695	765	751	555	389	706	774	741	501	-	701	751	755	571	409

In the Table 13. measurements have been taken from the edge varying between 20 to 40 µm. Measurements taken a bit deeper (1) vary from 66 to 120 µm and the depth below the surface measurements (2) vary between 106-191 µm below the surface.

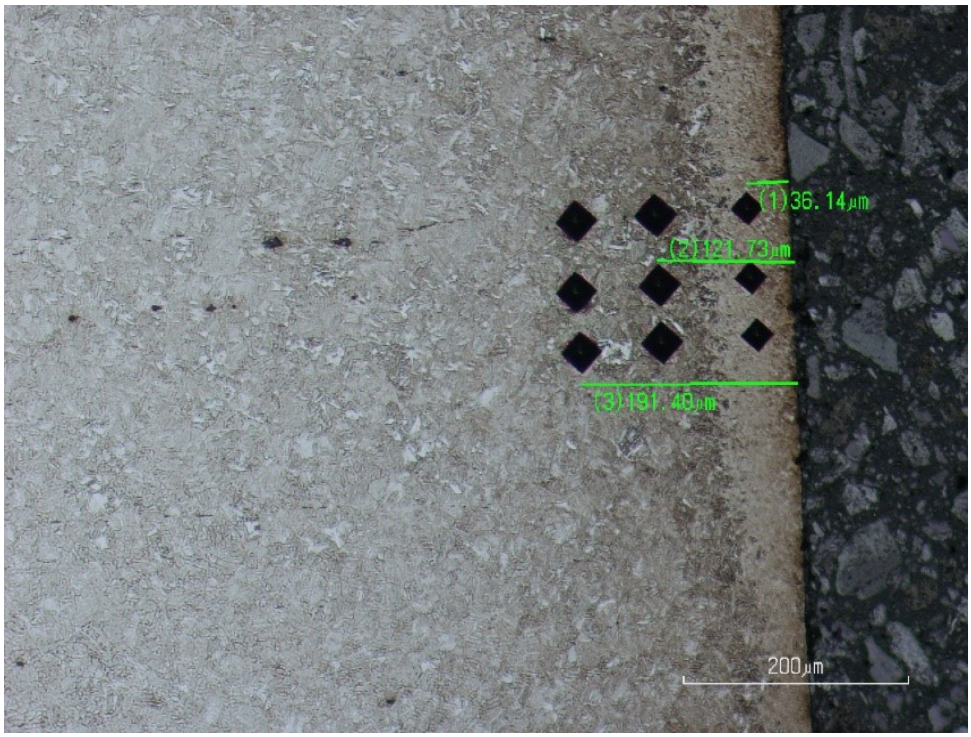

Figure 60. *Microhardness measurement taken from the TUT8 sample, area 4.*

In the Figure 60. the first near edge measurement had been taken from the white area to determine the hardness level difference between the visually different areas.

Microstructural observation of the intentionally caused grinding burn samples was the chosen measurement to observe the grinding burns and get a better understanding of the grinding burns in order to determine how accurate BN actually was. In Figure 61. is the N1 sample, in Figure 62. N2 and in Figure 63. is the N3 sample.

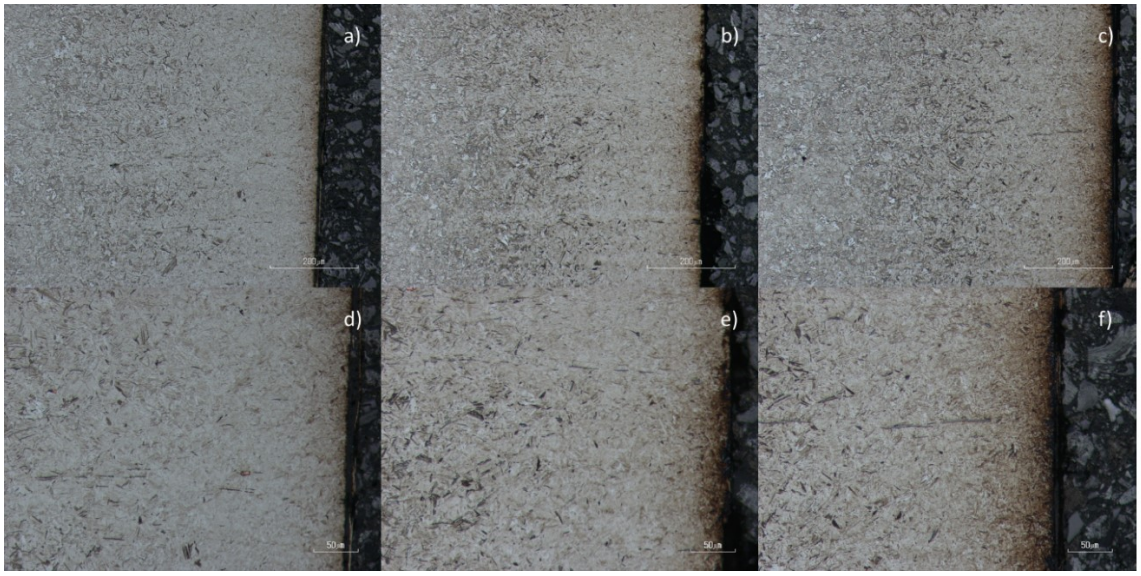

Figure 61. *N1 sample temper burn, top row magnification of x10 and bottom row x20. a and d) area 4, b and e) area 7 and c and f) area 10. Temper burn can be seen as the darker area on the right side of the sample.*

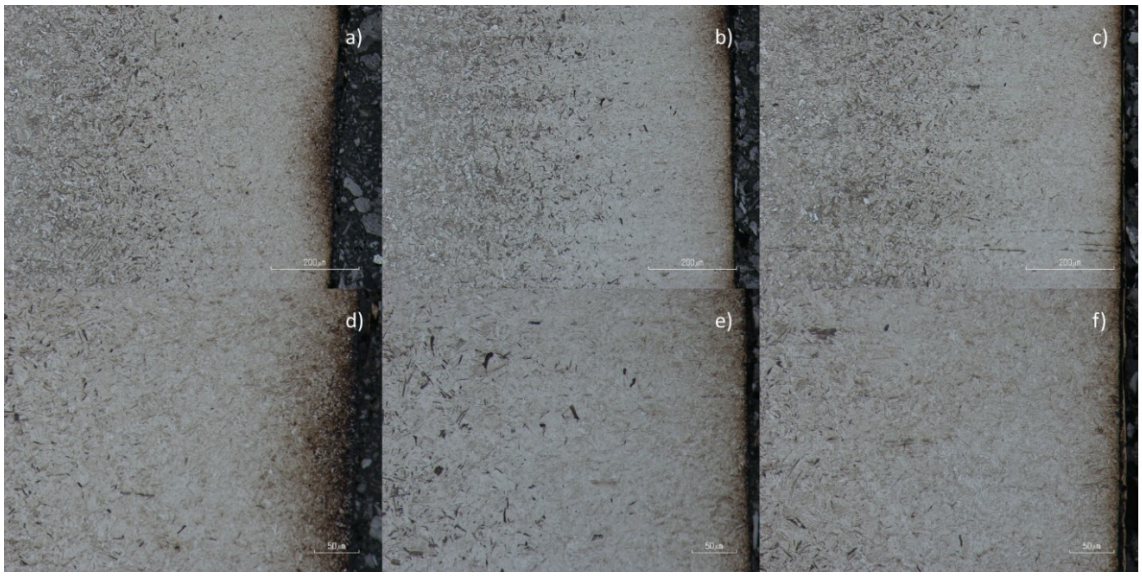

Figure 62. *N2 sample temper burn, top row magnification of x10 and bottom row x20. a and d) area 4, b and e) area 7 and c and f) area 10. Temper burn can be seen as the darker area on the right side of the sample.*

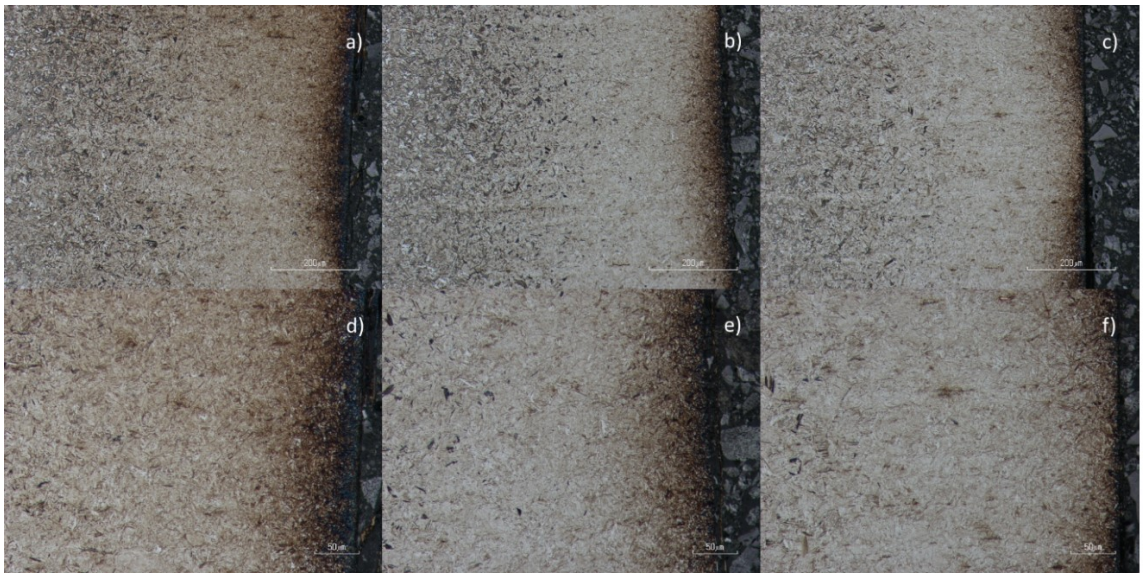

Figure 63. *N3 sample temper burn, top row magnification of x10 and bottom row x20. a and d) area 4, b and e) area 7 and c and f) area 10. Temper burn can be seen as the darker area on the right side of the sample.*

In Figures 61, 62 and 63. clear indications of temper burn appear below the surface. As mentioned in theoretical section of grinding burns, temper burn softens the material and lowers wear resistance meaning that the temperature has elevated over the tempering temperature during grinding. [28]

In sample N1 the visually more tempered area (microstructure) increased towards the more visually burned side (surface). Interesting part of the samples N2 and N3 was that the visually more tempered area (microstructure) was closer to the non-visually burned side rather than visually more burned side (surface). Comparing these two with known parameters of the grinding process and microstructural images to previously discussed literature indicated that the results were in line with each other. Since the N3 sample had more demanding grinding parameters, it should have evolved more thermal damage compared to other N samples. These results were also in line with the residual stress measurements taken with XRD when comparing BN results to the images the RMS value correlates well, offering the lowest value to minor burn and higher to the more serious burn. One possible explanation for the low RMS values compared to the values gathered from the normally ground samples is that the BN values have been measured slightly under the surface where the hardness is higher, as can be seen from the microhardness Table 13. RMS values should have been higher if the measurement would have been from the very surface layer but no significant change can be detected.

TUT6 sample's microstructure is presented in Figure 64. It is hard to determine the thermal damage since the case depth has been ground off and with the gathered data no obvious solution can be said.

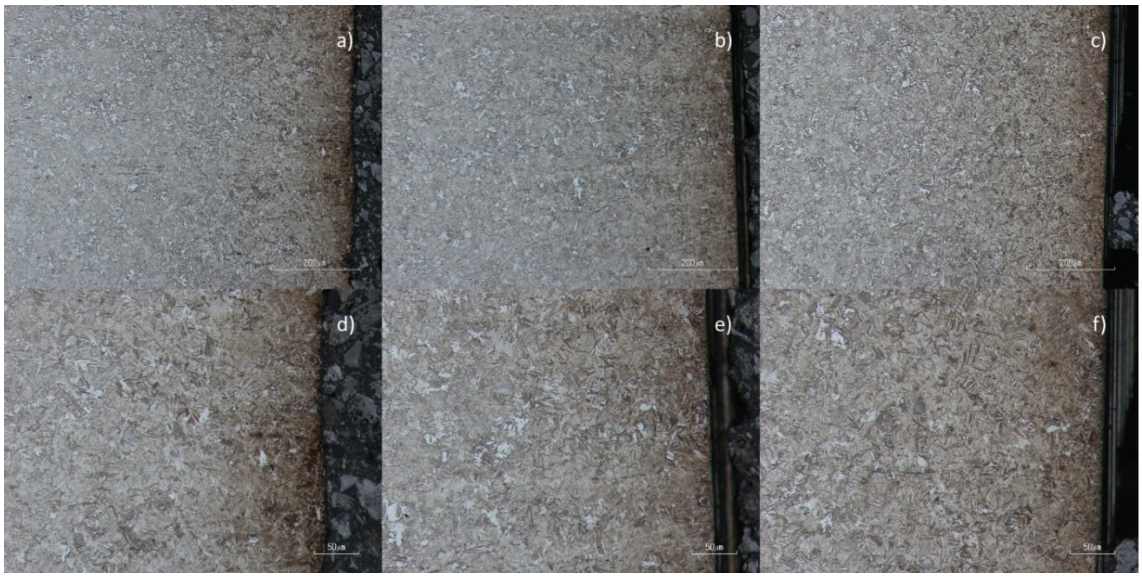

Figure 64. *TUT6 sample, top row magnification of x10 and bottom row x20. A and d) area 4, b and e) area 7 and c and f) area 10.*

TUT8 sample is showcased in Figure 65. Compared to BN measurements, highest RMS value was gathered from the area 7 with quite significant deviation from the other two. Instead of the educated guess of overtempering, microhardness measurements and microstructural observation confirmed rehardening as the thermal damage type. Thus offering information that the grinding process has elevated to the temperature over 850 ºC or the the plastic deformation induced phase change. Due to this, sample surface has become harder and brittle. Thus offering explanation to the drop in surface hardness after surface layer. One possible explanation for the RMS values could be that the untempered martensite white layer is thin and the BN has taken the values under the rehardened layer (softer layer). Or there could be layers of rehardening and tempering varying while the measurement collects the information mainly from the tempered areas.

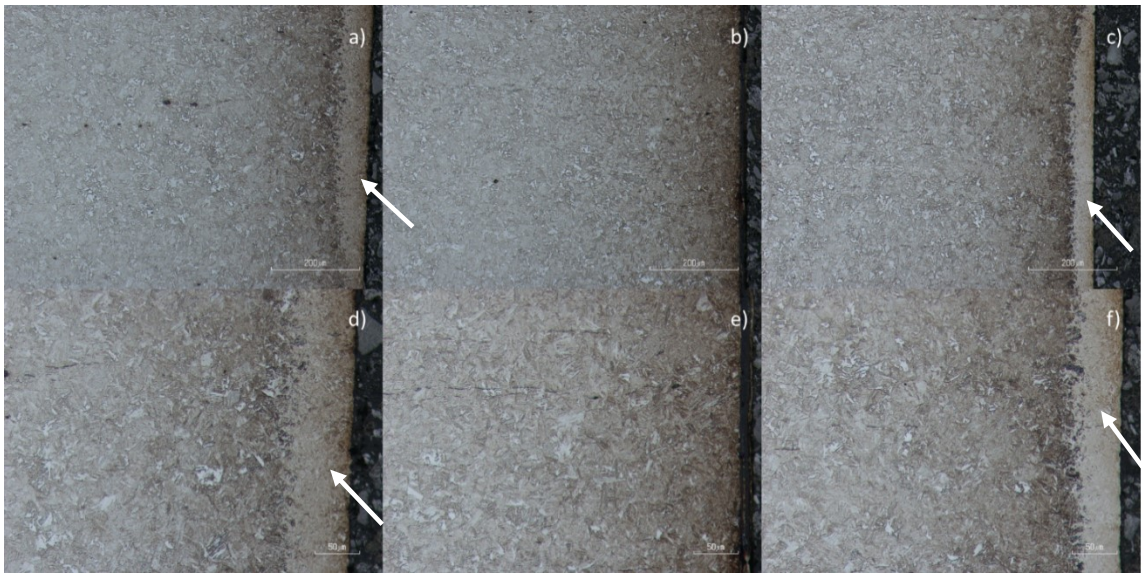

Figure 65. *TUT8 sample rehardening layer, top row magnification of x10 and bottom row x20. a and d) area 4, b and e) area 7 and c and f) area 10. Rehardened layer (white arrow)*

From the images of the TUT6 and TUT8 samples can be observed that the whole case depth layer has been ground off. Meaning that the softer material has been under the grinding forces, thus making thermal damage easier to be generated since the heat treatment produced protective case is minimal or completely lost from the surface layer. This makes the grinding burns observed questionable.

6.2 Conclusions drawn from the measurement results and comparison to literature

Based on the measurement results and comparing the normally ground sample batches Al_2O_3, CBN B126 and B181, significant differences could not be found. Based on literature and studies found, the results should have been favoring the CBN wheel. This can be explained with the study being quite unfair towards the CBN wheels since the initial grinding was done with the same low speed with the conventional wheel Al_2O_3. The speed wasn't nearly high enough to see the potential benefits that the higher thermal conductivity CBN possesses. Based on literature and studies found with higher grinding speeds used with the CBN wheels, the results should have been favoring the superabrasive CBN. For example in the "Principles of Modern Grinding Technology" it is stated [53] that advantage of CBN is in its thermal conductivity and low spesific energy. This is backed up with figures where the grits are same (200), wheel speeds are 30 m/s and work speeds are 0.25 m/s. Grinding with vitrifield CBN showed significantly lower specific energy and lower temperatures than Al_2O_3 wheel. [53] It would have been nice to know

the temperatures during grinding in order to make more detailed comparison based on this source. If the CBN grinding wheels have showed less temperature rise during grinding or would the grinding circumstances have been too low to define a difference for the temperature values?

Same book offers a study concerning the cost efficiency of the grinding based on different grinding parameters between Al_2O_3 and CBN wheels. The study includes the selection of the best grinding conditions through basic trials that were put through confirmation trials to be confirmed. This study found that optimal conditions for conventional speed Al_2O_3 and vitrifield CBN are different. In the study the wheel speed was same for both (45 m/s) but the work speed and removal rate were different. For the Al_2O_3, work speed was 20 m/min and removal rate was 1 mm^3/mms. For the vitrifield CBN, work speed was 26 m/min and removal rate was 4 mm^3/mms. [53] Based on this, in order to have better indication of the differences between the wheels, work speed and removal rate could have been increased for CBN. For the high-speed vitrifield CBN wheel the work speed was kept same as conventional vitrifield CBN but the wheel speed was increased up to 120 m/s, while the removal rate was increased to 20 mm^3/mms. The study made comparison between the costs of different wheels and speed using the parameters mentioned. Cost per part was by far the lowest with the high speed vitrifield CBN while the conventional speed vitrifield CBN was second most efficient. These resulted significantly lower costs than the conventional speed Al_2O_3 ground parts. The higher re-dress life based on the speed and the removal rate affected decreasingly to the cost compared to Al_2O_3. [53] Since the CBN wheel costs more than the Al_2O_3 wheel based on the result gathered (without the knowledge of the temperatures during grinding) it could be said that the amount of the components needing to be ground is the main factor influencing to the selection of the wheel based on these parameters with the surface quality. Based on the longer re-dress life of the CBN it is more suitable for high quantity grinding while Al_2O_3 is more suitable in small batch grinding. In order to see more variation in the results more sample sets should have been done and ground using different parameters regarding wheel speed, work speed and infeed rate.

Based on the thermal conductivity, differences in the temperatures during grinding would have offered value as well. Since the experimental study by Srivastava and Pavel [54] about the temperatures during Al_2O_3 and CBN gave significantly different temperatures between the grinding wheels. Although the grit sizes and bonds weren't similar to eachother the conclusion of higher temperatures involved with Al_2O_3 grinding can be drawn. The study shows that temperatures were quite a lot higher with Al_2O_3 with grinding fluid compared to dry grinding with CBN. With the information related to temperatures

it would have been easier to draw conclusions based on the differences with this important parameter included. [54]

Further support for CBN grinding wheel can be found in experimental study made by Yao et al. who studied [55] the grinding force and grinding temperature between CBN wheel and alumina wheels (white and single). The study included experimental portion of determining the thermal distribution with parameters: work speed 14 m/min, wheel speed of 25 m/s and grinding depth of 0.015 mm. Total heatflux values measured were: single alumina 91.18, white alumina 78.11 and CBN 66.48 W/mm^2. Based on the study clearly the best thermal conductivity is offered by CBN wheel. This leads to significantly lower temperature during grinding. Since the parameters are relatively close the once used in experimental part of this thesis, the results including temperature could have given indication of CBN being the better option. With grinding temperature information available comparison would have been easier to do and offered much needed information to further diagnose the wheels. [55]

Based on the results, the issues notified by the grinding wheel CBN B181 user, are not reliable detected. This is due to the fact that the deviation noticed in few of the measurements can be explained with normal deviation or possible with the likely differences between the samples in initial heat treatment process. So it is hard to determine what kind of effect if any these issues have caused during grinding.

The hardness depth profile measurements revealed the deviation in the case depths in the normally ground samples. The cause of that was further studied by measuring the hardness depth profiles of two more non-ground samples to get the accurate information about the possibility for the reason being in the initial heat treatment process.

Intentionally caused grinding burn samples offered clear differences in grinding damage department. Al_2O_3 ground samples (N1, N2 and N3) have suffered from temper burn while CBN TUT8 seems to have suffered rehardening. RMS values for the N samples are quite low compared to normally ground sample batch despite the clear thermal damage. Since earlier in the study it was already been established that temper burn lowers hardness and lower hardness means higher RMS value, it is bit odd to see next no rise in the RMS value between normally ground samples. One explanation could be that the BN values originate slightly under the surface layer from the harder layer and this explanation is backed up by the microhardness measurements.

Even though the TUT6 and TUT8 had the case depth ground off and therefore questionable grinding burn results, the finding is a good example of the nature of the grinding

burns. Grinding burns aren’t the easiest thing to study and generate on purpose. Sometimes the surface after grinding looks really badly burned while the microstructural changes are minimal. Or like in this case, surface had only minimal signs of grinding burn but the further measurements and microstructural observation revealed changes in the surface layer of TUT8 sample.

7. ANALYZING SOURCES OF ERRORS

This chapter is dedicated to inform the possible sources of error in the results presented in the thesis and in use of measurement devices. It doesn't matter how well the measurements are done, there is always possibility of error to occur in the results. That's why tolerances are used since it is extremely difficult to produce materials with exactly the same parameters and characteristics. The sources of errors mentioned in this chapter are based mainly on writer's own thoughts, common sense and information learned while writing this thesis. Not every single minor detail is going to be mentioned, only the most likely and reasonably realistic ones that can cause deviation in the results.

Grinding

Most of the common sources of error are due to the operator, the one that is using the machine. The possible sources of error in this case are new equipment, wrongly set parameters, defected grinding wheels or internally broken machine that is creating slightly wrong parameters while on the outside everything looks good.

Related to thesis there is possibility of defects in the grinding wheel or the fact that operators had limited experience in using CBN grinding. They also informed us that there was some kind of issues in the grinding process with the B181 grinding wheel. The measurements didn't reveal anything certain that would support this claim, some indications could be seen but nothing that could only be explained by grinding wheel issues. For the sample B126 0.1, the remaining case depth was according to the measurements only 0.36 mm and not even near the 0.8 mm determined from the non-ground sample. This could be due to heat treatment flaw (based on the other two non-ground hardness depth profile measurements done showing deviation) or for some reason too much of material was ground away from the surface so it would appear that the remaining case depth would be lower than the earlier measurements suggest.

Error sources occurring during the measurements

XRD

In XRD measurements the most of the common sources of error are due to the measurer using the device. The possible sources of error are: carrying out measurements while forgetting calibration, using too short exposure time (leading to less than 40 Intensity

(Imax) values and affecting the calculation of the results), placement of the sample deviates (meaning polishing) when the measurements are repeated from the same spot.

When the residual stress depth profiles are taken into account, the use of a polishing depth measurement device, Mitutoyo Absolute gauge, had few possible error causing sources. The arrangement of the start position was clumsy and small movement can occur if not correctly attached. Small hits to the device can move it and mess up the measuring place or/and depth. Deviation of the placement of the sample under the device causes error to the depth. Mostly errors are caused by the measurer since he or she is the one responsible of preparing the device. Also the sample's possible uneven polishing hole in polishing could become a problem especially if the marking of the measurement place is done poorly.

Barkhausen noise

The sensor S4740 was not flat and thus poor contact to the surface can deviate the results as well as the sensor's possible vibration during the measurements. Also measuring with only supporting the sensor with measurer's hands, can change the angle of the measurement sensor. Residual magnetism also effects to the BN response by alternating the formation of BN pulses [56]. This was also noticed in the first BN measurements done to AL_2O_3 ground samples when testing Rollscan and sensor (Figure 20.). The out look of the BN pulses was not such they should have been and testing the samples with Residumeter II model EMUD2K revealed the residual magnetism. Retained austenite can also alternate the result, content of over 40% volume decreases the BN value [56].

The amount of measurements per sample could possible be too low so that the results might have measurements shifting the results. Main worry is the one measurement taken from the grinding burn samples, even thought preliminary testing seemed to provide quite constant values. [32]

Error sources during the preparation for destructive measurements

Sources of errors in cutting of the sample are mainly due to the user of the device. Of course there is possibility of an error to occur in the machine (broken part, error in the system…). If manual cutting is used, there is possibility of cutting from the wrong area, using wrong wheel or using too much force. For the mounting process measurer can for example use wrong resin or settings.

In polishing process errors occur by using wrong sandpaper, too high speeds or forces without enough lubricant in the mix. Electropolishing for residual stress depth profile measurements results are quite depending on the one who does the measurements. What comes to measuring of the depth with Mitutoyo Absolute (capable of showing, 0,1 µm changes) it is hard to adjust to its place and minor shocks can influence the reading as well as the minor differences in the positioning of the sample. Etching can go wrong when it is used for too long or not long enough.

8. DISCUSSION OF BN ACCURACY

The focus of this discussion section is on the experimental study portion of the thesis and results. Based on the RMS measurements done by sensor S6387 it was correctly indicated what the hardness depth profile later on revealed. The value of RMS started to rise rapidly after 0.6 mm ground off sample indicating softening of the material, which turned out to be close to the hardness depth profiles (non-ground samples) defined effective case depth at 0.8 mm. This was clearly seen in each of the sample sets.

In the RMS avg – residual stress measurements the BN followed the correlation to residual stress as it should, only giving deviation to the curve in the early samples in B126 batch. Integral area – residual stress measurement gave similar results with the RMS average.

BN FWHM avg– residual stress measurement gave possibly even better correlation with the residual stress than RMS avg. Even though these measurements are correlating well, these should be measured as average values instead of single measurements due to the deviation of the measurement results.

In similar fashion, BN peak position avg – residual stress measurement correlated well offering higher peak values in higher stresses and lower values in lower stresses. This was the only measurement where some deviation in the B181 batch to perpendicular direction was noticed. It is difficult to say is the deviation related to the mentioned issue with the grinding wheel B181 (which can't really be noticed in any other of the experiments to the normally ground samples, maybe slightly in case depth measurement from the sample images after cutting) or something else. For example deviation in all of the three measurements giving deviant reading.

The PCCaseDepth gives reliable data from the measurements. Effective case depth area was visible due to rapid rise of the values in general area near the effective case depth (~0.8 mm). Similar relations was detected with the 20 Hz and 125 Hz slopes.

From the start, when there was no information that the effective case depth was 0.8 mm the results looked to be odd, but the hardness depth profile done to the non-ground sample revealed this information that the effective case depth was shallower than what was unticipated. This finding made the results look like as expected for most of the measurements.

RMS data gathered from the intentional grinding burn samples was done using sensor S4740. Two measurements were taken from each marked point, one for the grinding direction and one in the perpendicular direction. RMS values in N1 sample didn't follow the pattern that other samples did, since the values in the direction of grinding are not always higher than to the perpendicular direction. The values go back and forth close to each other, most of the measuring points still offering higher value in grinding direction. The measured values, themselves, are in order based on the study referenced in the results. Despite the obvious grinding burn in the N samples the RMS values stayed similar than in normally ground samples. One possible explanation could be that the BN measurements were taken slightly under the surface layer, from the harder layer. Overall the RMS values correlate well with the residual stress in the intentional grinding burn samples.

Purely based on BN measurements and not knowing about the intentionally caused grinding burn samples TUT6 and TUT8 samples would have been easy to isolate as possible grinding burns based on the normally ground batches. Al_2O_3 ground intentionally burned samples would have been much harder to isolate due to similar RMS values obtained as normally ground batch.

Overall, to collect more accurate data from the BN studies, more measurements per sample could have been done.

9. FUTURE OF GRINDING BURN DETECTION

Measurements and conclusions regarding the samples given for the thesis have been done. In this chapter one possible future quality inspection method is introduced regarding Barkhausen noise. With this non-destructive method, once finalized and hopefully standardized, quality inspection would be easier with no waste of valuable material during the inspection. This would make it possible to use all the material going through inspection if it passes the quality control.

9.1 Grinding temperature modeling

A study was done by Uppiliappan et al. [52] where prediction of thermal damage was done successfully independent of grinding variables for bearing steels using Malkin's grinding energy partition model with BNA. For example, retempering and rehardening were successfully detected with various intensities. The results were validated using metallography and residual stress analysis. The result of this study by Uppiliappan et al. shows [52] that prediction of thermal damage material specific models can be used as long as the models are independent of grinding process variables. [52]

Since the current method is semi-quantitative, lots of samples are needed with versatile levels of thermal damage in order to find the acceptable levels to be able to consistently detect acceptable products. This is both time consuming and quite empirical method. RMS average can be misleading since the difference between thermal damaged and non-damaged part may not vary substantially. To counter this, response that BNA gives had been correlated to other parameters but the issue remains when at least one parameter is changed. This method has a new point of view to the issues that BNA testing at the moment is facing. In the method, grinding thermal partition model has been related to BNA. [52]

Using grinding thermal model to determine the maximum grinding zone temperature to compactly summarize all of the grinding process variables. After calculations, it is correlated to material response characterizations and BNA. From the results it can be seen that the temperature can be selected to satisfy the requirements of residual stress and surface integrity. Imagining the grinding wheel as a moving heat source, it is possible to approximate the grinding zone temperatures. The influence of variability is minimal since the material transformation is verified with BNA and temperatures anticipated are relative. [52]

In the same study similar RMS values can be found in the 275 ºC as what can be seen at 175-225 ºC with the samples that had retempering. The risk is to under-predict the thermal damage intensity by trusting to RMS values alone. This risk is mitigated when the prediction includes mass of variables while correlated with BNA response. BNA RMS value relates well to maximum subsurface residual stress and predicted grinding zone temperature. Additional features like BNA peak position and FWHM parameters (envelope curves) offer information related to residual stresses and microstructure. Peak position relates well with material hardness. In the study both FWHM and RMS values follow each other almost linearly up to 800 MPa similarly with no damage or with retemper grinding damage. [52]

Depending on the maximum residual stress found in the measurements included in the study, the maximum residual stress level can be used to determine the allowed, predicted grinding temperature. After the grinding parameters that result as predicted temperature below the limit are solved measurements can be done. Upper limits for peak position and RMS can be determined using relationships like functional and fatique life requirements as guideline. [52]

To summarize the grinding temperature modelling, it compactly summarizes the grinding process variables and predicts the maximum grinding zone temperature based on several grinding parameter combinations. The predictions of grinding temperature correlates well with BNA while also correlating with residual stress profile and cross-sectional thermal damage. Grinding induced thermal damage can be detected accurately when the grinding zone temperature rise is correlated with RMS. This removes the need for destructive verification. [52]

When all of the grinding process variables are considered as one compact parameter (grinding zone temperature), several grinding conditions and impacts on surface integrity can be compared to BNA directly. There is a possibility to develop this further to effectively detect thermal damage unoccupied by process variables with material-specific grinding temperature-BNA relation. If the RMS measurement is extended to include envelope peak position, the prediction of unacceptable subsurface residual stresses can be made. This is when either retempering or rehardening related injury occuring while grinding. [52]

10. FINAL CONCLUSIONS

In the conclusions of the results, the data have been analyzed and correlation between literature and experimental results have been studied. Overall the results gave promising base to keep building up the reliability of the BN measurement method for analysis of ground surfaces. Based on the results gathered with CBN B181 wheel (informed issues while grinding) it is difficult to determine what kind of difference the issues caused (besides the signs of waviness that operator noticed). The deviation detected in few of the measurements could be explained with normal deviation and possible diffenrences caused by the initial heat treatment process. Since the measurement results are constant, it would require comparison with new batch of the samples ground with another CBN B181 wheel to determine the possible affects that the issues may have caused.

Initial questions for the thesis were: How accurate the BN is detecting grinding induced damage and suitability for quality control, how different grinding parameters or selection of the grinding wheel affects to the BN results and finally, what are the issues affecting to the outcome of the grinding and to the surface characteristics?

Based on the measurements done and data collected during experimental studies for the normally ground batches, results were quite accurate. The normally ground batches didn't have any indication of grinding burns which was confirmed with other destructive methods as well. BN method correctly identified zones where the effective and total case depth were and responded as expected, offering higher RMS values near and the hardened layer was ground off. For the intentionally caused grinding burn samples BN gave consistent results based on the other measurements. The RMS values even though correlated in each sample, the overall levels of RMS in the larger scale were a bit odd, offering relatively low values for Al_2O_3 temper burned samples. This could be explained with the theory that the RMS values were measured under surface where the material was harder, although this might not be only explanation. The CBN B126 ground intentionally caused grinding burn samples offered questionable grinding burn result since the case depth was basically ground off. CBN results still gave valuable indication that the grinding burn damage severity can't be determined based on the visual severity of the burn.

There are multiple parameters affecting to the BN results and it is hard to define only one individual effect since the result is the sum of all the affecting parameters. Grinding wheel

selection for the normally ground samples had no significant effect based on the measurements with the parameters that were available. This didn't include the temperature during the grinding and the results are discussed without the knowledge of temperature. The most defining differences can be seen in the cost of the wheels and surface roughness. The intentionally caused grinding burn samples offered theory supported relation to each other based on the results. Comparing the results to CBN ground samples is unreasonable since the whole case depth was ground off from these. Main conclusion is that effecting parameters were those involved in influencing to the temperature during grinding.

Many things can influence to the outcome and surface characteristics of the samples. Few of the main influencers are: temperature during grinding, grinding wheel material and parameters and grinding parameters.

All in all, the Barkhausen noise studies offered reliable information about the studied material and its response to the grinding wheel variations and grinding burns. Generally it is difficult to say what kind of possible thermal damage has happened to material and indicate the burn in some cases without support of other inspection methods besides BN. To further improve the BN method standards would be helpful, even though standards would be challenging to create due to multiple parameters that are hard to analyse individually when using Barkhausen noise.

After grinding trials, some thoughts of what could have been done differently to require more decisive results. Main idea related to the grinding plan. By optimising the grinding parameters for each grinding wheel, the experimental part would have offered more conclusive result regarding the specific wheel. Also addition of temperature observation during grinding would have revealed a lot more information about the grinding. The fact is that the machines provided and partners involved could not have been able to increase for example the grinding speed due to limitations of the grinding equipment. Other option would have been to use different grain sizes of the grinding wheels and vary the parameters in the limits of the machines to create further comparison.

In optimal conditions few different grinding plans would have been nice to have, at least one more that would have included optimal grinding parameters for Al_2O_3 and CBN. This would have created more realistic, real life usage scenarios. Or atleast enough difference between the CBN and Al_2O_3 grinding parameters to see more deviation in the results. Of course, the temperatures during grinding would have also offered a lot more information concerning the grinding wheels.

REFERENCES

[1] M. Blaow, J.T. Evans, B.A. Shaw, The effect of microstructure and applied stress on magnetic barkhausen emission in induction hardened steel, Journal of Materials Science, Volume 42, Issue 12, Feb 2007, pp. 4364-4371.

[2] T. Inoue, M.A.H. Howes, G.E. Totten, Handbook of residual stress and deformation of steel, Materials Park, Ohio, ASM International, 2002.

[3] Introduction to Surface Hardening of Steels, ASM handbook, Volume 4A, Steel Heat Treating Fundamentals and Processes, ASM International, Revised by M.J. Schneider, S. Madhu. https://pdfs.semanticscholar.org/0790/3c9150fbcf8193776c6fe9a1df755b0a71fe.pdf, 14.3.2019

[4] G.F. Vander Voort, Understanding and measuring decarburization, Advanced materials & processes, Feb 2015. https://www.google.com/url?sa=t&rct=j&q=&esrc=s&source=web&cd=2&ved=2ahUKEwjvwZvf7OTkAhUq4aYKHaHfC8EQFjABegQIABAC&url=https%3A%2F%2Fwww.asminternational.org%2Fc%2Fportal%2Fpdf%2Fdownload%3FarticleId%3D23559195%26groupId%3D10192&usg=AOvVaw3NPAILfwhuH3QxXw2DoGei, 12.7.2019

[5] R.B. Ross, Decarburizing, Handbook of metal treatments and testing (2nd edition), 1988. https://books.google.fi/books?id=TO9dSoi0P6gC&pg=PA88&dq=Handbook+of++decarburising&hl=en&sa=X&ved=0ahUKEwjrlvz0wJPjAhUJs4sKHSJeC2MQ6AEIMTAC#v=onepage&q=Handbook%20of%20%20decarburising&f=false, 12.7.2019

[6] M. Neslušan, J. Čížek, K. Kolařík, P. Minárik, M. Čilliková, O. Melikhova, Monitoring of grinding burn via barkhausen noise emission in case-hardened steel in large-bearing production, Journal of Materials Processing Technology, Volume 240, Feb 2017, pp. 104-117.

[7] Learning Center, Understanding effective vs total case depth, Paulo. https://www.paulo.com/understanding-effective-vs-total-case-depth/, 13.6.2019

[8] Vickers hardness testing (HV), Struers. https://www.struers.com/en/Knowledge/Hardness-testing/Vickers#application, 13.6.2019

[9] M. Vashista, A. Gaddam, S. Paul, Study of surface integrity of ground bearing steel using barkhausen noise technique, International Journal of Advanced Manufacturing Technology, Volume 63, Issues 5-8, Nov 2012, pp. 771-783.

[10] W. Ding, L. Zhang, Z. Li, Y. Zhu, H. Su, J. Xu. Review on grinding-induced residual stresses in metallic materials, The International Journal of Advanced Manufacturing Technology, Volume 88, Issue 9, 2017, pp. 2939-2968.

[11] S. Santa-aho, M. Vippola, A. Sorsa et al, Development of barkhausen noise calibration blocks for reliable grinding burn detection, Journal of Materials Processing Technology, Volume 212, Issue 2, Feb 2012, pp. 408-416.

[12] C. Yao, T. Wang, W. Xiao, X. Huang, J. Ren, Experimental study on grinding force and grinding temperature of aermet 100 steel in surface grinding, Journal of Materials Processing Technology, Volume 214, Issue 11, Nov 2014, pp. 2191-2199.

[13] J. Chen, Q. Fang, L. Zhang, Investigate on distribution and scatter of surface residual stress in ultra-high speed grinding, The International Journal of Advanced Manufacturing Technology, Volume 75, Issues 1-4, 2014, pp. 615-627.

[14] I.D. Marinescu, M.P. Hitchiner, E. Uhlmann, W.B. Rowe, I. Inasaki, Handbook of machining with grinding wheels (2nd edition), 2016.

[15] A. Thanedar, G.G. Dongre, R. Singh, S.S. Joshi, Surface integrity investigation including grinding burns using barkhausen noise (BNA), Journal of Manufacturing Processes, Volume 30, Dec 2017, pp. 226-240.

[16] W.B. Rowe, 3 - Grinding Wheel Developments, Principles of Modern Grinding Technology (2nd edition), 2014, pp. 35-62.

[17] S. Malkin, C. Guo, Grinding Technology Theory and Applications of Machining with Abrasives, (2nd edition), 2008. https://books.google.fi/books?hl=fi&lr=&id=I3260ZF_PfQC&oi=fnd&pg=PR7&dq=grinding+technology&ots=V46x6F2SdQ&sig=xm7c8mfQITTlOqN7lKE7KmASu_w&redir_esc=y#v=snippet&q=heavy%20duty&f=false, 9.4.2019

[18] T. Yu, A.F. Bastawros, A. Chandra, Experimental and modeling characterization of wear and life expectancy of electroplated CBN grinding wheels, International Journal of Machine Tools and Manufacture, Volume 121, Oct 2017, pp. 70-80.

[19] S. Malkin, C. Guo, Thermal analysis of grinding, CIRP Annals, Volume 56, Issue 2, 2007, pp. 760-782.

[20] T. Hussein, M. Marwa, Study Some Properties for Manufactured Grinding Wheels by Use Different Abrasive Materials, Australian journal of basic and applied sciences, Feb 2017, pp. 50-59. http://www.ajbasweb.com/old/ajbas_February_2017.html , 13.5.2019

[21] M.J. Jackson, B. Mills, Materials applied to vitrified alumina & CBN grinding wheels, Journal of Materials Processing Technology, Volume 108, Issue 1, Dec 2000, pp. 114-124.

[22] How to Use a Surface Grinder Machine, American Machine Tools Co. http://www.americanmachinetools.com/how_to_use_a_surface_grinder.htm, 4.3.2019

[23] X. Chen, W.B. Rowe, R. Cai, Precision grinding using CBN wheels, International Journal of Machine Tools and Manufacture, Volume 42, Issue 5, Apr 2002, pp. 585-593.

[24] Grinding wheels, Dr. Kaiser precision through diamond, 2012. https://www.google.com/url?sa=t&rct=j&q=&esrc=s&source=web&cd=4&ved=2ahUKEwjLwteX6-TkAhWxw8QBHSWTC80QFjADegQIARAC&url=https%3A%2F%2Fm.drkaiser.de%2Ffileadmin%2Fuser_upload%2Fdrkaiser_de%2Fdocuments%2FEN%2FDR-KAISER-Grinding-Wheels.pdf&usg=AOv-Vaw3kUoV8cfVHTItkftGwSihA, 15.8.2019

[25] R.P. Upadhyaya, J.H. Fiecoat, Factors affecting grinding performance with electroplated CBN wheels, CIRP Annals, Volume 56, Issue 1, 2007, pp. 339-342.

[26] M. Deveci, Stresstech bulletin 7: The importance of residual stresses. https://www.stresstech.com/en/knowledge/articles/stresstech-bulletin-7-importance-residual-stresses/, 4.6.2019

[27] S. Shen, B. Li, W. Guo, Residual stresses distributions in grinding of 3J33 maraging steel with miniature electroplated CBN wheel, MATEC Web of Conferences, Volume 256, Article 01002, 2019. https://www.researchgate.net/publication/330558661_Residual_Stresses_Distributions_in_Grinding_of_3J33_Maraging_Steel_with_Miniature_Electroplated_CBN_Wheel, 10.7.2019

[28] W.B. Rowe, Chapter 7 - Avoiding Thermal Damage. Principles of Modern Grinding Technology (1st edition), 2009, pp. 105-112.

[29] T.W. Krause, A. Samimi, Micromagnetic techniques, ASM handbook, volume 17 - nondestructive evaluation of materials, ASM International, 2018. https://dl.asminternational.org/handbooks/book/55/chapter/648758/Micromagnetic-Techniques, 1.5.2019

[30] B. He, C. Wei, S. Ding, Z. Shi, A survey of methods for detecting metallic grinding burn, Measurement, Volume 134, Feb 2019, pp. 426-439.

[31] M. Deveci, Stresstech bulletin 12: Measurement Methods of Residual Stresses. https://www.stresstech.com/en/knowledge/articles/stresstech-bulletin-12-measurement-methods-residual-stresses/, 4.6.2019

[32] Communications with grinding operators and the partners of FUNBARK project

[33] T. Nguyen, L.C. Zhang, Performance of a new segmented grinding wheel system, International Journal of Machine Tools and Manufacture, Volume 49, Issues 3-4, Mar 2009, pp. 291-296.

[34] M.W. Seidel, A. Zösch, K. Härtel, Grinding burn inspection, Forschung im Ingenieurwesen, Volume 82, Issue 3, Sep 2018, pp. 253-259. https://doi.org/10.1007/s10010-018-0270-4, 20.3.2019

[35] Barkhausen noise analysis, Stresstech. https://www.stresstech.com/en-fi/products/barkhausen-noise-equipment/barkhausen-noise-analysis/, 4.6.2019

[36] G.Gu, Z. Yang, L. Pan, W. Wei, Evolution of the microstructure, mechanical properties, and high-order modal characteristics of AISI 1045 steel subjected to a simulative environment of surface grinding bur, The International Journal of Advanced Manufacturing Technology, Volume 82, Issue 1, 2016, pp. 253-263.

[37] A.F. Chávez-González, J.A. Pérez-Benítez, J.H. Espina-Hernández, R. Grössinger, J.M. Hallen, Influence of frequency of the excitation magnetic field and material's electric conductivity on domain wall dynamics in ferromagnetic materials, Journal of Magnetism and Magnetic Materials, Volume 401, Mar 2016, pp. 287-295.

[38] V. Moorthy, B.A. Shaw, P. Mountford, P. Hopkins, Magnetic barkhausen emission technique for evaluation of residual stress alteration by grinding in case-carburised En36 steel, Acta Materialia, Volume 53, Issue 19, Nov 2005, pp. 4997-5006.

[39] M. Deveci, Stresstech bulletin 1: Barkhausen noise analysis. https://www.stresstech.com/en/knowledge/articles/stresstech-bulletin-1-barkhausen-noise-analysis/, 4.6.2019

[40] W.B. Rowe, 9 – cost reduction, Principles of Modern Grinding Technology (1st edition), 2009, pp. 145-161

[41] M. Čilliková, B. Mičieta, M. Neslušan, D. Blažek, Nondestructive magnetic monitoring of grinding damage, Procedia Materials Science, Volume 12, 2016, pp. 54-59.

[42] C.H. Gür, Nondestructive characterization of microstructures of heat-treated steels by magnetic barkhausen noise technique, Characterization of Minerals, Metals and Materials 2017, pp. 371-376.

[43] Grinding of tool steel, Uddeholm. https://www.google.com/url?sa=t&rct=j&q=&esrc=s&source=web&cd=1&ved=2ahUKEwiEqtGt7eTkAhXOxcQBHeFfBwUQFjAAegQIAhAC&url=https%3A%2F%2Fwww.uddeholm.com%2Ffiles%2FTB_grinding-english.pdf&usg=AOvVaw0oG-AtQO0AICc4xiScdb05, 2.7.2019

[44] W.X. Pereira, A.E. Diniz, A. Hassui, Comparing different plunge cylindrical grinding cycles based on workpiece roughness and process vibration, Journal of the Brazilian Society of Mechanical Sciences and Engineering, Volume 31, Number 2, 2009. http://www.scielo.br/scielo.php?script=sci_arttext&pid=S1678-58782009000200009&lng=en&tlng=en, 11.7.2019

[45] European steel and alloy grades/numbers SteelNumber. http://www.steel-number.com/en/steel_composition_eu.php?name_id=177, 6.8.2019

[46] Catalogus and product leaflets, SBU, vitrified and resin bonded, Weiler. http://www.swatycomet.com/en/products/catalogues-and-product-leaflets/index.html, 16.8.2019

[47] FEPA Particle Size Conversion Chart. https://www.washingtonmills.com/resources/guides/fepa-particle-size-conversion-chart, 31.7.2019

[48] S. Santa-aho, Barkhausen Noise Method for Hardened Steel Surface Characterization – The Effect of Heat Treatments, Thermal Damages and Stresses, 2012. https://tutcris.tut.fi/portal/en/publications/barkhausen-noise-method-for-hardened-steel-surface-characterization--the-effect-of-heat-treatments-thermal-damages-and-stresses(56496ffd-bb0a-42de-9fd5-83baba4edfde).html, 25.7.2019

[49] M. Deveci, Nondestructive determination of case depth by barkhausen noise method, 2016. https://dspace.cc.tut.fi/dpub/handle/123456789/24049, 3.5.2019

[50] N. Sinha, Abrasive Machining Processes. https://www.google.com/url?sa=t&rct=j&q=&esrc=s&source=web&cd=25&ved=2ahUKEwjowoGe7uTkAhVb8aYKHXG3DbMQFjAYegQIAxAC&url=http%3A%2F%2Fhome.iitk.ac.in%2F~nsinha%2FAbrasive_machining_processes.pdf&usg=AOvVaw0sqeWOwWTzoam-LI0_6EPK, 30.8.2019

[51] M.J. Balart, A. Bouzina, L. Edwards, M.E. Fitzpatrick, The onset of tensile residual stresses in grinding of hardened steels, Materials Science and Engineering: A. 2004, Volume 367, Issues 1-2 , Feb 2004, pp.132-142.

[52] U. Sridharan, V. Bedekar, F.M. Kolarits, A functional approach to integrating grinding temperature modeling and barkhausen noise analysis for prediction of surface integrity in bearing steels, CIRP Annals, Volume 66, Issue 1, 2017, p. 333-336.

[53] W.B. Rowe, 18 – Temperatures in grinding, Principles of Modern Grinding Technology (1st edition), 2009, pp. 365-398

[54] R. Pavel, A. Srivastava, An experimental investigation of temperatures during conventional and CBN grinding, The International Journal of Advanced Manufactoring Technology, Volume 33, Issues 3-4, Jun 2007, pp. 412-418.

[55] C. Yao, T. Wang, W. Xiao, X. Huang, J. Ren, Experimental study on grinding force and grinding temperature of aermet 100 steel in surface grinding, Journal of Materials Processing Technology, Volume 214, Issue 11, Nov 2014, pp. 2191-2199.

[56] M. Deveci, Stresstech bulletin 2: The properties of barkhausen noise. https://www.stresstech.com/en/knowledge/articles/properties-barkhausen-noise/, 4.6.2019

[57] ISO 18203:2016. https://www.iso.org/standard/61748.html, 18.9.2019